Supporting Information

Subcomponent Exchange Transforms an $Fe^{II}_4L_4$ Cage from High- to Low-Spin, Switching Guest Release in a Two-Cage System

Anna J. McConnell, Catherine M. Aitchison, Angela B. Grommet and Jonathan R. Nitschke*

Table of Contents

1 Materials and Methods

Reagents and solvents were purchased from commercial suppliers and used without further purification, unless otherwise specified. All manipulations involving cage **1** were carried out in a glovebox using CD_3CN that had been dried over calcium hydride and distilled *in vacuo*.

Centrifugation of cage samples was carried out using a Grant-Bio LMC-3000 low speed benchtop centrifuge.

UV/visible spectra were recorded on a Perkin Elmer Lambda 750 UV-Vis-NIR spectrophotometer fitted with a PTP-1 Peltier temperature controller accessory. Spectra were obtained in double beam mode recording the spectra using the front beam with air in the rear beam. A background spectrum of CH_3CN was recorded using the analyte beam prior to each experiment and a baseline correction was applied using the Perkin Elmer WinLab software suite.

IR spectra were recorded on a Perkin Elmer Spectrum One FT-IR Spectrometer fitted with a University ATR Sampling Accessory. A background spectrum was recorded prior to each experiment, and spectra were obtained over 16 scans.

1.1 NMR Spectroscopy

All NMR spectra were recorded on Bruker 400 MHz Avance III HD Smart Probe (paramagnetic and routine ^{1}H NMR experiments) and Bruker 500 MHz DCH Cryoprobe (^{13}C NMR experiments) NMR spectrometers. The following pulse programs were used: zg30 (^{1}H), ledbpgp2s (DOSY), zgfhigqn (^{19}F), cosygpmfqf (routine COSY), cosyqf90 (COSY of cage **1**), hsqcetgpsisp2.2 (HSQC), hmbcetgpl3nd (HMBC), zgpg30 (^{13}C). Chemical shifts are expressed in parts per million (ppm) and reported relative to the resonance of the residual methyl proton and carbon of CD_3CN (δ_H = 1.94 ppm, δ_C = 1.32 ppm) or residual proton and carbon of CD_2Cl_2 (δ_H = 5.32 ppm, δ_C = 53.84 ppm). ^{19}F chemical shifts (δ) are reported relative to hexafluorobenzene (dissolved in CD_3CN in a capillary) at -164.90 ppm. All measurements were carried out at 298 K unless reported otherwise. The following abbreviations are used to describe signal multiplicity for ^{1}H, ^{13}C and ^{19}F NMR spectra: s: singlet, d: doublet, t: triplet, dd: doublet of doublets; m: multiplet, b: broad.

1.1.1 Paramagnetic ^{1}H NMR spectra

Paramagnetic ^{1}H NMR spectra were recorded using the zg30 pulse program with a 407 ppm sweep width centred at 130 ppm. The delay, D1, was set at a value five times the longest T1 value of the signals and a minimum number of 120 scans were recorded. The NMR spectra were processed applying a line broadening of 20 Hz.

1.1.2 T_1 Measurements

It was not possible to measure the T_1 values for all cage signals simultaneously in the 240 ppm range of the paramagnetic ^{1}H NMR spectrum. Therefore, the T_1 value for each signal was measured with a sweep width of 10 ppm centred on the signal or group of signals within the sweep width. Initially, the T_1 value for each signal was estimated using the t1ir1d pulse program in order to set an appropriate D1 value (five times the estimated T_1 value) and variable delay list for measuring an accurate T_1 value using the t1ir pulse program. Data was collected for a minimum of 25 delays using 8 scans and processed using Dynamics Center 2.3.3. As a small sweep width had been used, the data was fit using the inversion recovery with partial inversion fitting function (Eq. 1) with an error estimation by fit to obtain the T_1 value.

$$I(t) = Io(1 - ae^{-t/T1}) \qquad \text{Eq. 1}$$

1.1.3 COSY Spectra

COSY NMR spectra for cage **1** were recorded using a cosyqf90 pulse program with a 120 ppm spectral width centred at 10 ppm using 28 scans, 2048 increments and acquisition times of 0.34 s and 0.021 s in the F2 and F1 dimensions, respectively. The COSY spectra were

processed using a line broadening of 20 Hz in the F2 dimension, and a sine function with a sine bell shift of 2 in the F1 dimension.

1.1.4 Magnetic Susceptibility Measurements

Magnetic susceptibility measurements in solution were determined by the Evans' method[1] using variable temperature NMR data obtained using the same parameters as for the paramagnetic ^{1}H NMR spectra (Section 1.1.1). Cage **1** binds a variety of guests in CD_3CN and commonly used internal references for mass susceptibility measurements, such as *tert*-butanol and cyclohexane, were found to bind in the cavity of the cage. *p*-Xylene was chosen as the internal reference since it only binds in traces amounts according to host-guest studies in Section 3 in order to minimise the interactions with the cage at the concentrations of internal reference required for the measurements. In a glovebox, a 1 mL solution of *p*-xylene (30.0 µL) and CD_3CN was prepared in a volumetric flask. This solution was added to a 5 mm NMR tube. In a glovebox, a 1 mL solution of **1** (6.64 mg, 1.50 µmol), *p*-xylene (30.0 µL), and CD_3CN was prepared in a volumetric flask. This solution was used to fill a standard melting point capillary, which was then inserted into the NMR tube containing the *p*-xylene/CD_3CN solution. Data and results are included in Section 9.2.

1.2 Mass Spectrometry

Low resolution electrospray ionisation mass spectrometry (ESI-MS) was carried out on a Micromass Quattro LC (cone voltage 4-14 eV, desolvation temp. 313 K, ionisation temp. 313 K) infused from a Harvard syringe pump at a rate of 10 µL per minute.

High resolution electrospray ionisation mass spectrometry (ESI-MS) was carried out by the EPSRC UK National Mass Spectrometry Facility at Swansea University on a LTQ Orbitrap XL hybrid ion trap-orbitrap mass spectrometer.

Gas-chromatography-mass spectrometry (GC-MS) was carried out using a Shimadzu QP2010-SE fitted with a SHIM-5MS column (30 m, 0.25 mm, 0.25 µm film) for MS analysis.

2 Cage 1

2.1 Synthesis

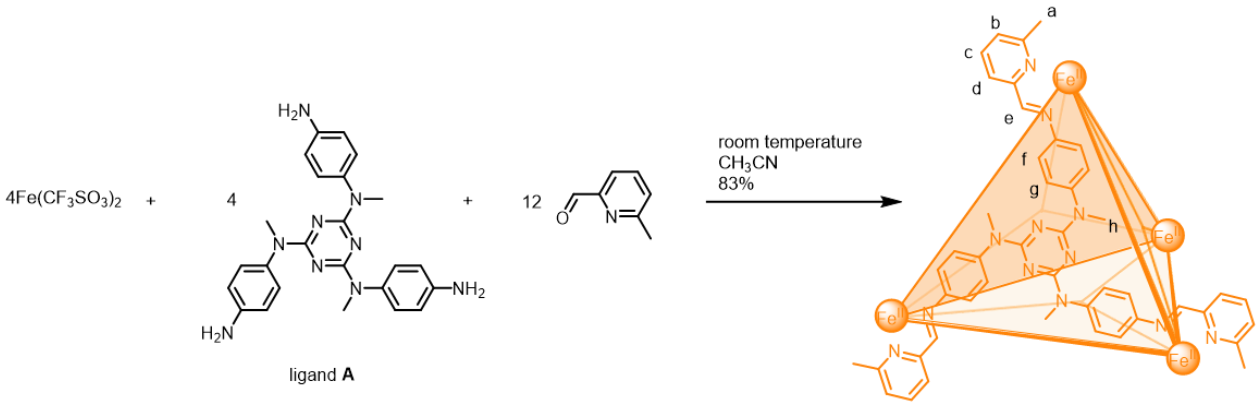

Scheme S1. Synthesis of cage **1**.

$Fe(OTf)_2$ (80.06 mg, 0.23 mmol), ligand **A**[2] (99.78 mg, 0.23 mmol) and commercially available 2-formyl-6-methylpyridine (82.11 mg, 0.68 mmol) were added to a Schlenk flask containing degassed MeCN (15 mL). The mixture was degassed by freeze-pump-thaw three times and stirred under N_2 at room temperature for 21 h. The reaction mixture was added dropwise to diethyl ether (60 mL) to precipitate **1** and the mixture was centrifuged, the supernatant decanted and the solid was washed with diethyl ether two times. The orange solid was dried under a vacuum to give **1** (0.21 g, 83%).

^{1}H NMR (400 MHz, CD_3CN, 298 K) δ (ppm): 193.6 (H_e), 54.7 (H_b, H_d), 8.5 (H_c), 4.7 (H_g), -4.1 (H_h), -18.8 (b, H_f), -36.7 (H_a)

^{19}F NMR (376 MHz, CD_3CN, 298 K, referenced to C_6F_6) δ (ppm): -74.5 (b, OTf^-)

High Resolution ESI-MS *m/z*: 587.5174 (calcd 587.5181) for [**1** + 2OTf]$^{6+}$

ESI-MS *m/z*: 482.3 [**1** + OTf]$^{7+}$, 587.6 [**1** + 2OTf]$^{6+}$, 734.9 [**1** + 3OTf]$^{5+}$, 955.9 [**1** + 4OTf]$^{4+}$, 1324.0 [**1** + 5OTf]$^{3+}$

2.2 Characterisation

2.2.1 NMR Spectra

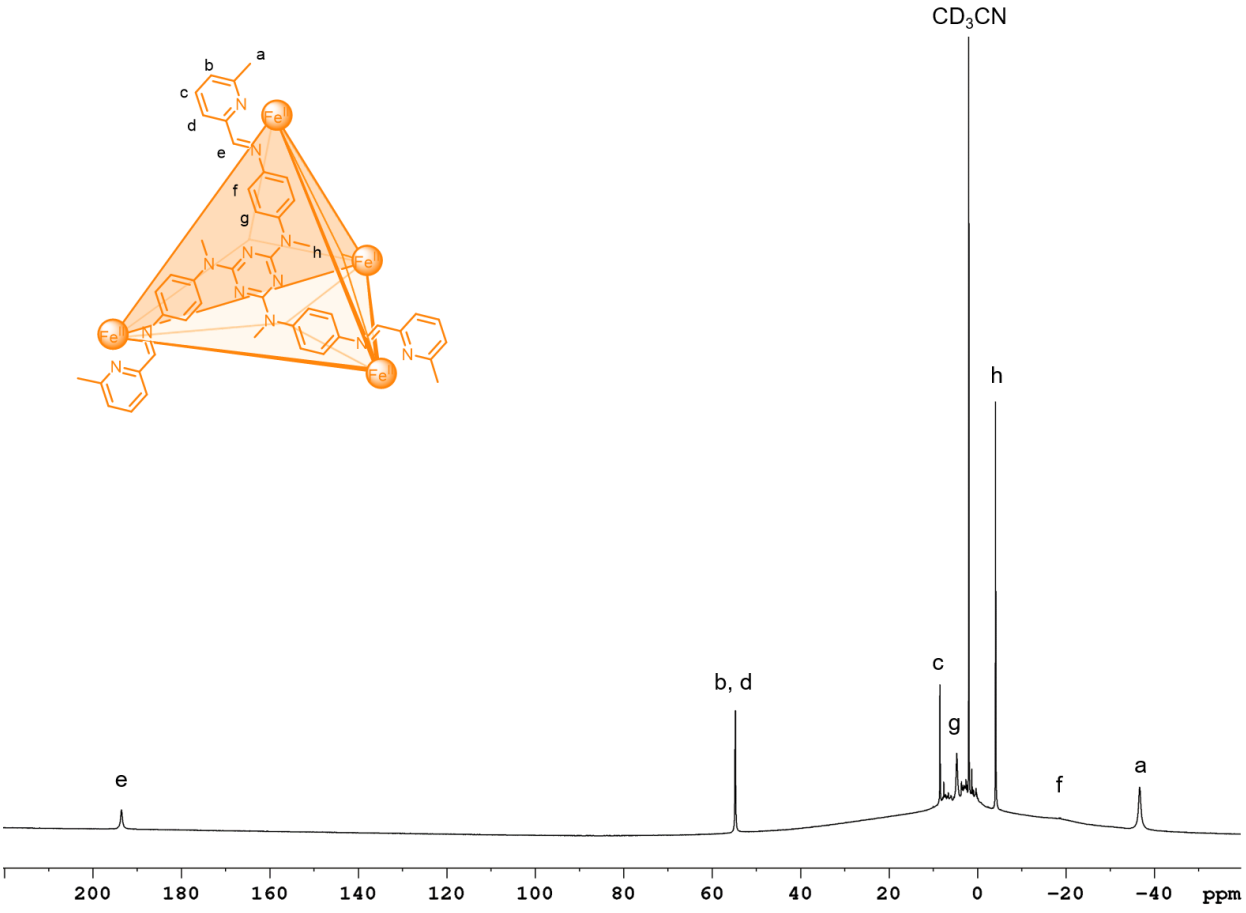

Figure S1. Paramagnetic ^{1}H NMR spectrum of [**1**](OTf)$_8$ in CD_3CN at 298 K.

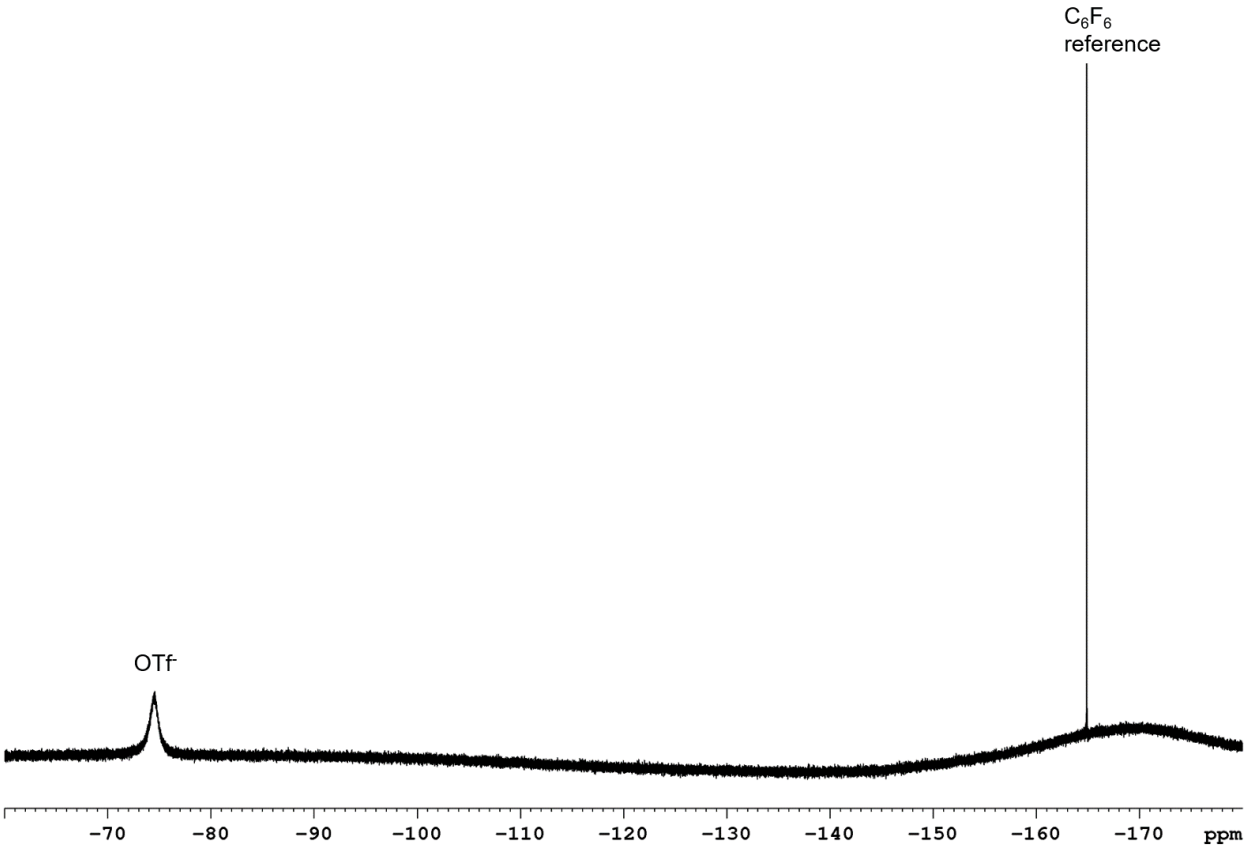

Figure S2. ^{19}F NMR spectrum of [**1**](OTf)$_8$ in CD_3CN at 298 K.

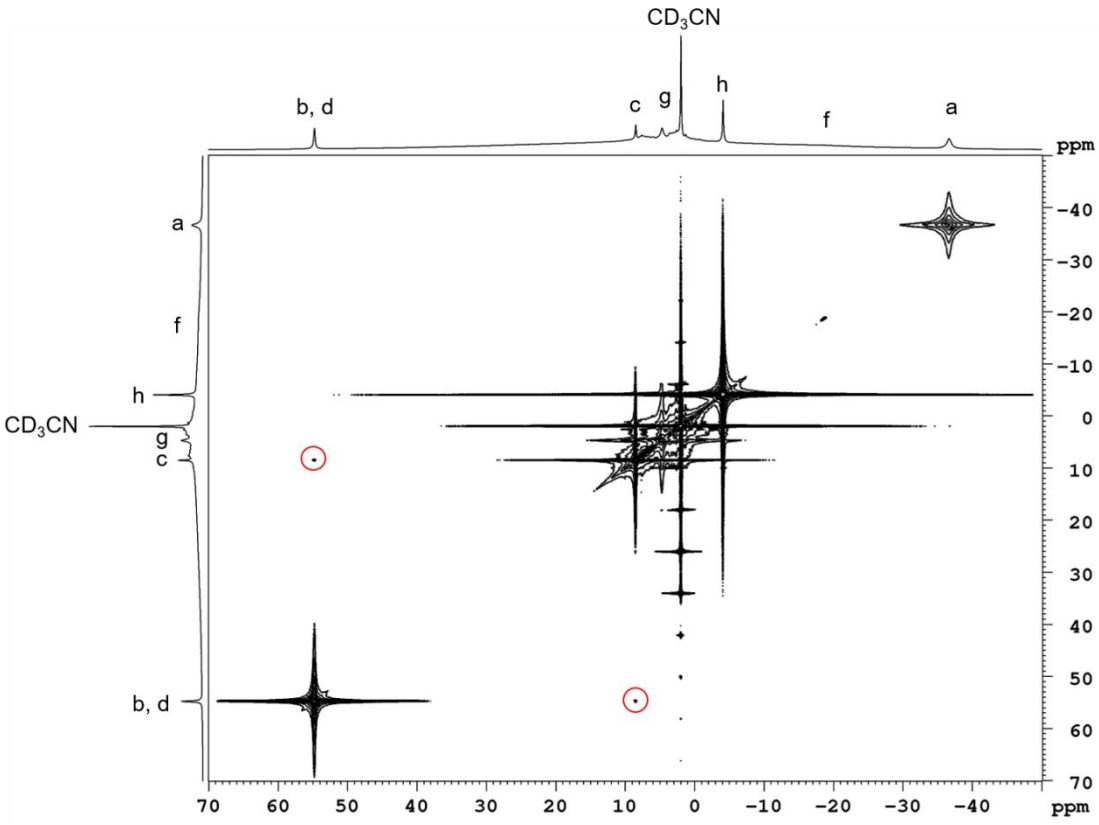

Figure S3. COSY NMR spectrum of [**1**](OTf)$_8$ in CD_3CN at 298 K.

2.2.2 Mass Spectra

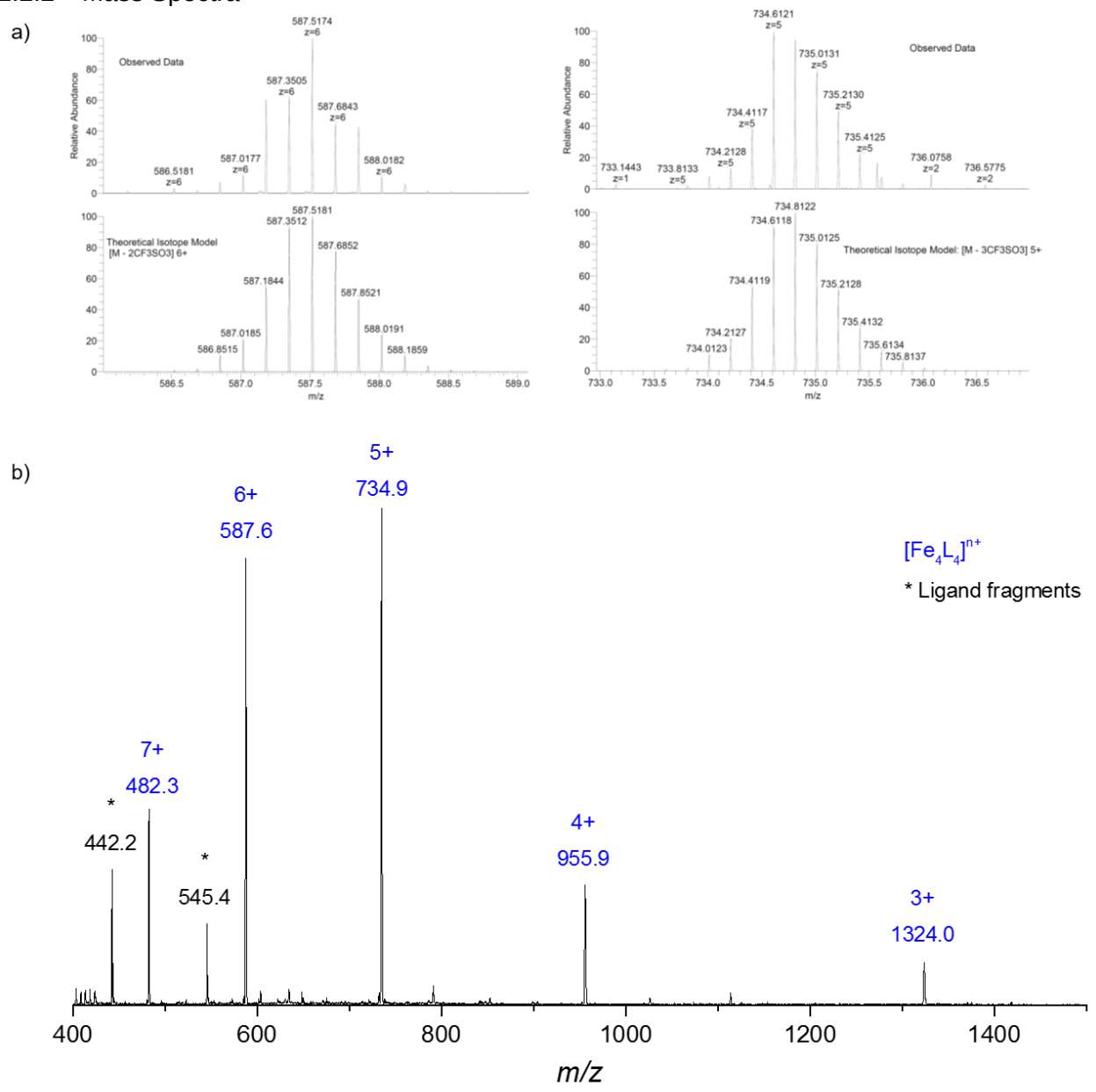

Figure S4. a) High resolution ESI-mass spectra for the 6+ and 5+ charges with the observed (top) and theoretical (bottom) isotope patterns. b) Low resolution ESI-mass spectrum of [**1**](OTf)$_8$.

2.2.3 VT NMR Studies

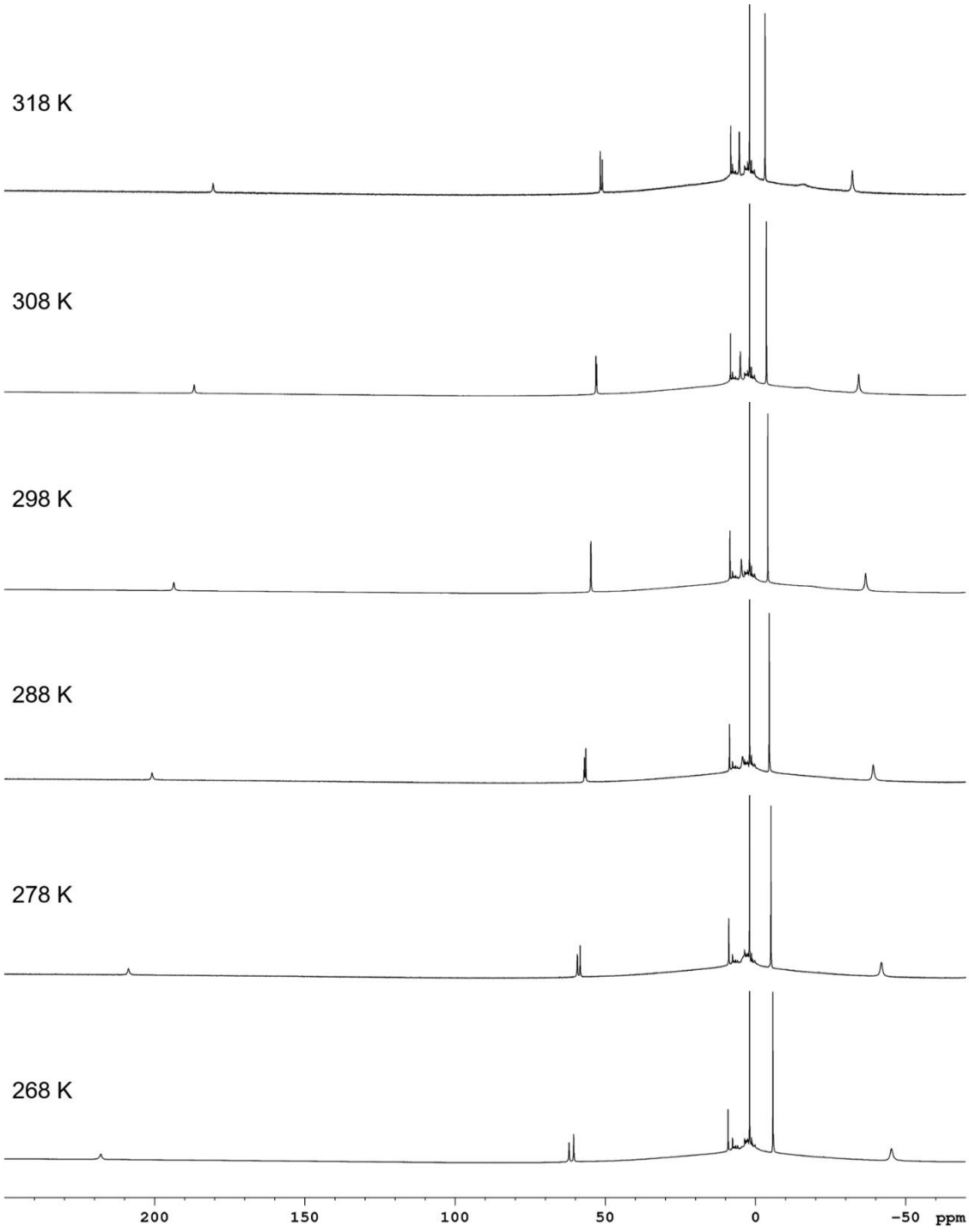

Figure S5. Variable temperature paramagnetic ^{1}H NMR spectra of [**1**](OTf)$_8$ in CD_3CN.

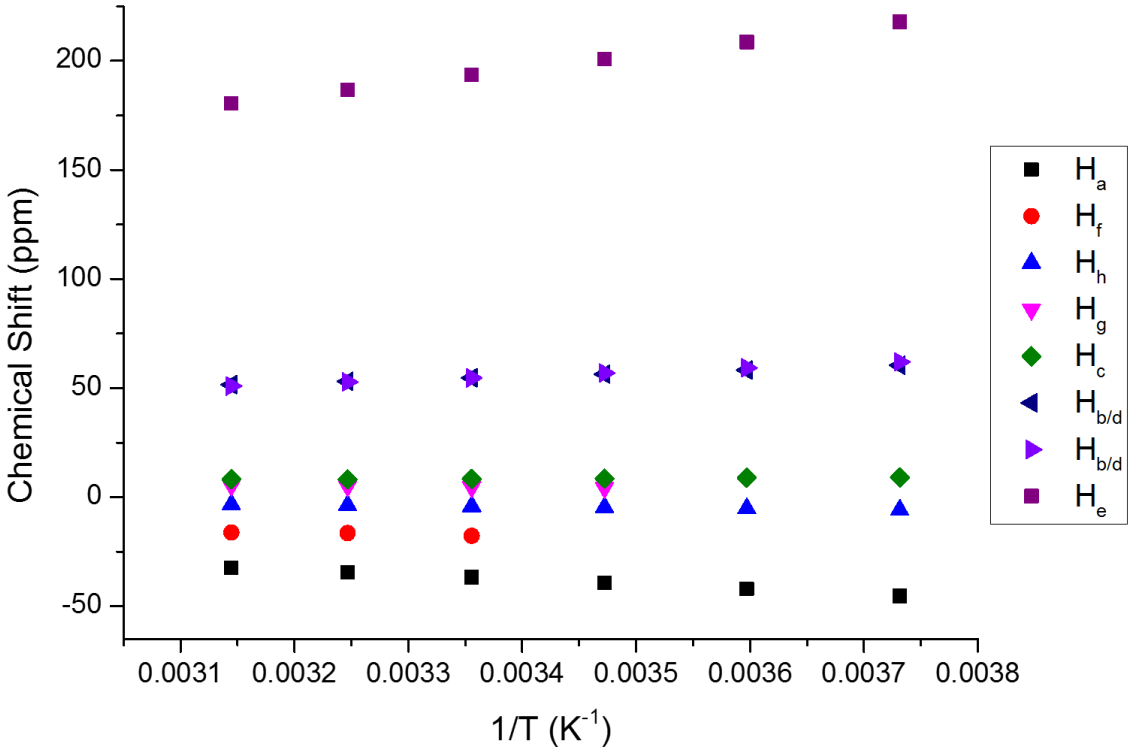

Figure S6. Curie-Weiss plot showing the chemical shift changes of cage **1** as a function of 1/T. The signals for H_f and H_g were too broad at low temperatures to accurately determine chemical shifts.

2.2.4 Proton Assignment through T_1 Measurements

In order to assign the paramagnetic signals of **1**, T_1 relaxation values were measured: T_1 is inversely proportional to $\Sigma(r_{ij})^{-6}$, where r_{ij} is the distance from the paramagnetic center to the proton, according to the Solomon equation.[3] For cage **1**, the T_1 values varied from 2.91 ms to 101 ms, although the broadness of the peak at -18.8 ppm precluded measurement of the T_1 value (Table S1, Figure S7). In the absence of a crystal structure for cage **1**, the Fe^{II}-proton distances from the crystal structure of the low spin analogue **2**[2] were used to calculate relative T_1 values (normalised to the imine peak at 193.6 ppm) and assign the proton signals, following the methods employed by Raehm[4] and Ward[5] for paramagnetic Co^{II} complexes. It was not possible to calculate the relative T_1 values normalised to the smallest measured T_1 value of 2.91 ms as cage **2** does not have an equivalent Fe^{II}-proton *a* distance in the crystal structure. There is good agreement (within a factor of 1.3) between the measured and calculated T_1 values with the exception of proton *h*. This discrepancy could be due to the increased flexibility of the cage in solution compared with the solid state.

Additional confirmation of the proton assignments by 2D NMR analysis was rendered difficult by the short T_1 values and wide spectral width of the paramagnetic spectrum. The cross-peaks observed in the COSY spectrum are consistent with our assignment of the pyridine protons (Figure S3), although correlations between protons *f* and *g* were not observed due to the broadness of the signal for proton *f.* Comparison to the calculated chemical shifts for a related high spin Fe^{II} mononuclear complex provided additional support for our ^{1}H NMR assignments.[6]

Table S1. T_1 relaxation values and ^{1}H NMR assignments for cage **1**.

δ/ppm	Measured T_1/ms	Normalised $[\Sigma(r_{ij})^{-6}]^{-1}$[a]	Normalised $[\Sigma(r_{ij})^{-6}]^{-1}$ /T_{1meas}	Proton assignment
-36.7	2.91	[b]	[c]	a
-18.8	[d]	4.8	[c]	f
-4.1	101	257	2.5	h
4.7	49.4	57	1.2	g
8.5	47.2	54	1.1	c
54.7	20.5	26, 21	1.3, 1.0	b, d
193.6	3.92	3.92	1	e

[a] Calculated from the X-ray crystal structure of cage $\mathbf{2}^{2}$ by averaging six Fe^{II}-proton distances for each type of proton.[4-5] The relative T_1 value was calculated by normalising $[\Sigma(r_{ij})^{-6}]^{-1}$ to the measured T_1 value for the peak at 193.6 ppm. [b] The T_1 value could not be calculated as the crystal structure of cage **2** does not have equivalent Fe^{II}-proton *a* distances. [c] Could not be calculated. [d] The signal was too broad to determine the T_1 value.

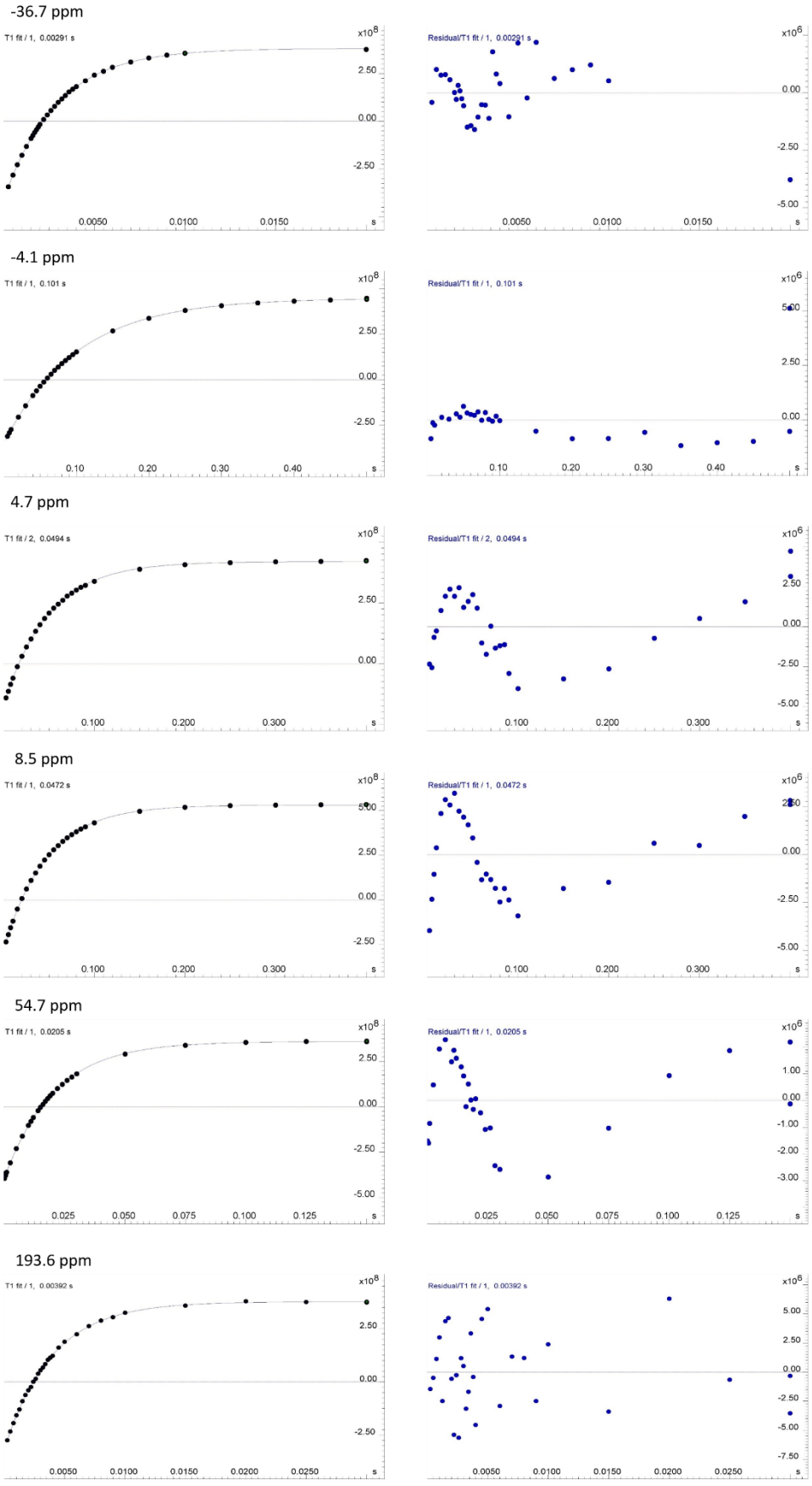

Figure S7. T_1 measurements for each signal in the paramagnetic ^{1}H NMR spectrum of [**1**](OTf)$_8$ in CD_3CN at 298 K.

3 Host-Guest Complexes with Cage 1

In a glovebox, 10-15 equivalents of the guest were added to a 2 mM solution of cage **1** in CD_3CN (0.5 mL) and the solution was transferred to a J Young NMR tube, sealed and left to equilibrate at 298 K. Paramagnetic ^1H NMR spectra were recorded over time and equilibration occurred in less than 4 hours. In some cases, signals corresponding to cage protons *f* and *g* were broadened into the baseline or obscured by resonances of excess non-encapsulated guest.

3.1 Comparison of Host-Guest Complexes

The paramagnetic Fe^{II} centers in cage **1** enabled the sensitive detection of guest encapsulation by ^1H NMR spectroscopy *via* two mechanisms. First, paramagnetism reduces the T_1 relaxation times of the guest and cage nuclei, allowing more scans in comparison with a diamagnetic analog to be recorded over the same time by reducing the acquisition time and relaxation delay.[7] Second, as noted by Ward,[8] paramagnetism also enhances the observation of host-guest complexes because the NMR signals are spread over a wider chemical shift range, thus reducing signal overlap and improving dispersion upon encapsulation.

Signals for the encapsulated guest were observed in all cases between -10 and -20 ppm and T_1 values were measured for signals having sufficient intensity (Table S2). Their values were of a similar magnitude to the T_1 value for proton *h* and reflect the isotropic shifts experienced by the guests within the paramagnetic host cavity.

3.1.1 Guest Signal Chemical Shifts and T_1 Measurements

Table S2. T_1 values for guest signals for host-guest complexes with cage **1**

Guest	Chemical shift/ppm	Measured T_1/ms
adamantane	-17.1	116
	-20.1	101
1-fluoroadamantane	-16.9	99.3
	-17.3	104
	-20.0	87.2
ferrocene	-15.2	376
cyclohexane	-18.4	405
cis-decalin	-16.7	[a]
	-17.8	190
	-18.7	[a]
trans-decalin	-15.7	[a]
	-16.9	[a]
	-17.0	[a]
	-17.6	[a]
	-17.7	[a]
	-18.6	[a]
	-18.8	[a]
	-19.5	[a]
	-19.6	[a]
benzene	-12.6	~274[b]
toluene	-12.6	[a]
	-12.7	[a]
	-12.9	[a]
	-16.9	[a]
R-limonene	[a]	[a]
o-xylene	-12.4	[a]
	-12.7	[a]
	-17.0	203
m-xylene	[c]	[c]
p-xylene	[c]	[c]

[a] Could not be accurately determined due to the multiple peaks and low signal intensity. [b] Could not be determined accurately as there was poor agreement between the experimental data and model. [c] Could not be determined as the host-guest complex forms in trace quantities.

3.1.2 Paramagnetic ^{1}H NMR Spectra

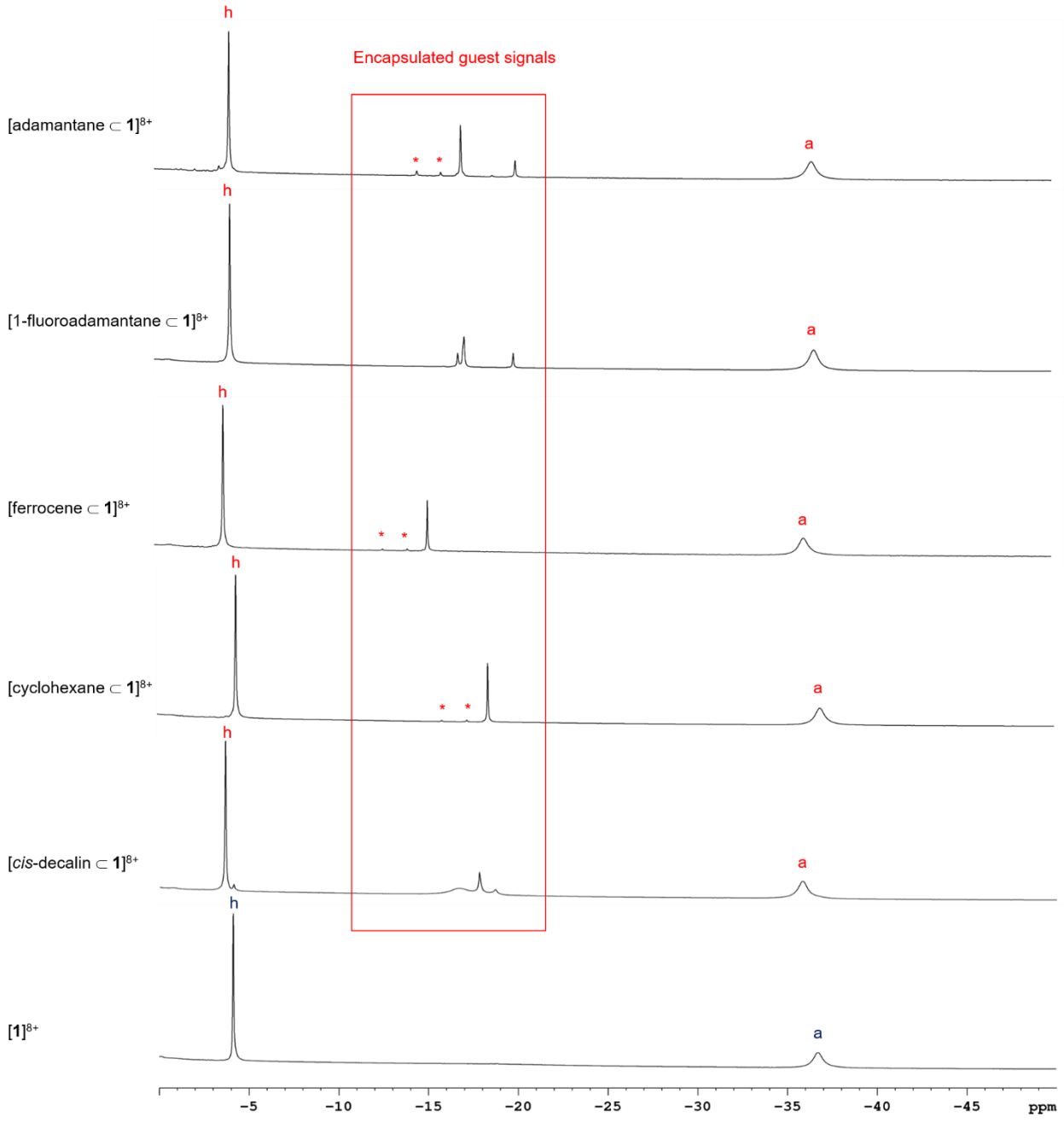

Figure S8. Comparison of NMR spectra for the host-guest complexes with strongly bound guests in CD_3CN at 298 K. Red labels refer to [guest ⊂ **1**](OTf)$_8$ and blue labels refer to empty cage **1**. Signals marked with * are attributed to encapsulation of trace impurities present in the sample of the guest.

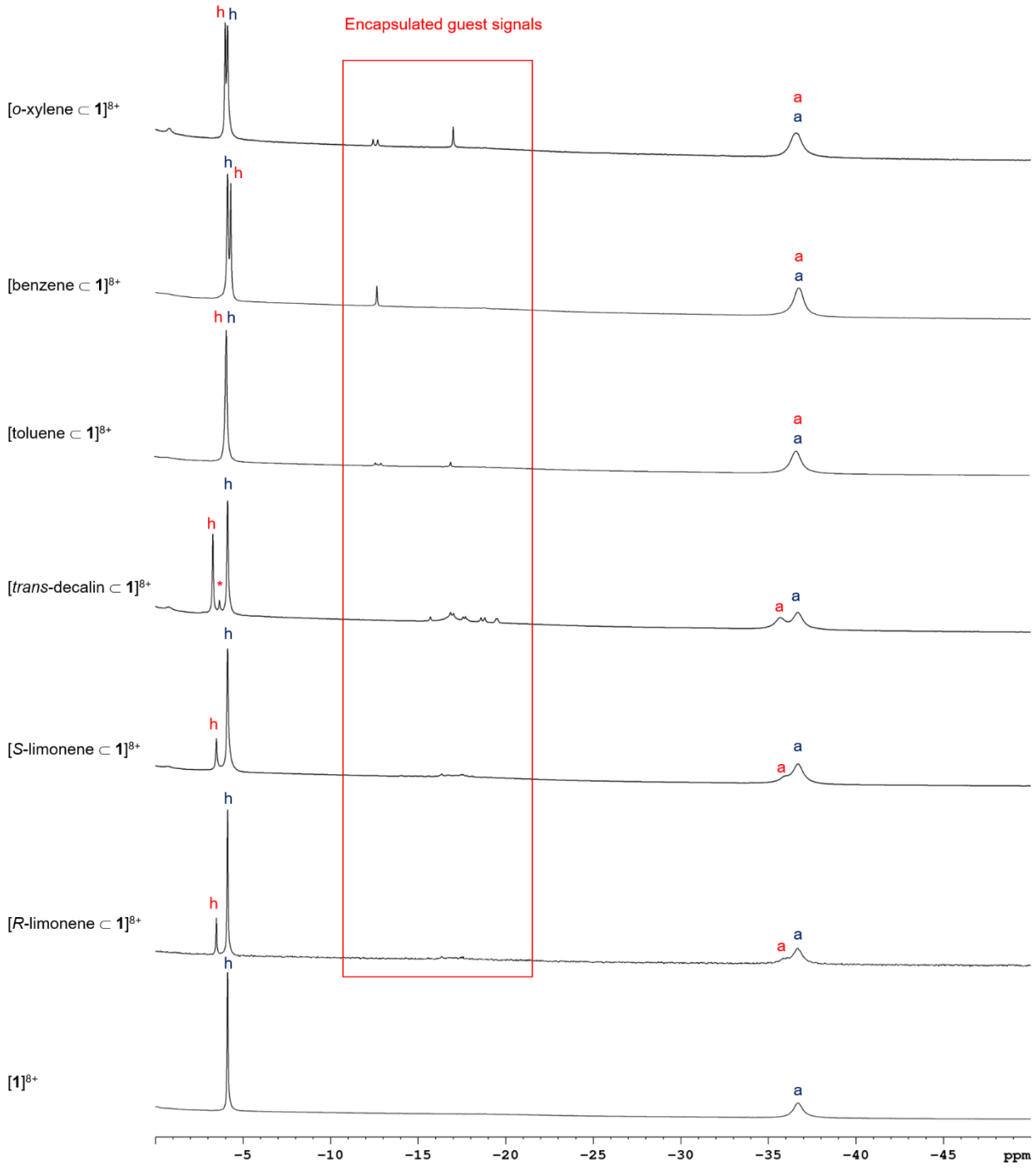

Figure S9. Comparison of NMR spectra for the host-guest complexes with weakly bound guests in CD_3CN at 298 K. Red labels refer to [guest ⊂ **1**](OTf)$_8$, blue labels refer to empty cage **1** and * is [*cis*-decalin ⊂ **1**]$^{8+}$.

3.1.3 GC-MS Analysis of Guest Purity

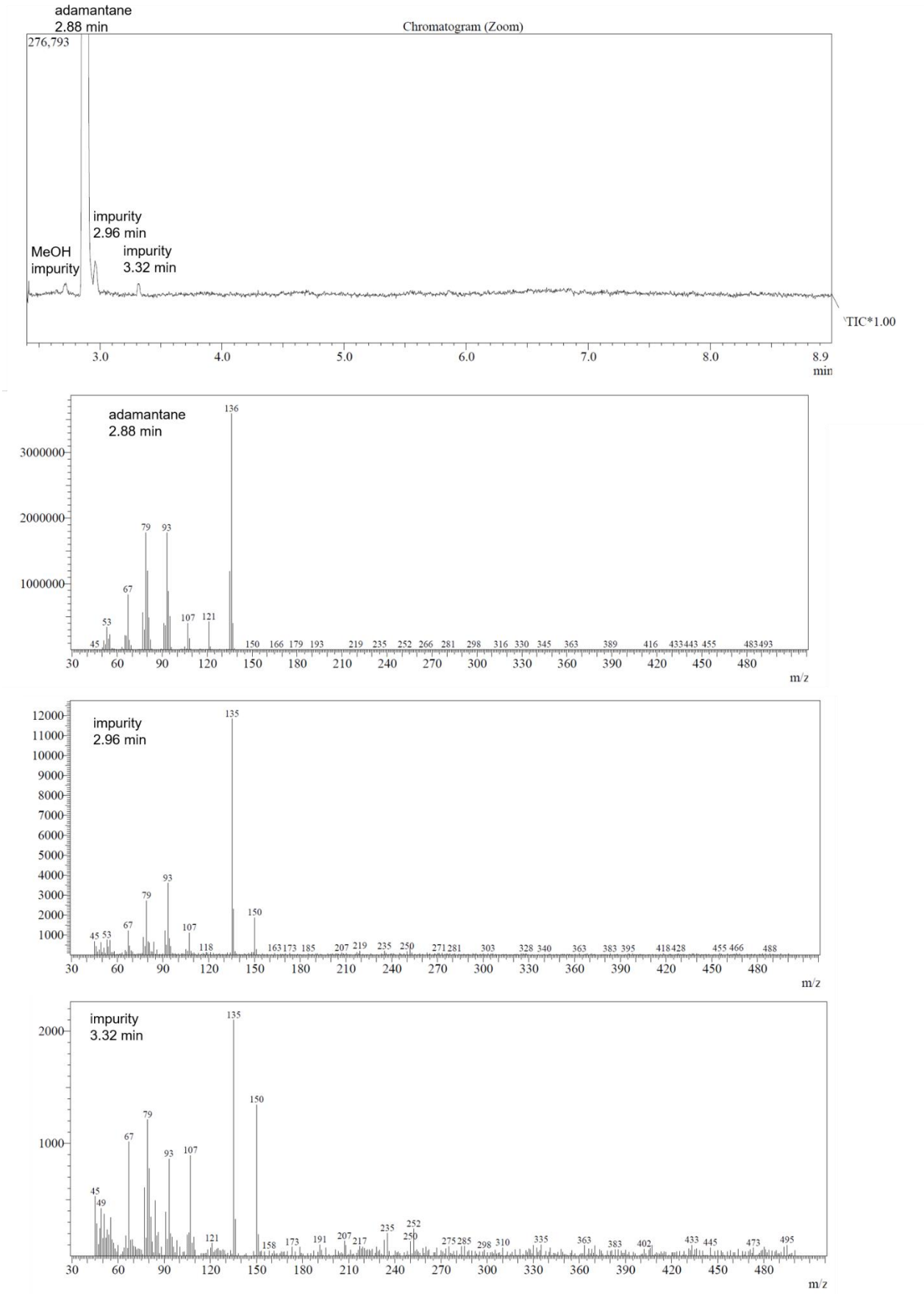

Figure S10. GC-MS chromatogram and mass spectra of adamantane.

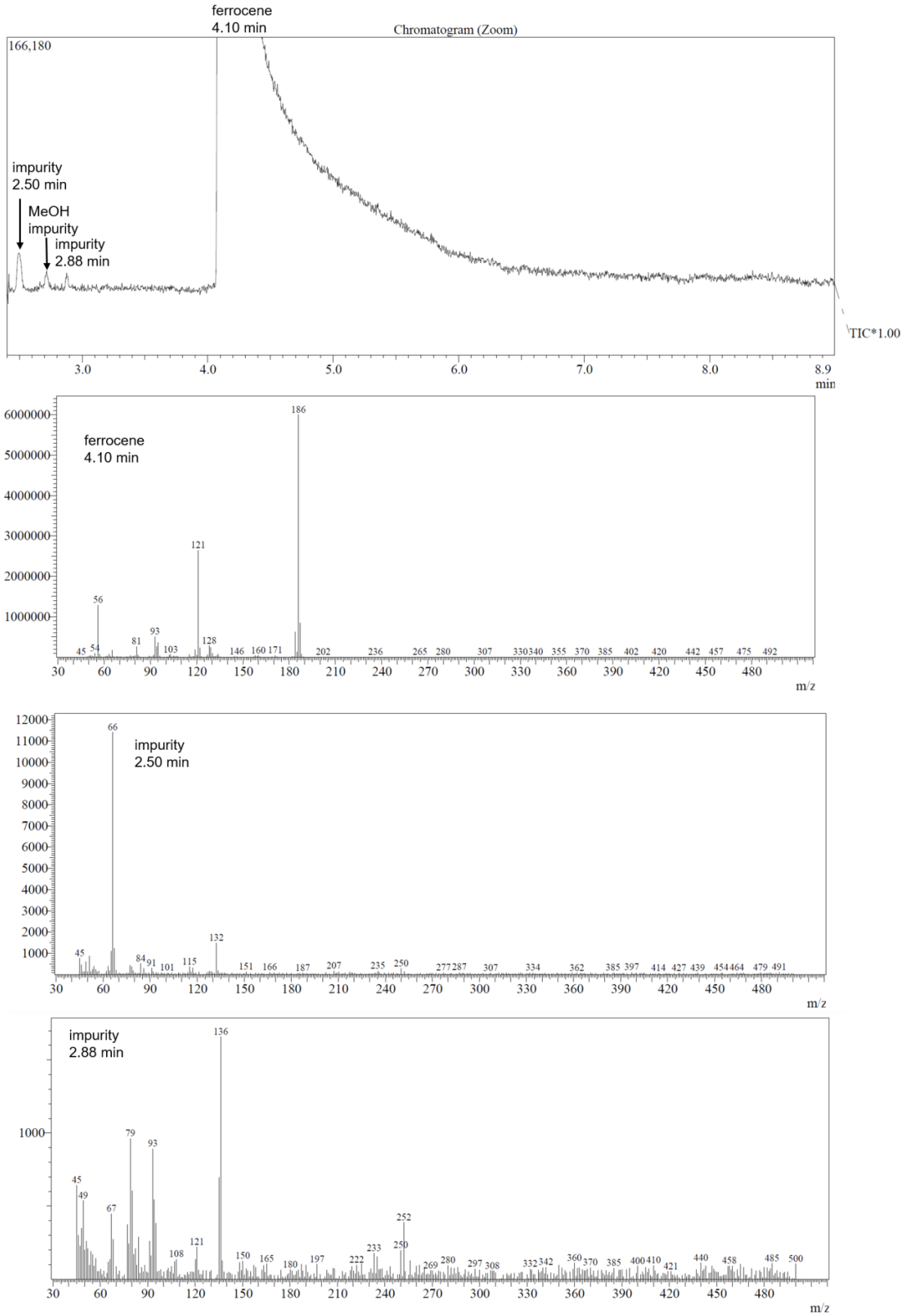

Figure S11. GC-MS chromatogram and mass spectra of ferrocene.

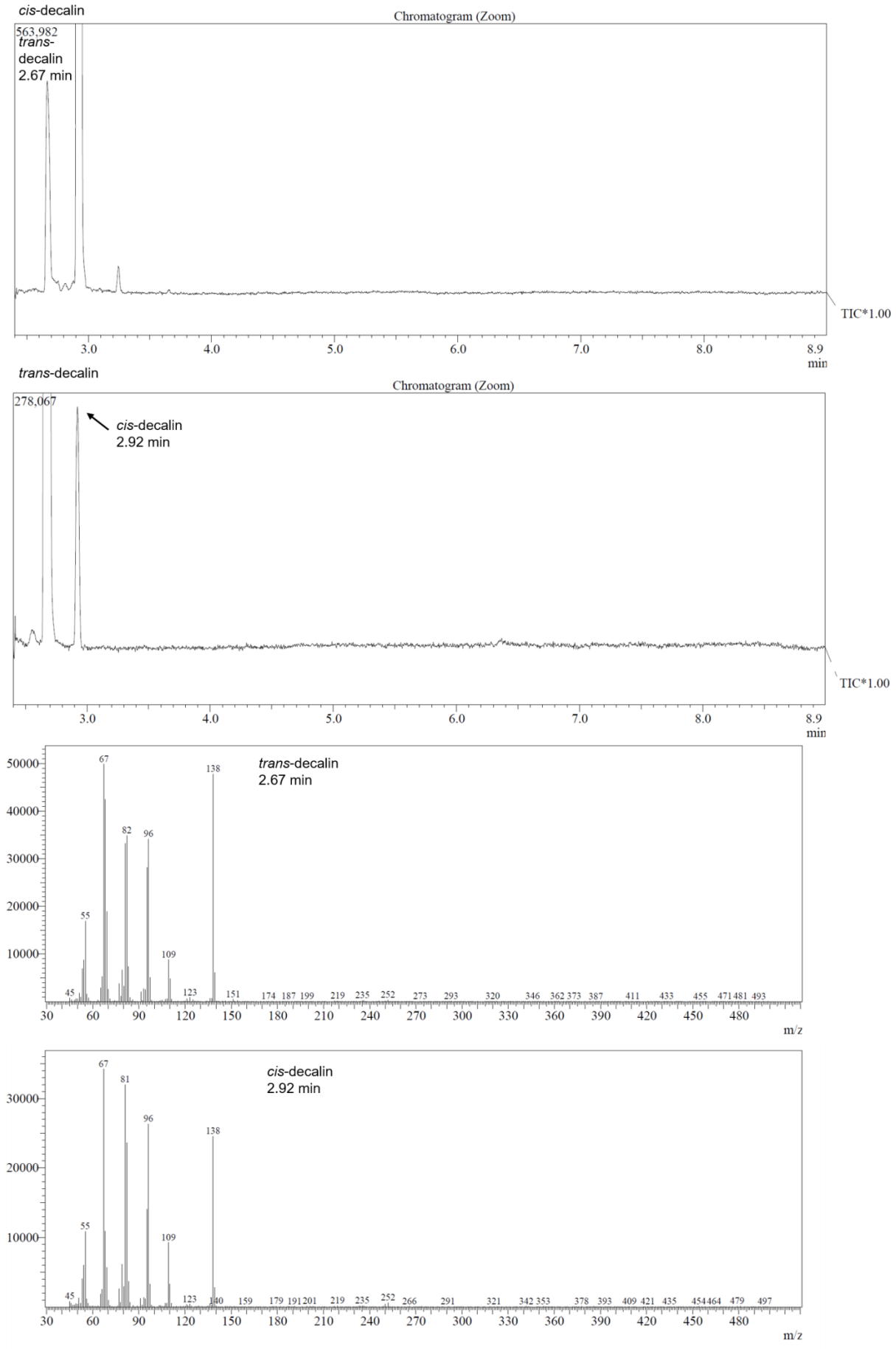

Figure S12. GC-MS chromatograms and mass spectra of *cis*- and *trans*-decalin.

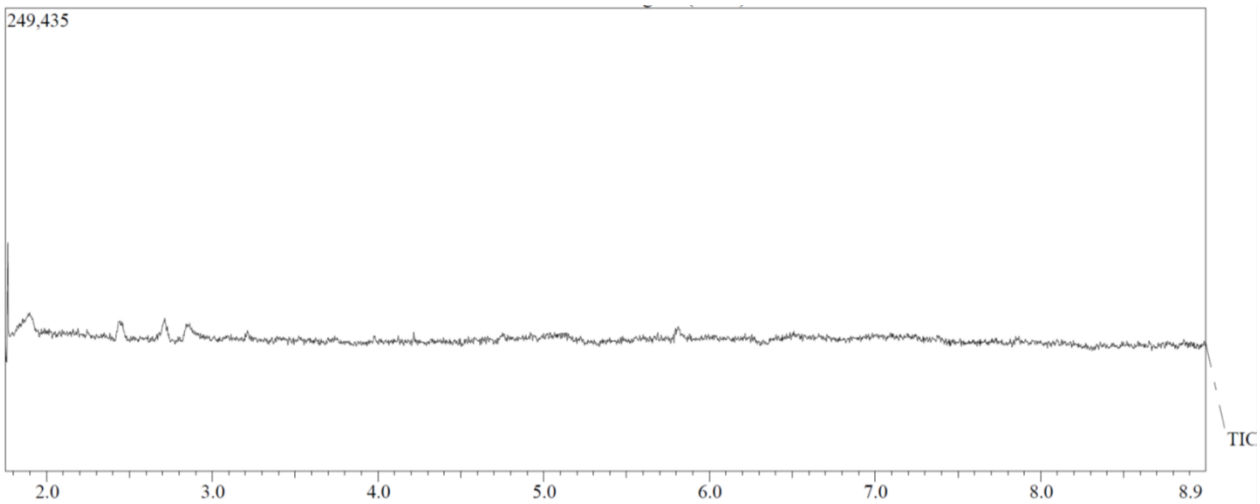

Figure S13. GC-MS chromatogram of cyclohexane.

3.2 Adamantane

^{1}H NMR (400 MHz, CD_3CN, 298 K) δ (ppm): 194.1 (H_e), 54.7 (H_b, H_d), 8.4 (H_c), -4.2 (H_h), -17.1 (H_2), -20.1 (H_1), -36.6 (H_a)

ESI-MS *m/z*: 501.6 [adamantane ⊂ **1** + OTf]$^{7+}$, 610.2 [adamantane ⊂ **1** + 2OTf]$^{6+}$, 761.7 [adamantane ⊂ **1** + 3OTf]$^{5+}$

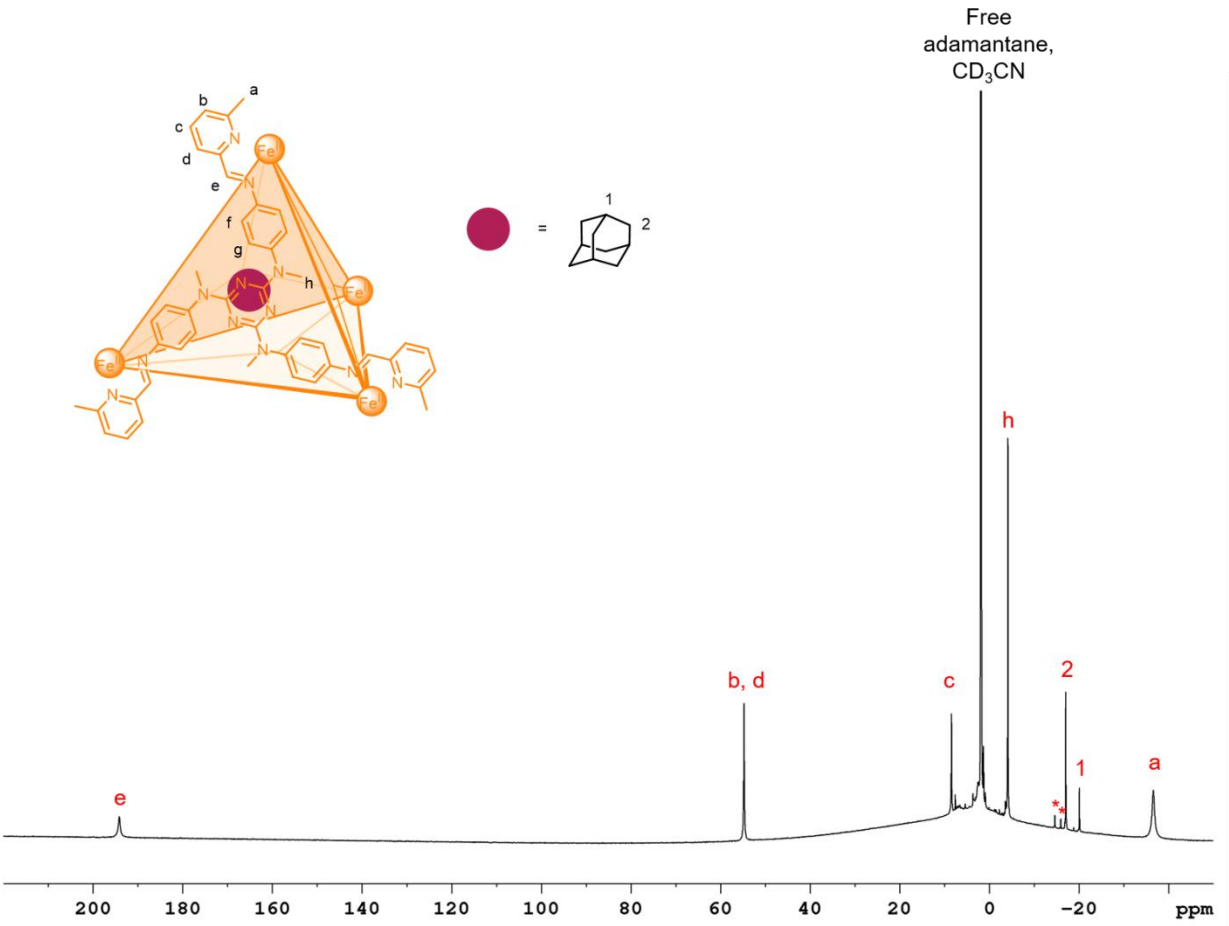

Figure S14. Paramagnetic ^{1}H NMR spectrum of [adamantane ⊂ **1**](OTf)$_8$ in CD_3CN at 298 K. Signals marked with * are attributed to encapsulation of trace impurities present in the sample of adamantane.

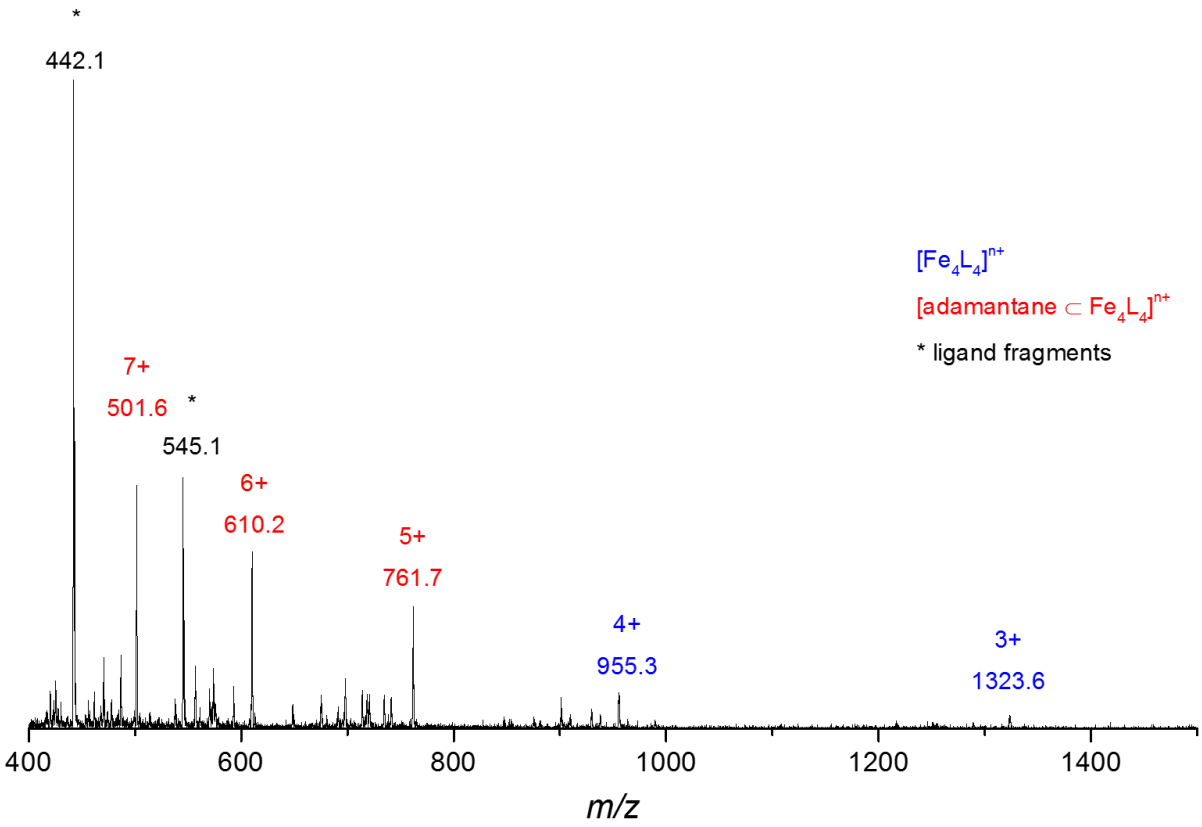

Figure S15. Low resolution ESI-mass spectrum of [adamantane ⊂ **1**](OTf)$_8$.

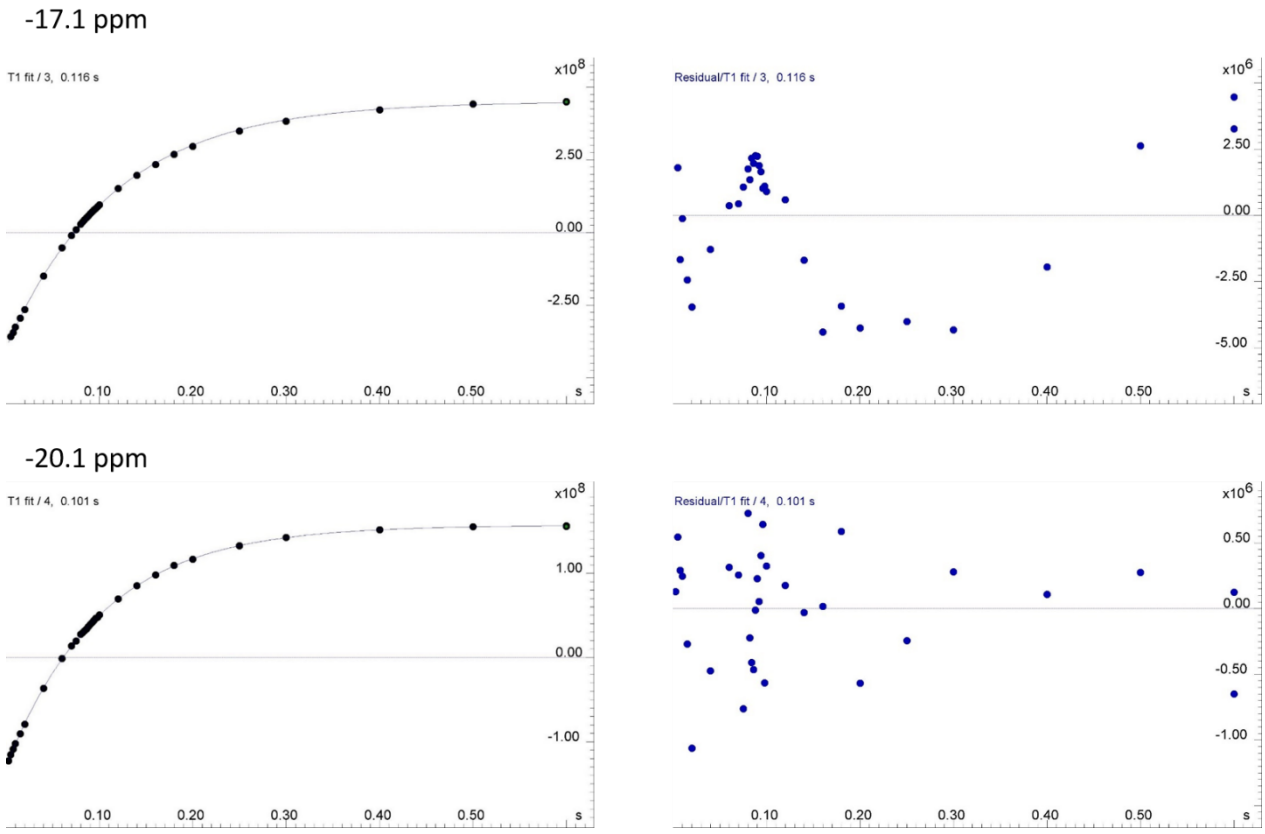

Figure S16. T_1 measurements for the encapsulated guest signals at -17.1 ppm and -20.1 ppm for [adamantane ⊂ **1**](OTf)$_8$ in CD_3CN at 298 K.

3.3 1-Fluoroadamantane

^{1}H NMR (400 MHz, CD_3CN, 298 K) δ (ppm): 193.6 (H_e), 54.7 (H_b, H_d), 8.5 (H_c), -4.2 (H_h), -16.9 (encapsulated 1-fluoroadamantane), -17.3 (encapsulated 1-fluoroadamantane), -20.0 (encapsulated 1-fluoroadamantane), -36.8 (H_a)

^{19}F NMR (376 MHz, CD_3CN, 298 K, referenced to C_6F_6) δ (ppm): -77.4 (OTf^-), -127.7 (free 1-fluoroadamantane), -145.9 (encapsulated 1-fluoroadamantane)

ESI-MS *m/z*: 504.3 [1-fluoroadamantane ⊂ **1** + OTf]$^{7+}$, 613.3 [1-fluoroadamantane ⊂ **1** + 2OTf]$^{6+}$, 765.5 [1-fluoroadamantane ⊂ **1** + 3OTf]$^{5+}$, 994.5 [1-fluoroadamantane ⊂ **1** + 4OTf]$^{4+}$, 1375.5 [1-fluoroadamantane ⊂ **1** + 5OTf]$^{3+}$

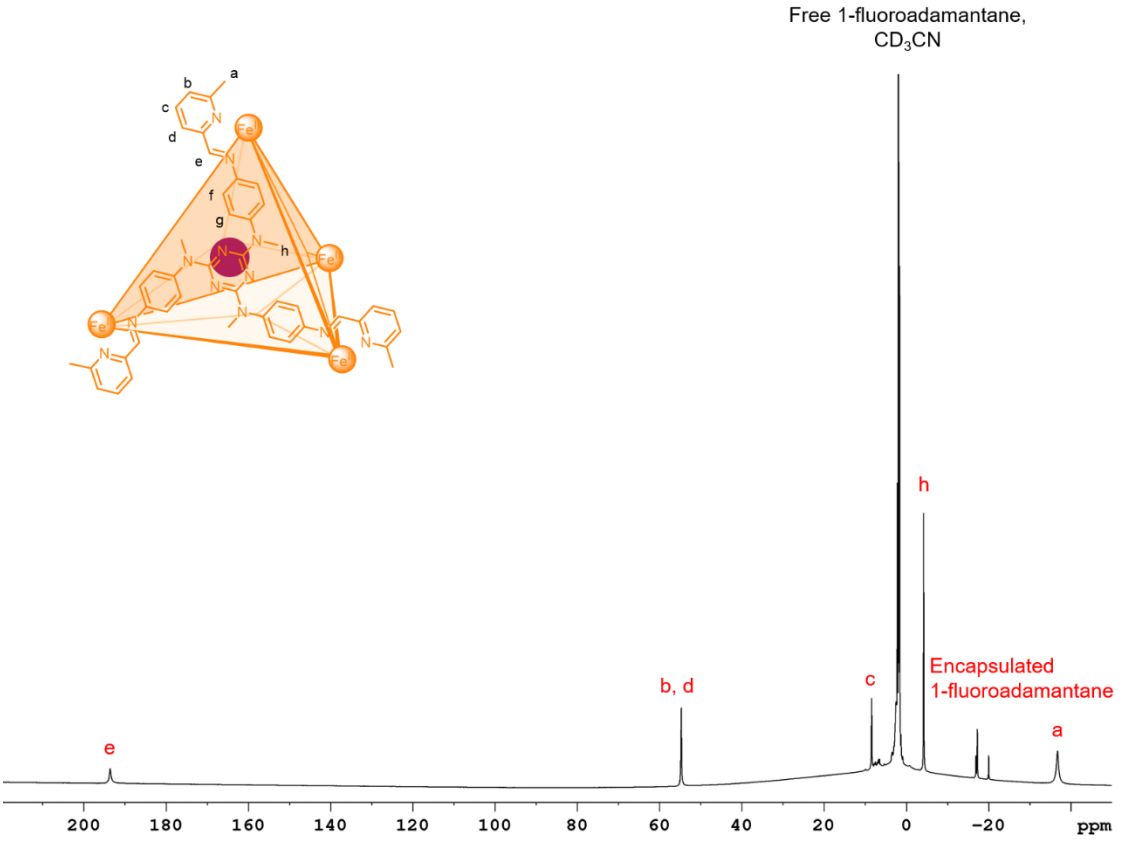

Figure S17. Paramagnetic ^{1}H NMR spectrum of [1-fluoroadamantane ⊂ **1**](OTf)$_8$ in CD_3CN at 298 K.

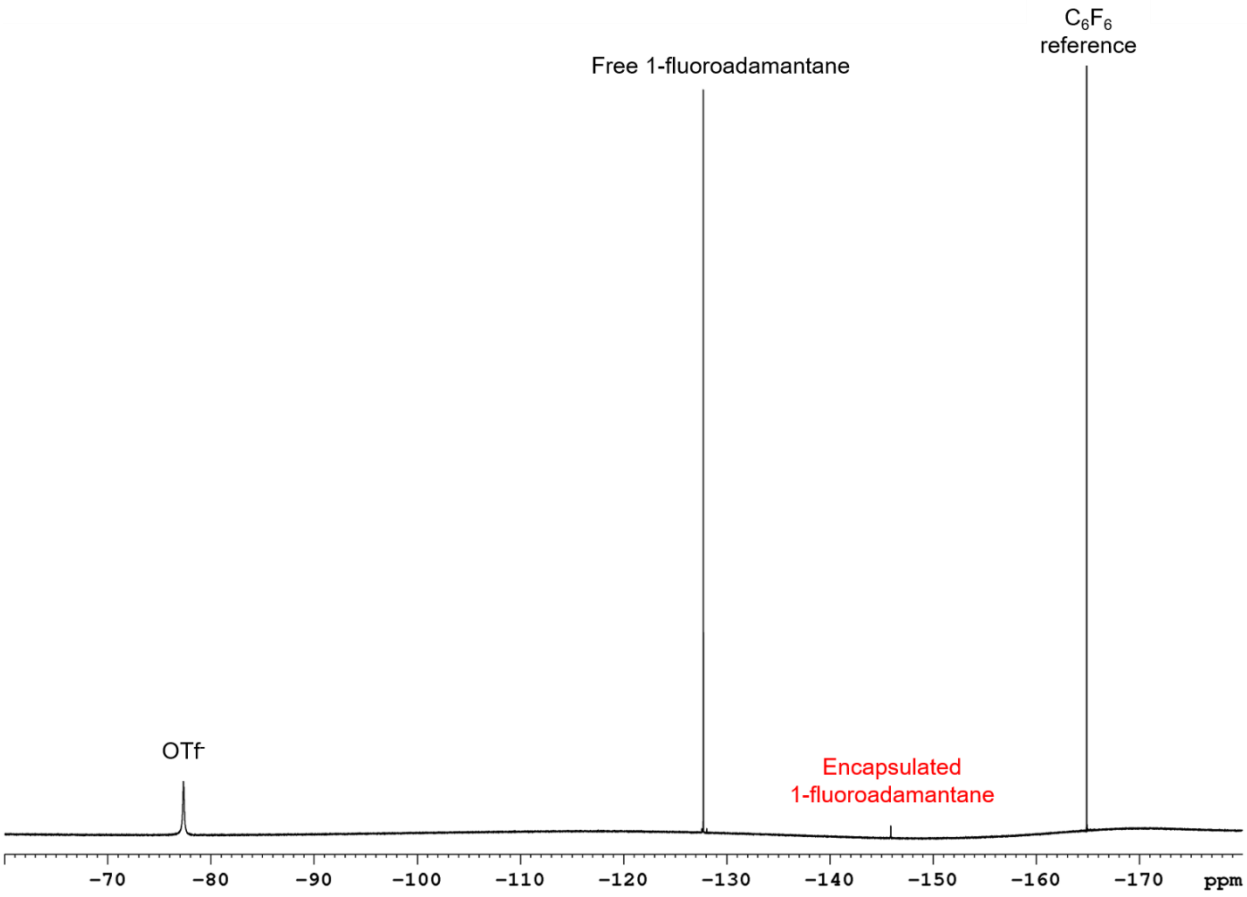

Figure S18. ^{19}F NMR spectrum of [1-fluoroadamantane ⊂ **1**](OTf)$_8$ in CD_3CN at 298 K.

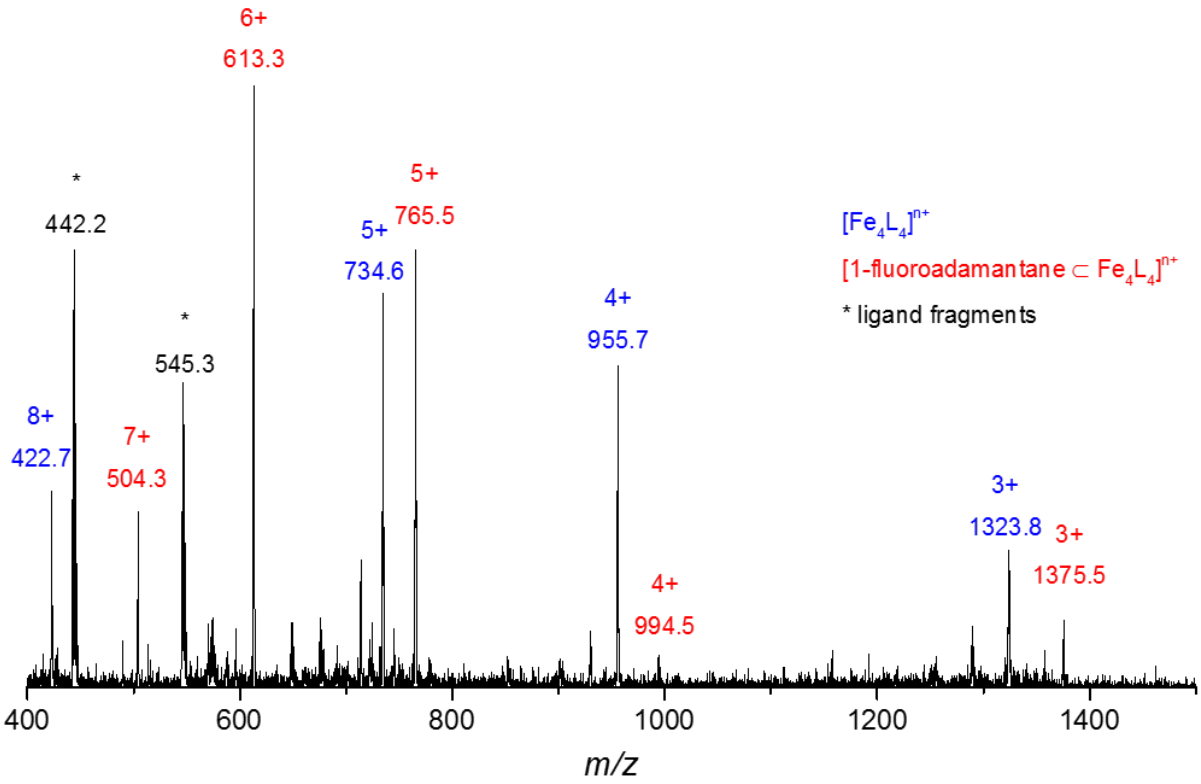

Figure S19. Low resolution ESI-mass spectrum of [1-fluoroadamantane ⊂ **1**](OTf)$_8$.

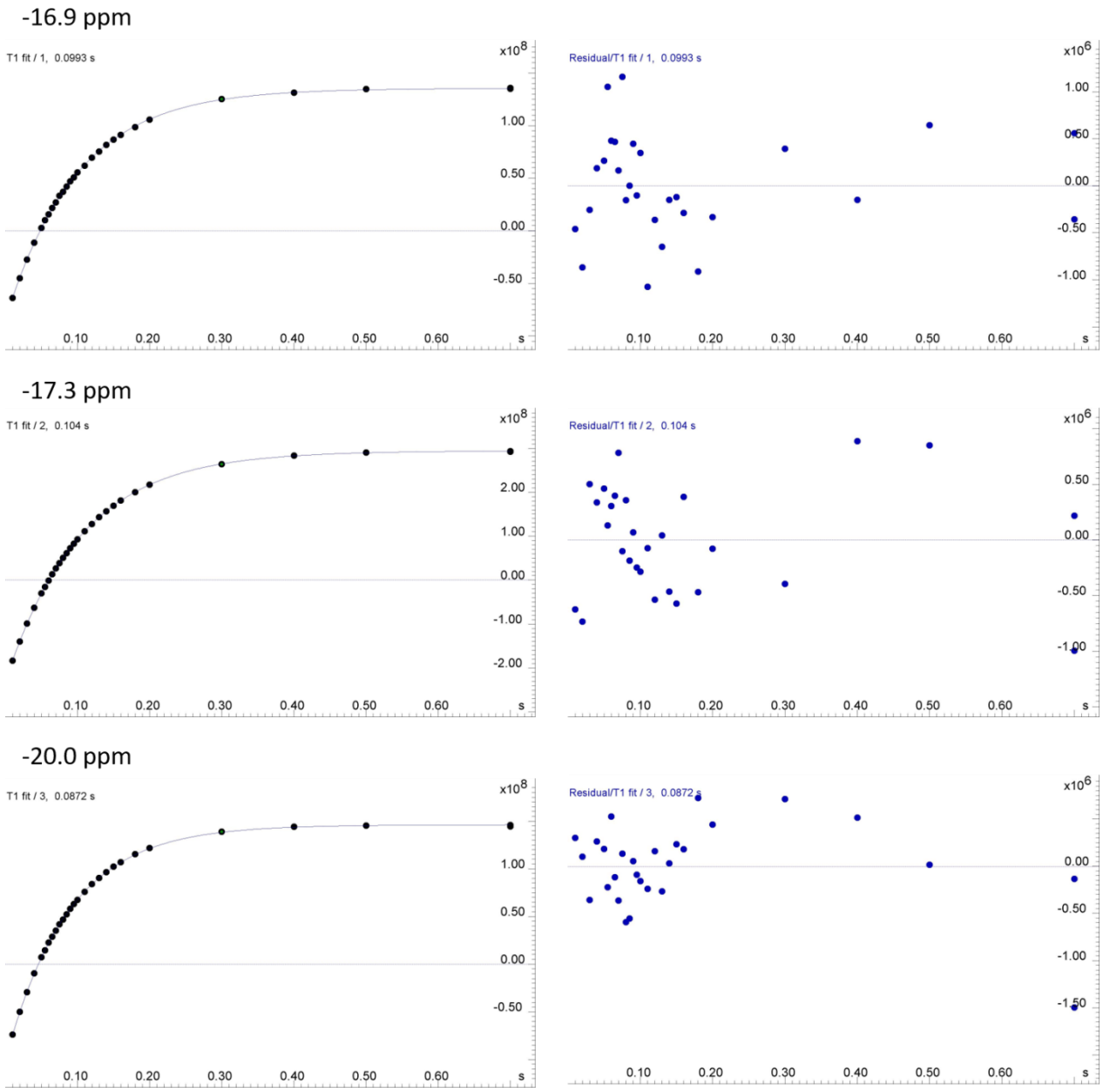

Figure S20. T_1 measurements for the encapsulated guest signals at -16.9, -17.3 ppm and -20.0 ppm for [1-fluoroadamantane ⊂ **1**](OTf)$_8$ in CD_3CN at 298 K.

3.4 Ferrocene

^{1}H NMR (400 MHz, CD_3CN, 298 K) δ (ppm): 193.8 (H_e), 54.8 ($H_{b/d}$), 54.6 ($H_{b/d}$), 8.4 (H_c), 5.2 (H_g), -3.8 (H_h), -15.2 (H_1), -36.2 (H_a)

ESI-MS *m/z*: 508.8 [ferrocene ⊂ **1** + OTf]$^{7+}$, 618.5 [ferrocene ⊂ **1** + 2OTf]$^{6+}$, 772.0 [ferrocene ⊂ **1** + 3OTf]$^{5+}$, 1002.3 [ferrocene ⊂ **1** + 4OTf]$^{4+}$

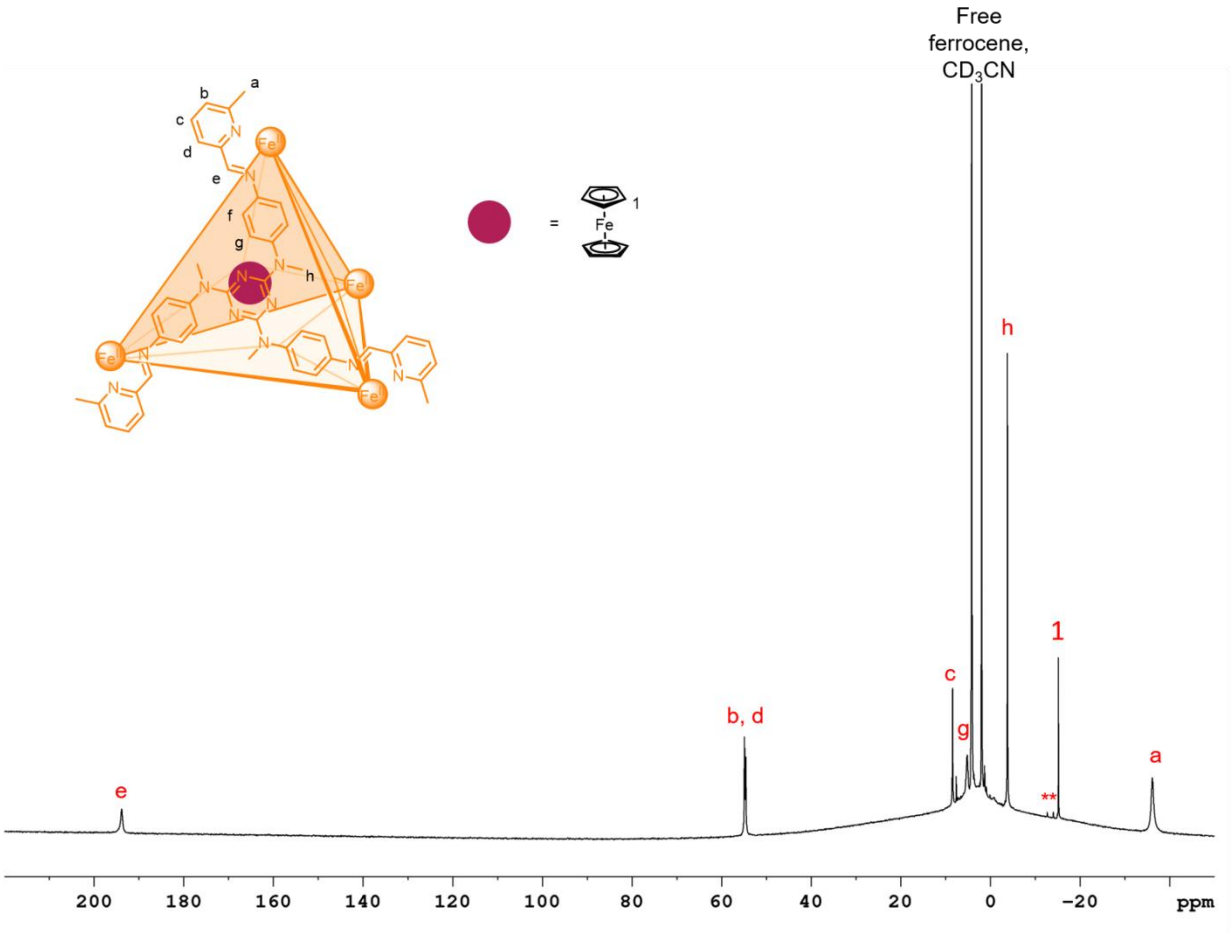

Figure S21. Paramagnetic ^{1}H NMR spectrum of [ferrocene ⊂ **1**](OTf)$_8$ in CD_3CN at 298 K. Signals marked with * are attributed to encapsulation of trace impurities present in the sample of ferrocene.

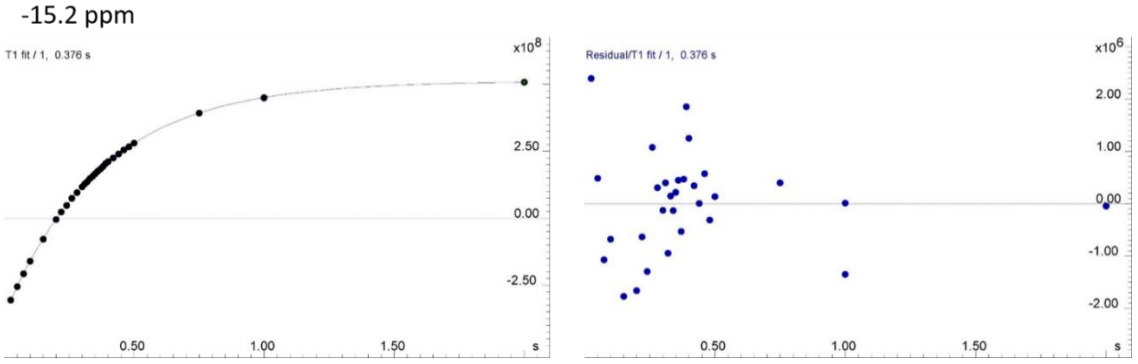

Figure S22. T_1 measurements for the encapsulated guest signal at -15.2 ppm for [ferrocene ⊂ **1**](OTf)$_8$ in CD_3CN at 298 K.

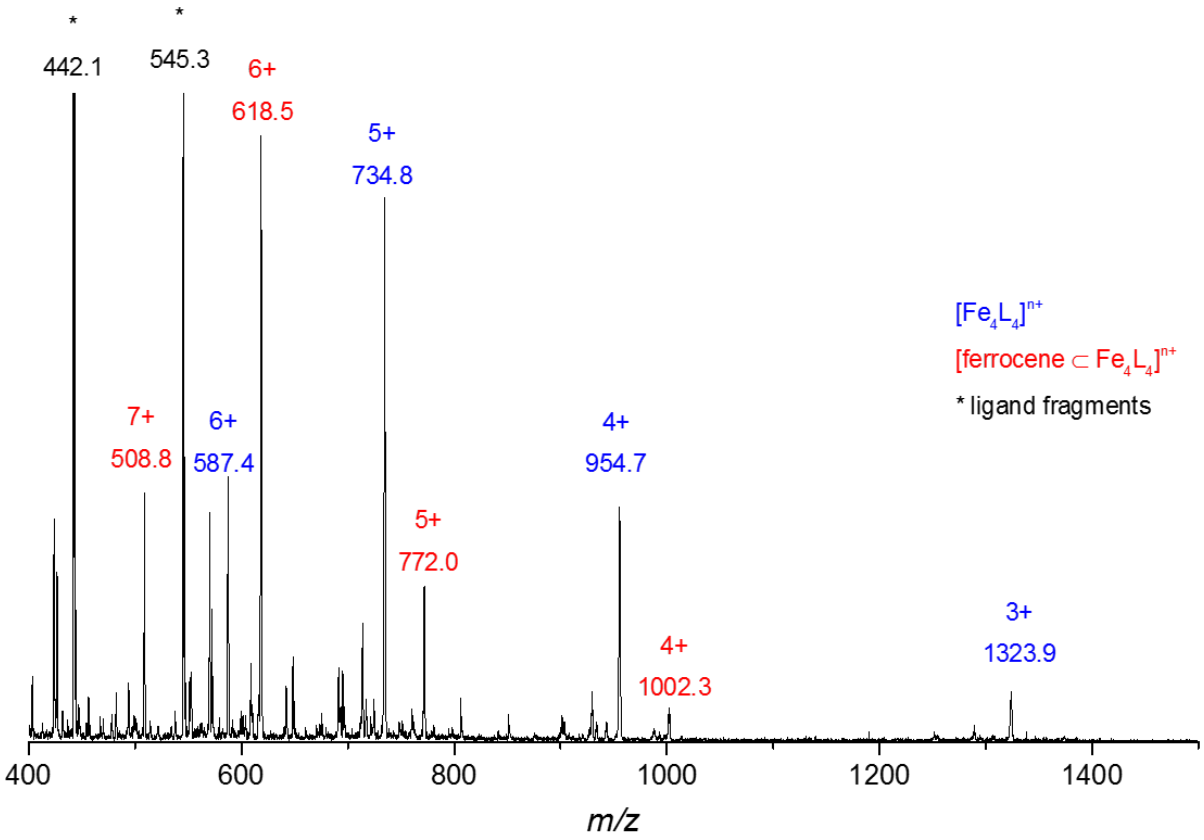

Figure S23. Low resolution ESI-mass spectrum of [ferrocene ⊂ **1**](OTf)$_8$.

3.5 Cyclohexane

^{1}H NMR (400 MHz, CD_3CN, 298 K) δ (ppm): 193.6 (H_e), 54.9 ($H_{b/d}$), 54.6 ($H_{b/d}$), 8.5 (H_c), -4.4 (H_h), -18.4 (encapsulated cyclohexane, H_1), -36.9 (H_a)

ESI-MS *m/z*: 601.6 [cyclohexane ⊂ **1** + 2OTf]$^{6+}$

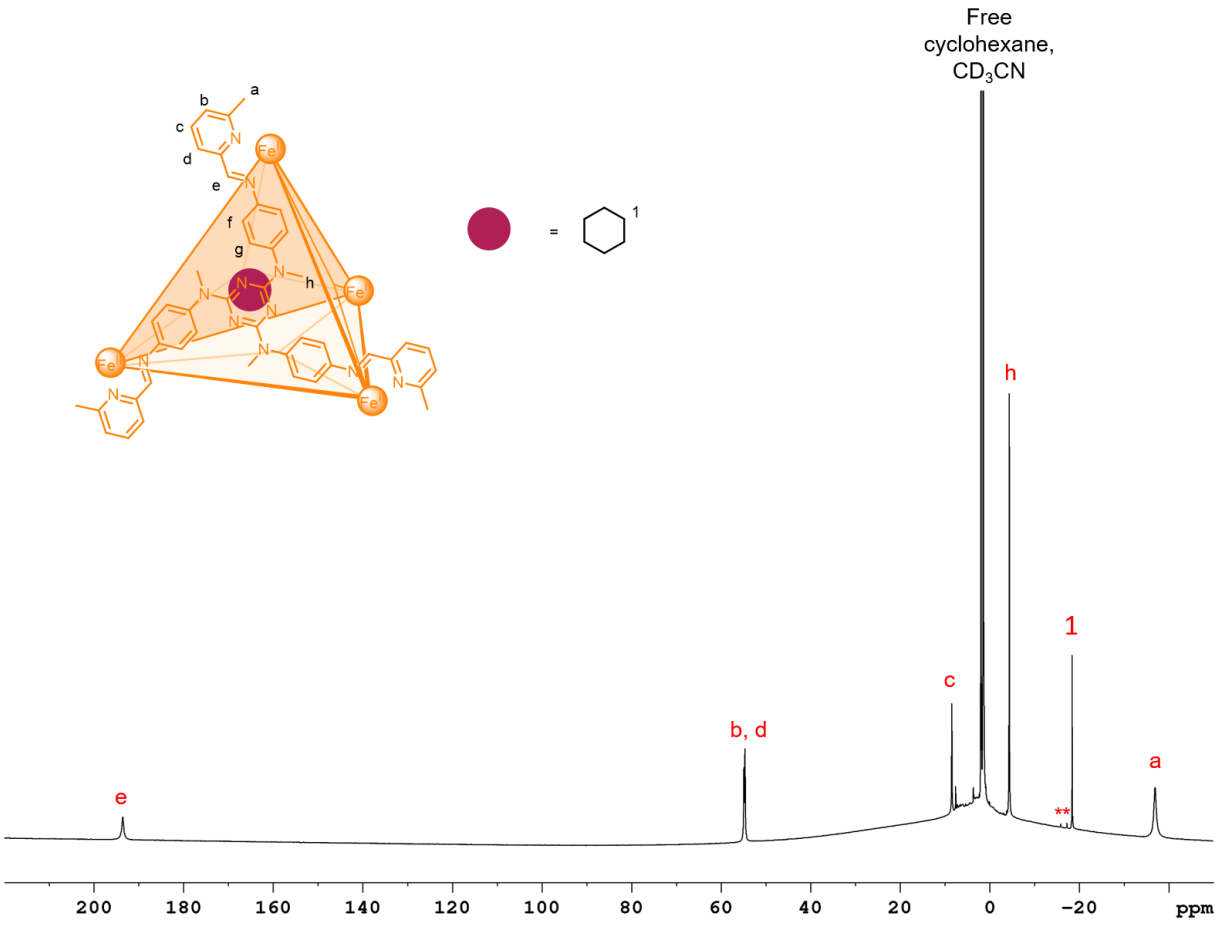

Figure S24. Paramagnetic ^{1}H NMR spectrum of [cyclohexane ⊂ **1**](OTf)$_8$ in CD_3CN at 298 K. Signals marked with * are attributed to encapsulation of trace impurities present in the sample of cyclohexane.

-18.4 ppm

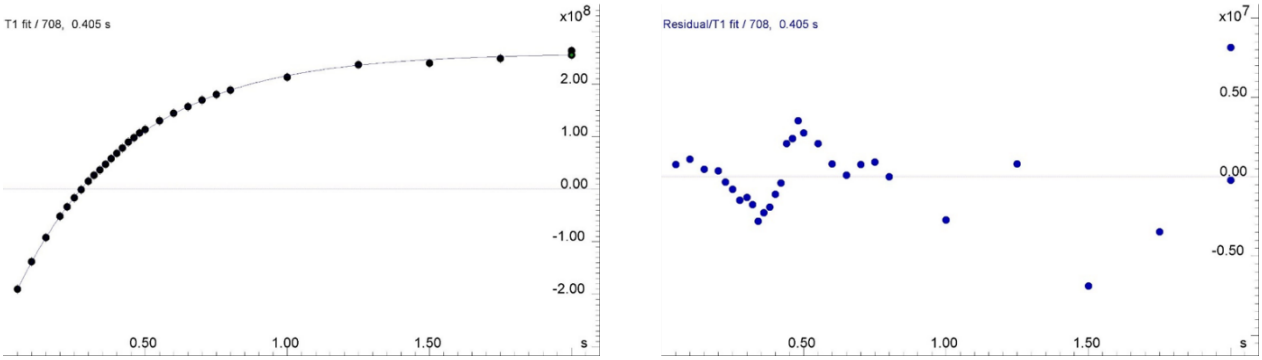

Figure S25. T_1 measurements for the encapsulated guest signal at -18.4 ppm for [cyclohexane ⊂ **1**](OTf)$_8$ in CD_3CN at 298 K.

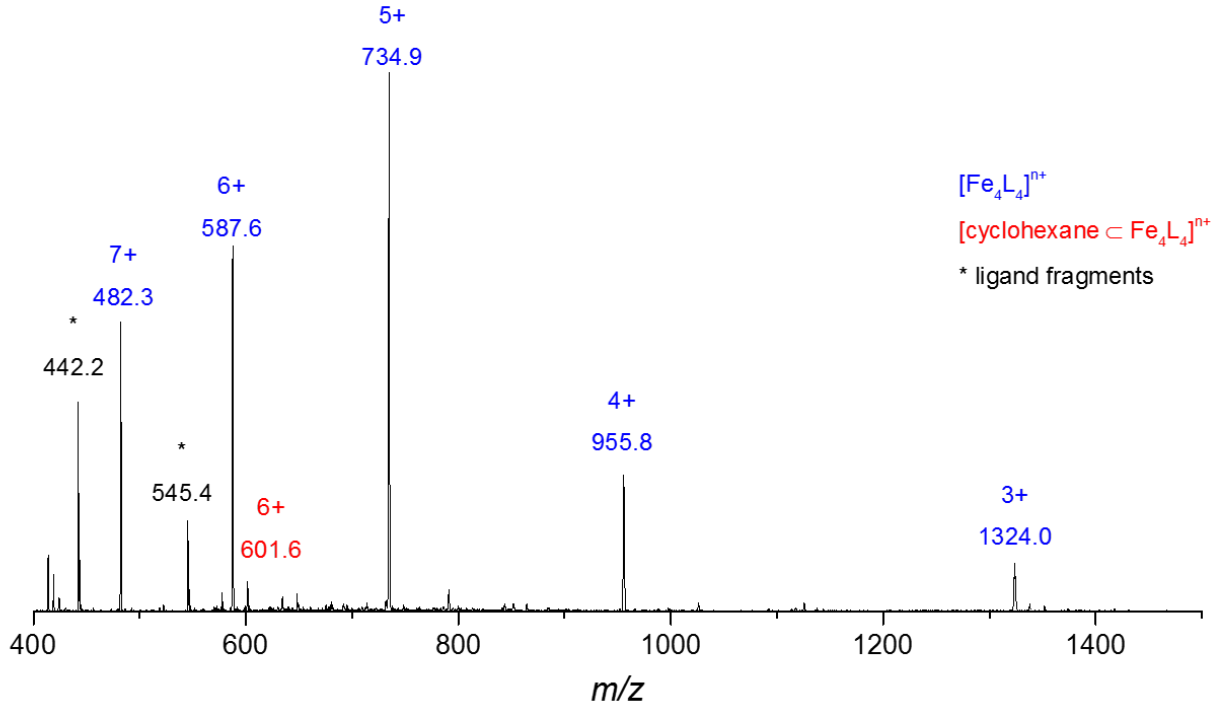

Figure S26. Low resolution ESI-mass spectrum of [cyclohexane ⊂ **1**](OTf)$_8$.

3.6 *cis*-Decalin

^{1}H NMR (400 MHz, CD_3CN, 298 K) δ (ppm): 193.1 (H_e), 54.9 ($H_{b/d}$), 54.5 ($H_{b/d}$), 8.4 (H_c), 5.5 (H_g), -3.7 (H_h), -16.7 (encapsulated *cis*-decalin), -17.8 (encapsulated *cis*-decalin), -18.7 (encapsulated *cis*-decalin), -35.9 (H_a)

ESI-MS *m/z*: 502.0 [*cis*-decalin ⊂ **1** + OTf]$^{7+}$, 610.3 [*cis*-decalin ⊂ **1** + 2OTf]$^{6+}$

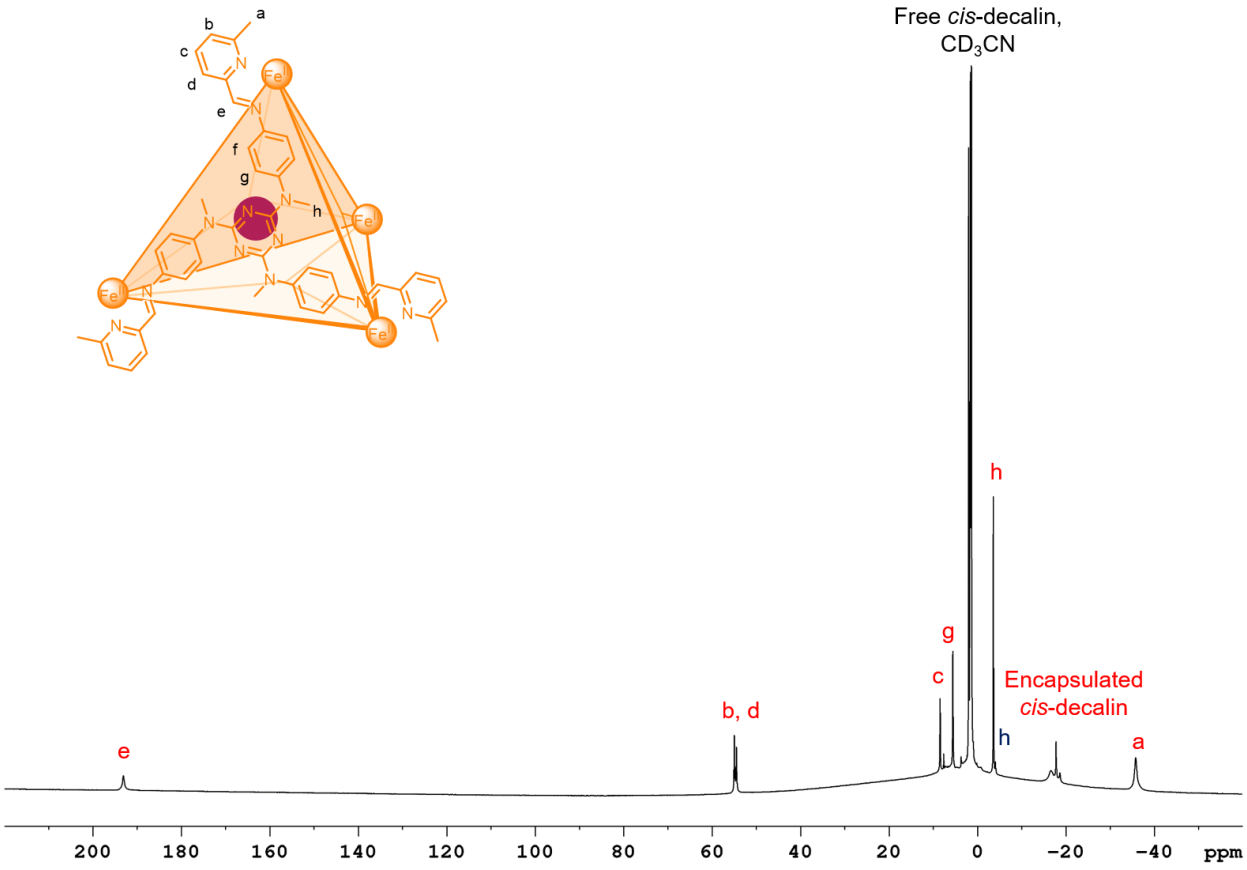

Figure S27. Paramagnetic ^{1}H NMR spectrum of [*cis*-decalin ⊂ **1**](OTf)$_8$ in CD_3CN at 298 K. Red labels refer to [*cis*-decalin ⊂ **1**](OTf)$_8$, blue labels refer to empty cage **1**.

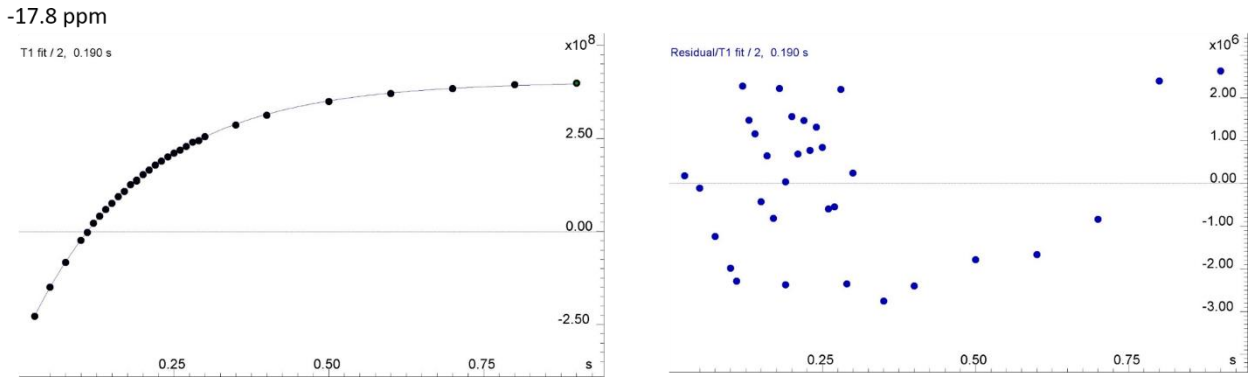

Figure S28. T_1 measurements for the encapsulated guest signal at -17.8 ppm for [*cis*-decalin ⊂ **1**](OTf)$_8$ in CD_3CN at 298 K.

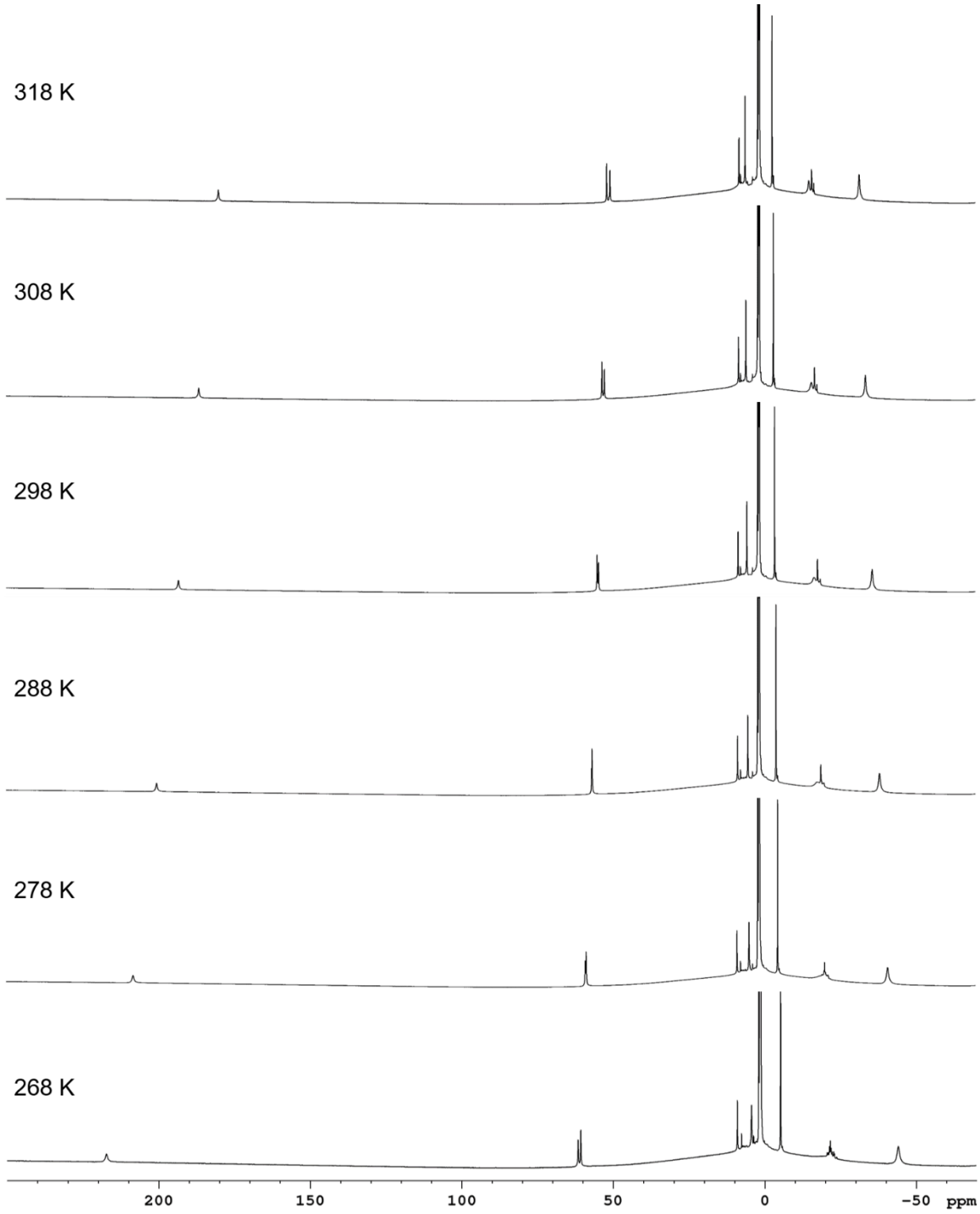

Figure S29. Variable temperature paramagnetic ^{1}H NMR spectra of [*cis*-decalin ⊂ **1**](OTf)$_8$ in CD_3CN.

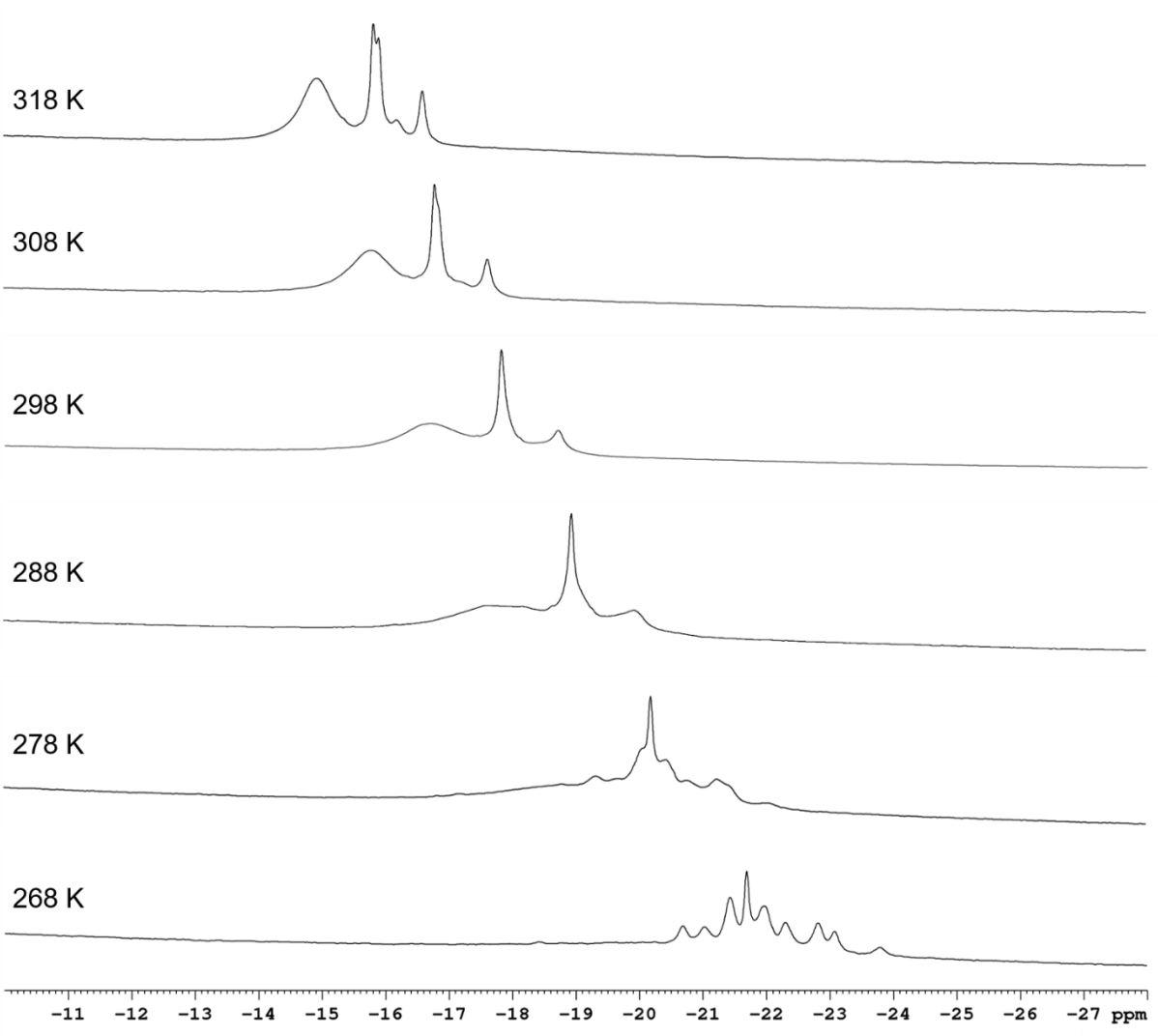

Figure S30. Variable temperature paramagnetic ^{1}H NMR spectra of [*cis*-decalin ⊂ **1**](OTf)$_8$ in CD_3CN showing the *cis*-decalin guest signals. The *cis*-decalin guest peaks were broad at room temperature, and although they sharpened upon cooling to 268 K, the conformers could not be distinguished.

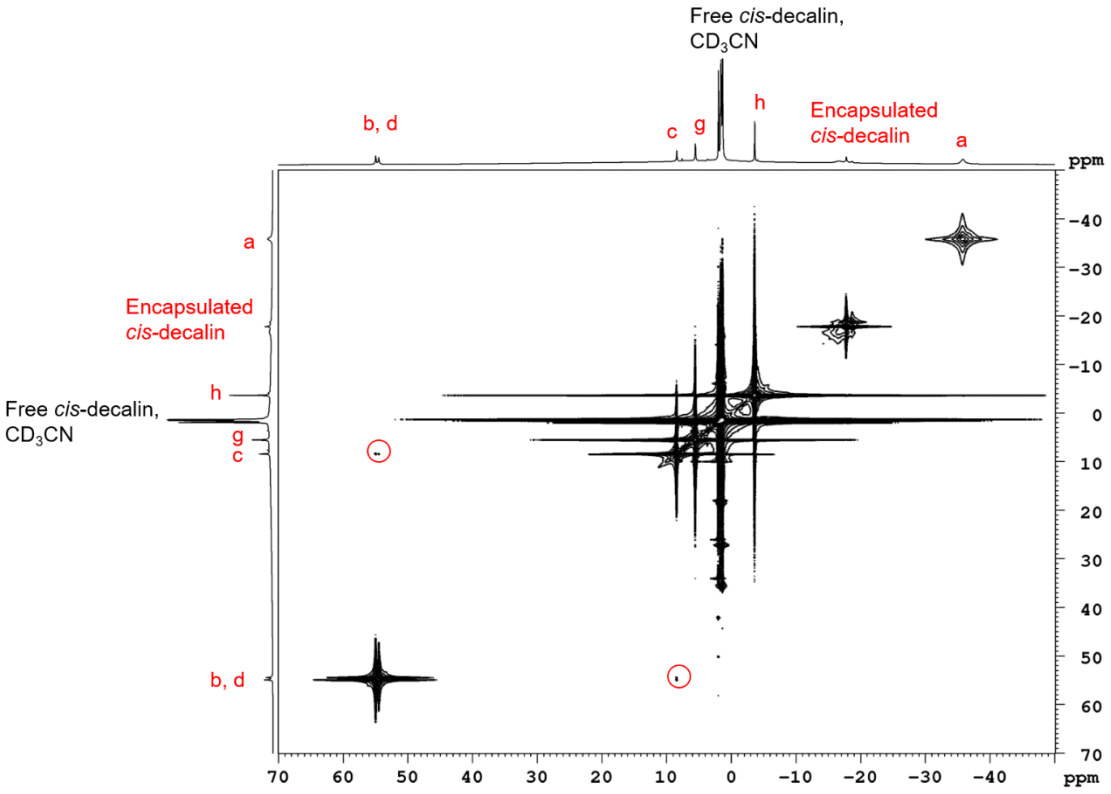

Figure S31. COSY NMR spectrum of [*cis*-decalin ⊂ **1**](OTf)$_8$ in CD_3CN at 298 K.

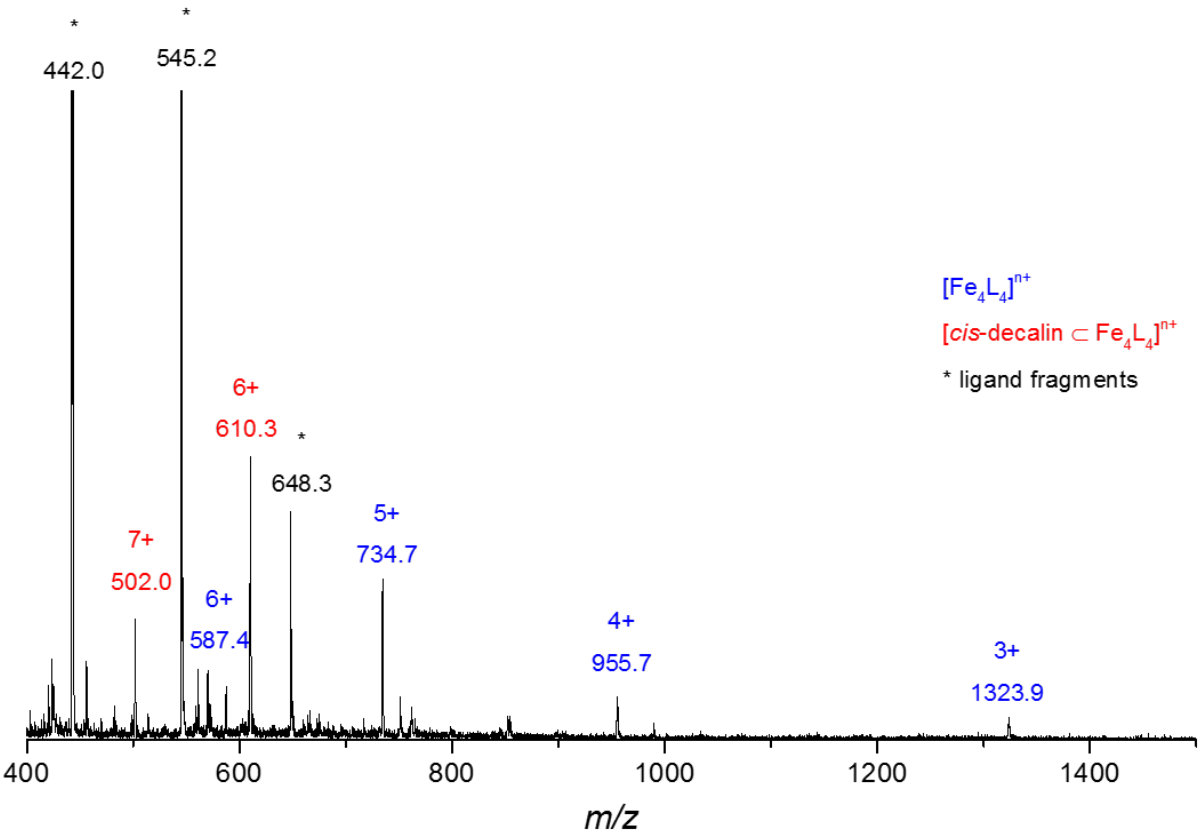

Figure S32. Low resolution ESI-mass spectrum of [*cis*-decalin ⊂ **1**](OTf)$_8$.

3.7 *trans*-Decalin

^{1}H NMR (400 MHz, CD_3CN, 298 K) δ (ppm): 193.8 (H_e), 55.1 ($H_{b/d}$), 54.5 ($H_{b/d}$), 8.4 (H_c), 5.8 (H_g), -3.3 (H_h), -15.7 (encapsulated *trans*-decalin), -16.9 (encapsulated *trans*-decalin), -17.0 (encapsulated *trans*-decalin), -17.6 (encapsulated *trans*-decalin), -17.7 (encapsulated *trans*-decalin), -18.6 (encapsulated *trans*-decalin), -18.8 (encapsulated *trans*-decalin), -19.4 (encapsulated *trans*-decalin), -19.5 (encapsulated *trans*-decalin), -35.7 (H_a)

ESI-MS *m/z*: 502.0 [*trans*-decalin ⊂ **1** + OTf]$^{7+}$, 610.5 [*trans*-decalin ⊂ **1** + 2OTf]$^{6+}$, 990.0 [*trans*-decalin ⊂ **1** + 4OTf]$^{4+}$

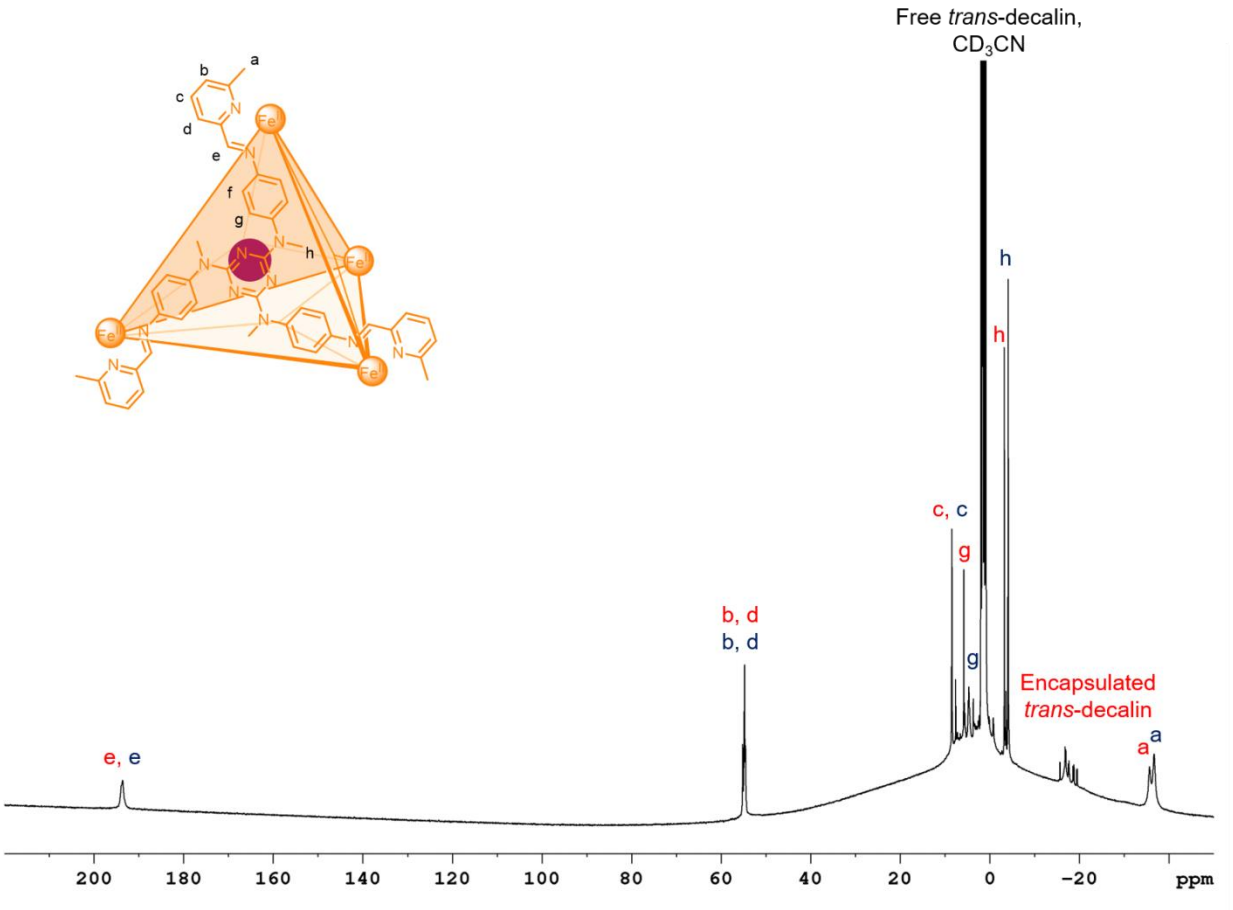

Figure S33. Paramagnetic ^{1}H NMR spectrum of [*trans*-decalin ⊂ **1**](OTf)$_8$ in CD_3CN at 298 K. Red labels refer to [*trans*-decalin ⊂ **1**](OTf)$_8$ and blue labels refer to empty cage **1**.

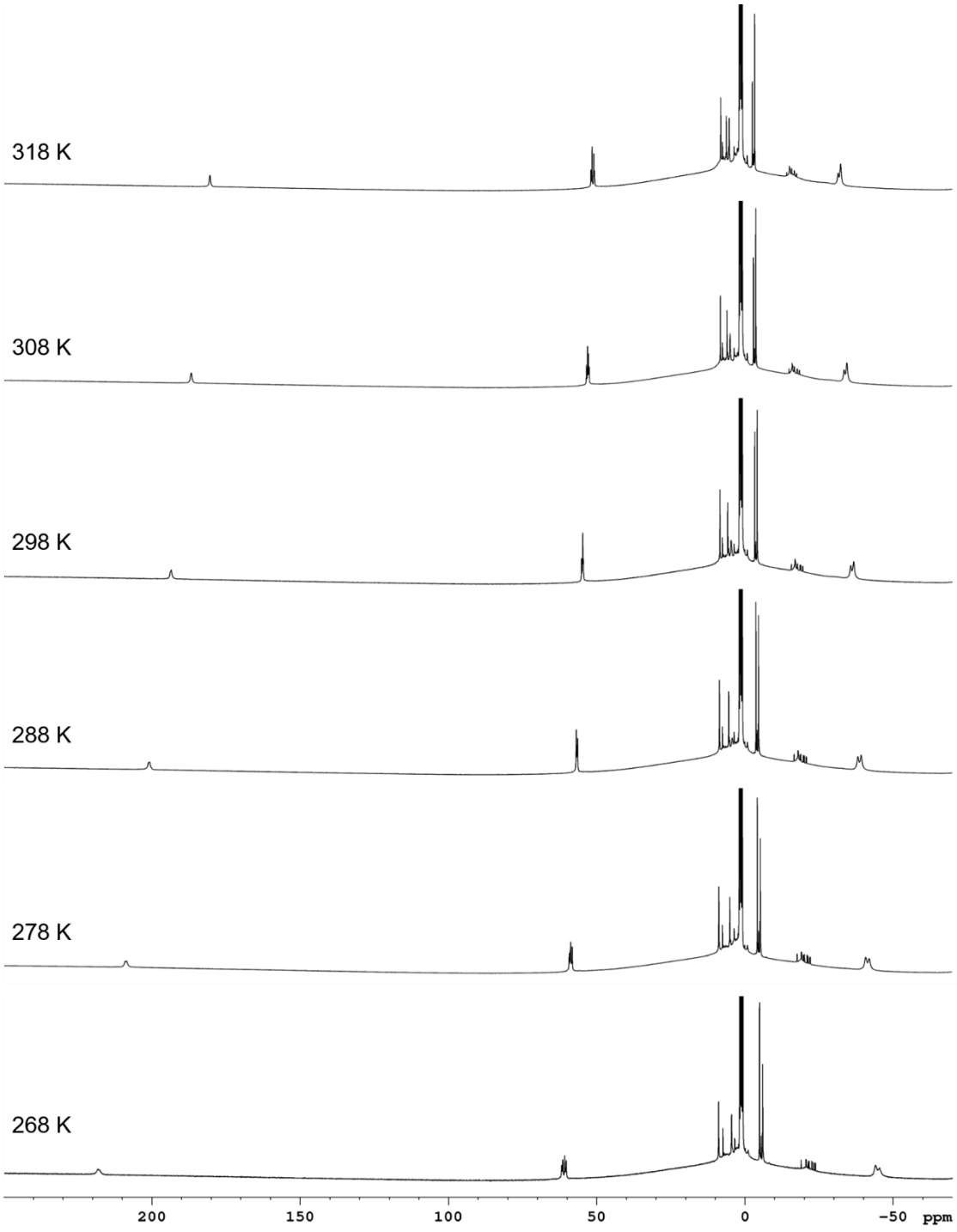

Figure S34. Variable temperature paramagnetic ^{1}H NMR spectra of [*trans*-decalin ⊂ **1**](OTf)$_8$ in CD_3CN.

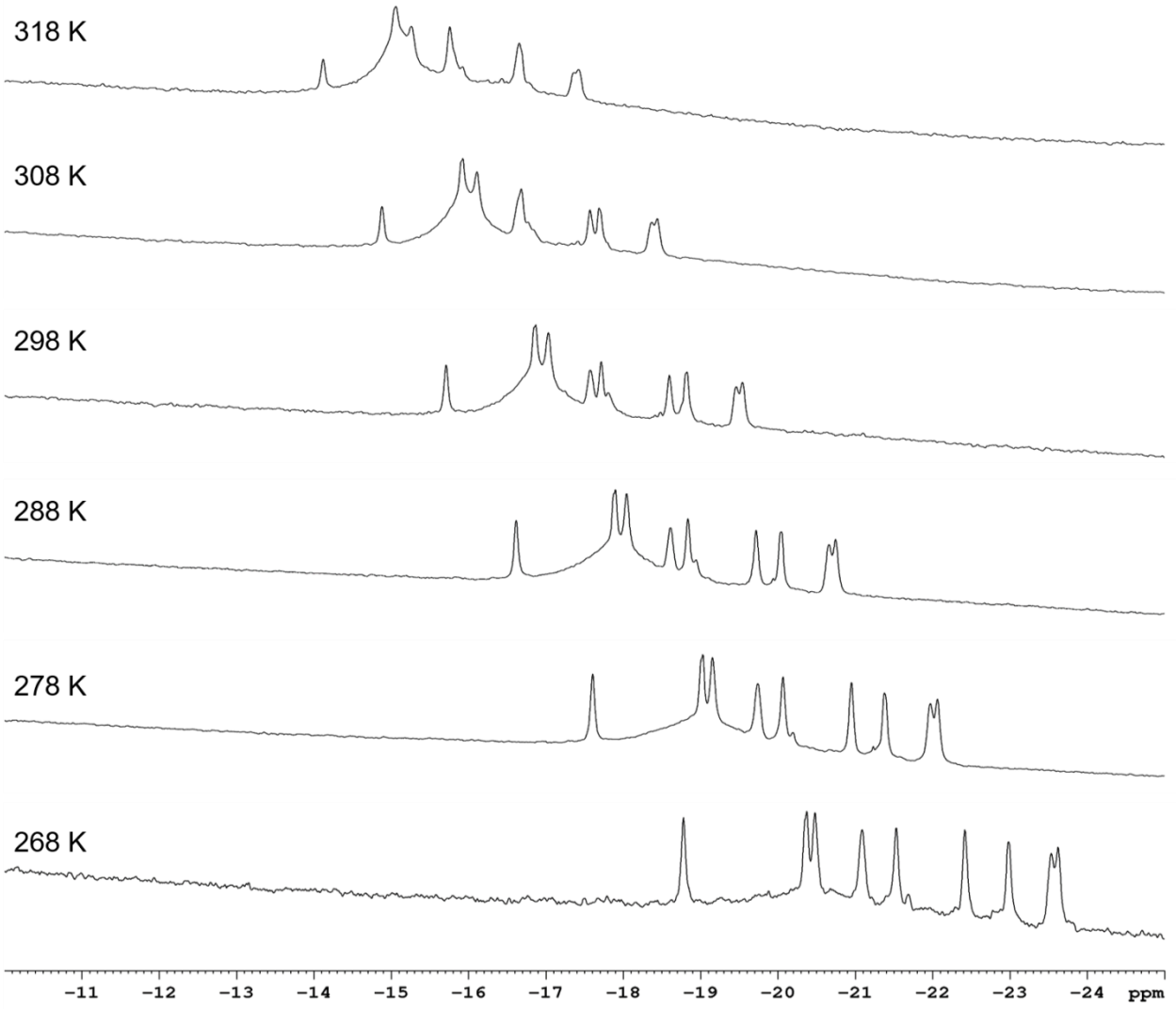

Figure S35. Variable temperature paramagnetic ^{1}H NMR spectra of [*trans*-decalin ⊂ **1**](OTf)$_8$ in CD_3CN showing the *trans*-decalin guest signals. The guest peaks for *trans*-decalin were sharper at room temperature than for *cis*-decalin (Figure S30) and further sharpened and split upon cooling to 268 K. The nine peaks observed are consistent with the adoption of a boat-boat (or twist-boat-twist-boat) conformation for *trans*-decalin within **2**.[2]

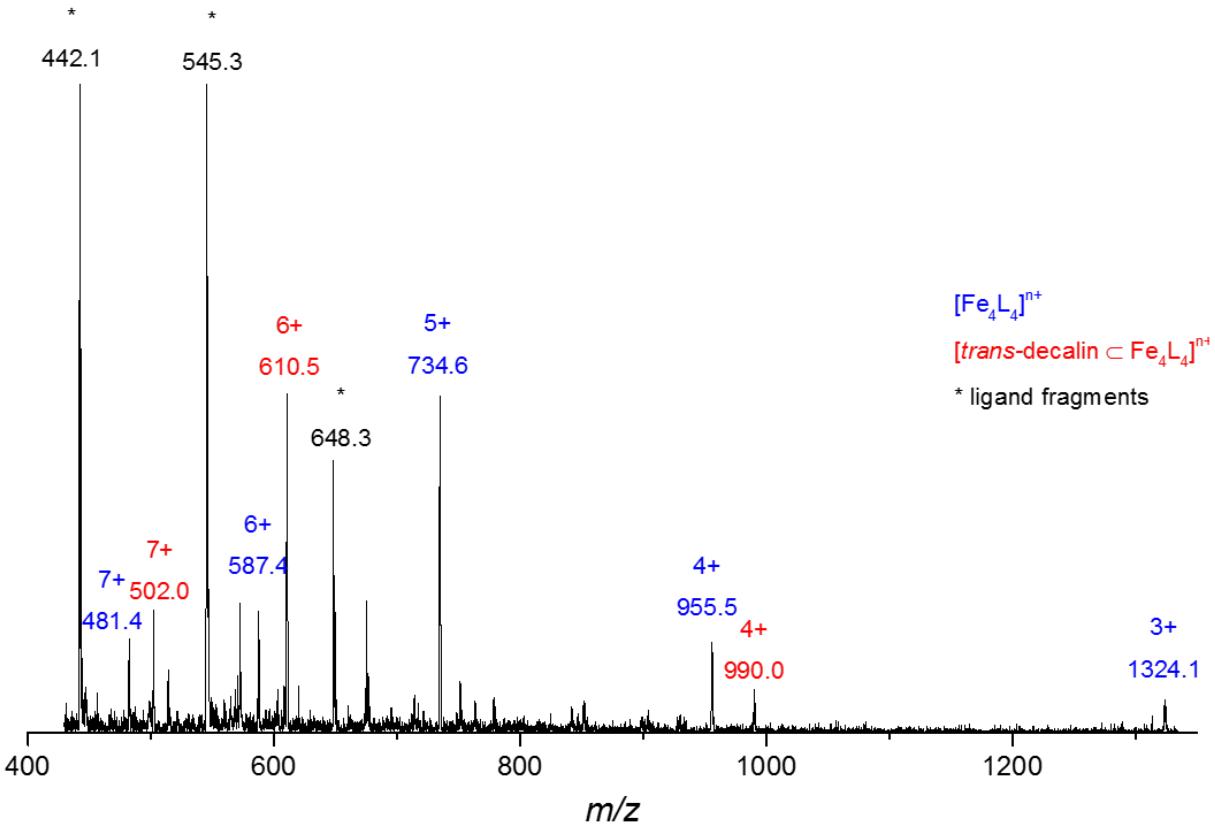

Figure S36. Low resolution ESI-mass spectrum of [*trans*-decalin ⊂ **1**](OTf)$_8$.

3.8 *o*-Xylene

^{1}H NMR (400 MHz, CD_3CN, 298 K) δ (ppm): 193.5 (H_e), 54.7 (H_b, H_d), 8.4 (H_c), 4.9 (H_g), -4.0 (H_h), -12.4 (encapsulated *o*-xylene), -12.7 (encapsulated *o*-xylene), -17.0 (encapsulated *o*-xylene), -36.6 (H_a)

ESI-MS *m/z*: 605.3 [*o*-xylene ⊂ **1** + 2OTf]$^{6+}$

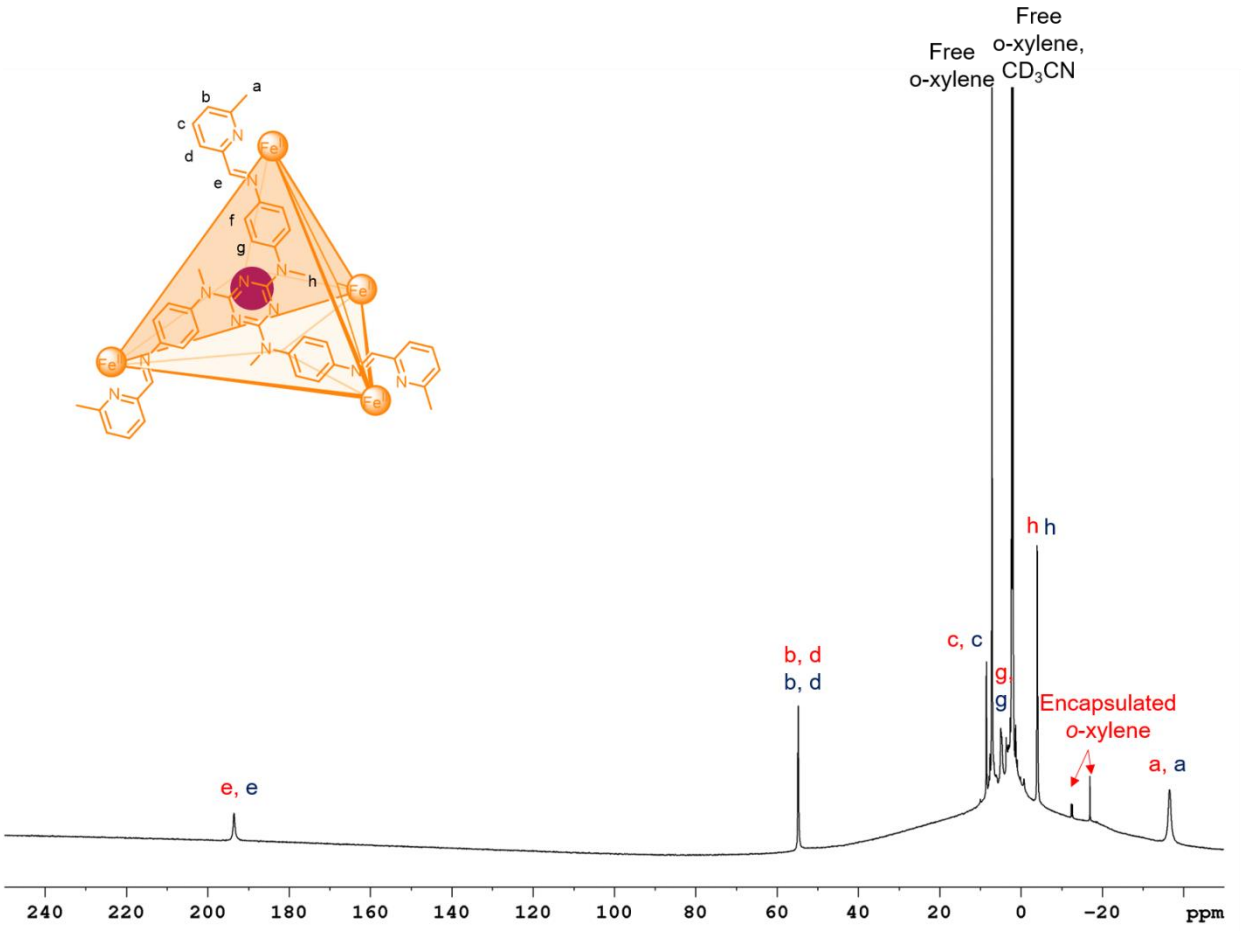

Figure S37. Paramagnetic ^{1}H NMR spectrum of [*o*-xylene ⊂ **1**](OTf)$_8$ in CD_3CN at 298 K. Red labels refer to [*o*-xylene ⊂ **1**](OTf)$_8$ and blue labels refer to empty cage **1**.

-17.1 ppm

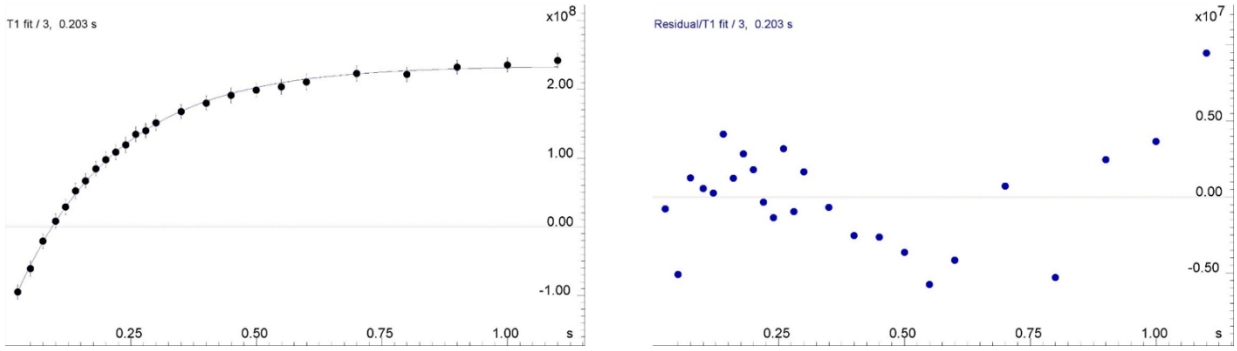

Figure S38. T1 measurements for the encapsulated guest signal at -18.4 ppm for [*o*-xylene ⊂ **1**](OTf)$_8$ in CD_3CN at 298 K.

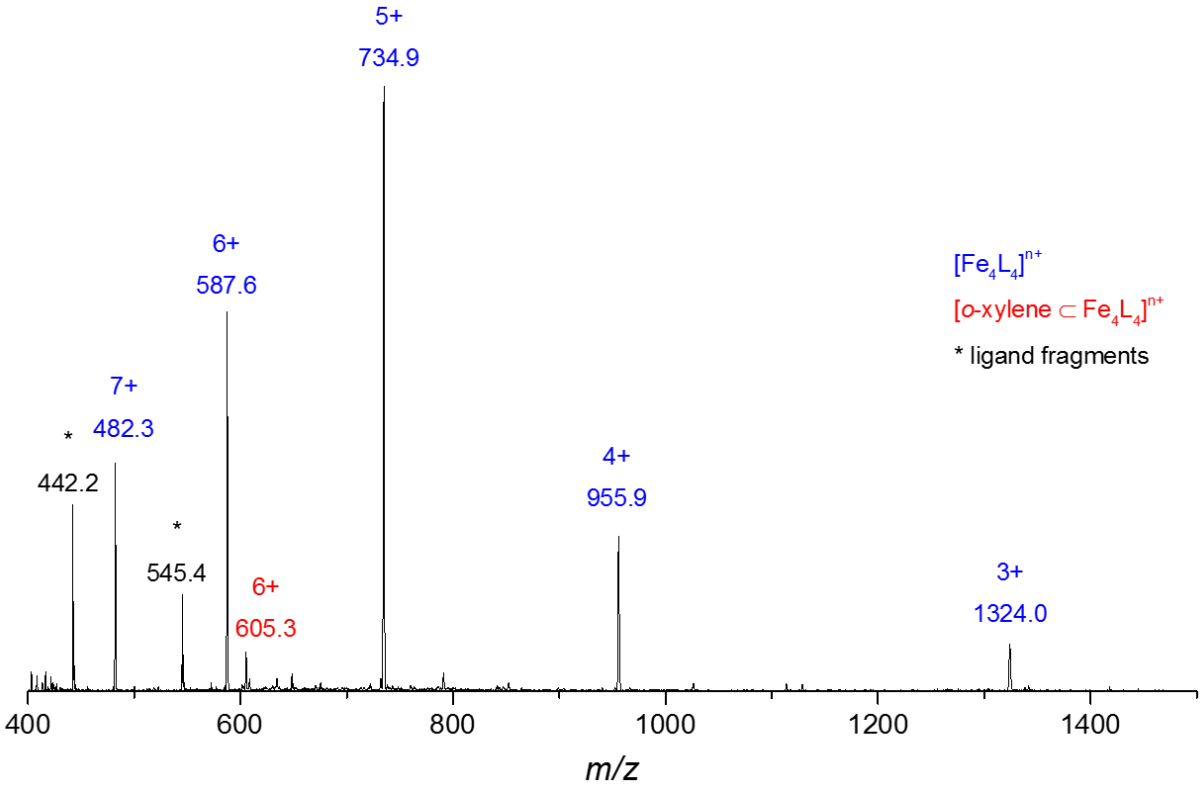

Figure S39. Low resolution ESI-mass spectrum of [*o*-xylene ⊂ **1**](OTf)$_8$.

3.9 Benzene

^{1}H NMR (400 MHz, CD_3CN, 298 K) δ (ppm): 193.5 (H_e), 54.7 (H_b, H_d), 8.5 (H_c), 4.7 (H_g), -4.3 (H_h), -12.6 (H_1), -36.8 (H_a)

Only the empty cage is observed in the ESI mass spectrum.

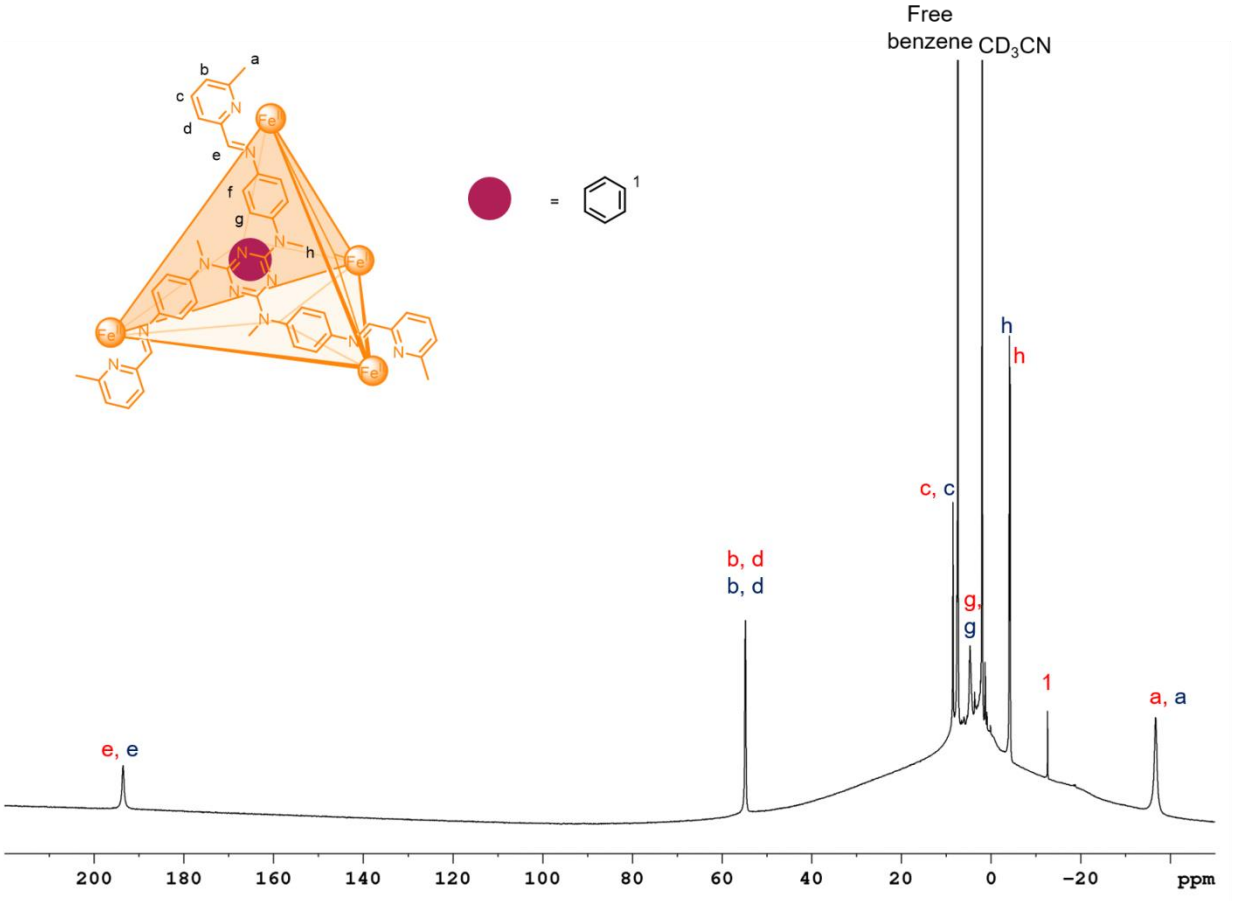

Figure S40. Paramagnetic ^{1}H NMR spectrum of [benzene ⊂ **1**](OTf)$_8$ in CD_3CN at 298 K. Red labels refer to [benzene ⊂ **1**](OTf)$_8$ and blue labels refer to empty cage **1**.

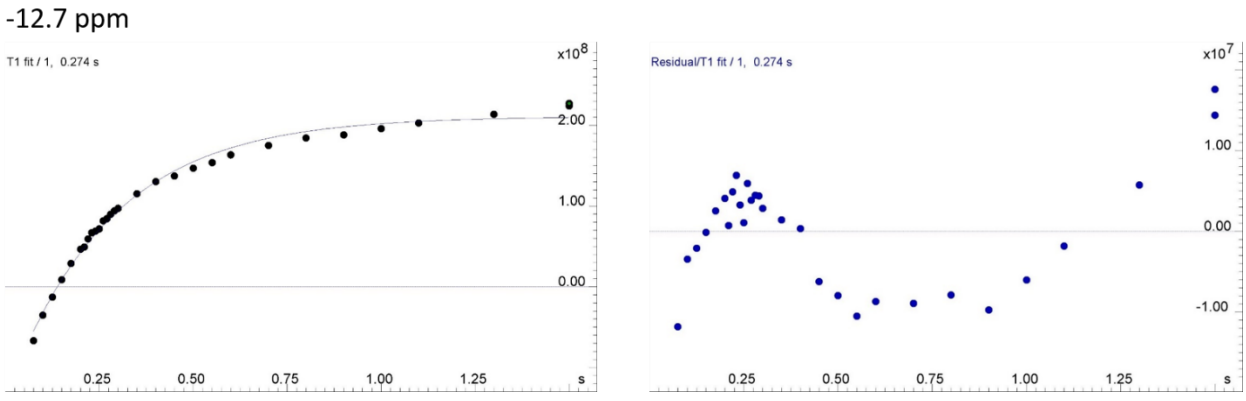

Figure S41. T_1 measurements for the encapsulated guest signal at -12.7 ppm for [benzene ⊂ **1**](OTf)$_8$ in CD_3CN at 298 K.

3.10 Toluene

^{1}H NMR (400 MHz, CD_3CN, 298 K) δ (ppm): 193.5 (H_e), 54.7 (H_b, H_d), 8.4 (H_c), 4.7 (H_g), -4.1 (H_h), -12.6 (encapsulated toluene), -12.7 (encapsulated toluene), -12.9 (encapsulated toluene), -16.9 (encapsulated toluene), -36.7 (H_a)

Only the empty cage is observed in the ESI mass spectrum.

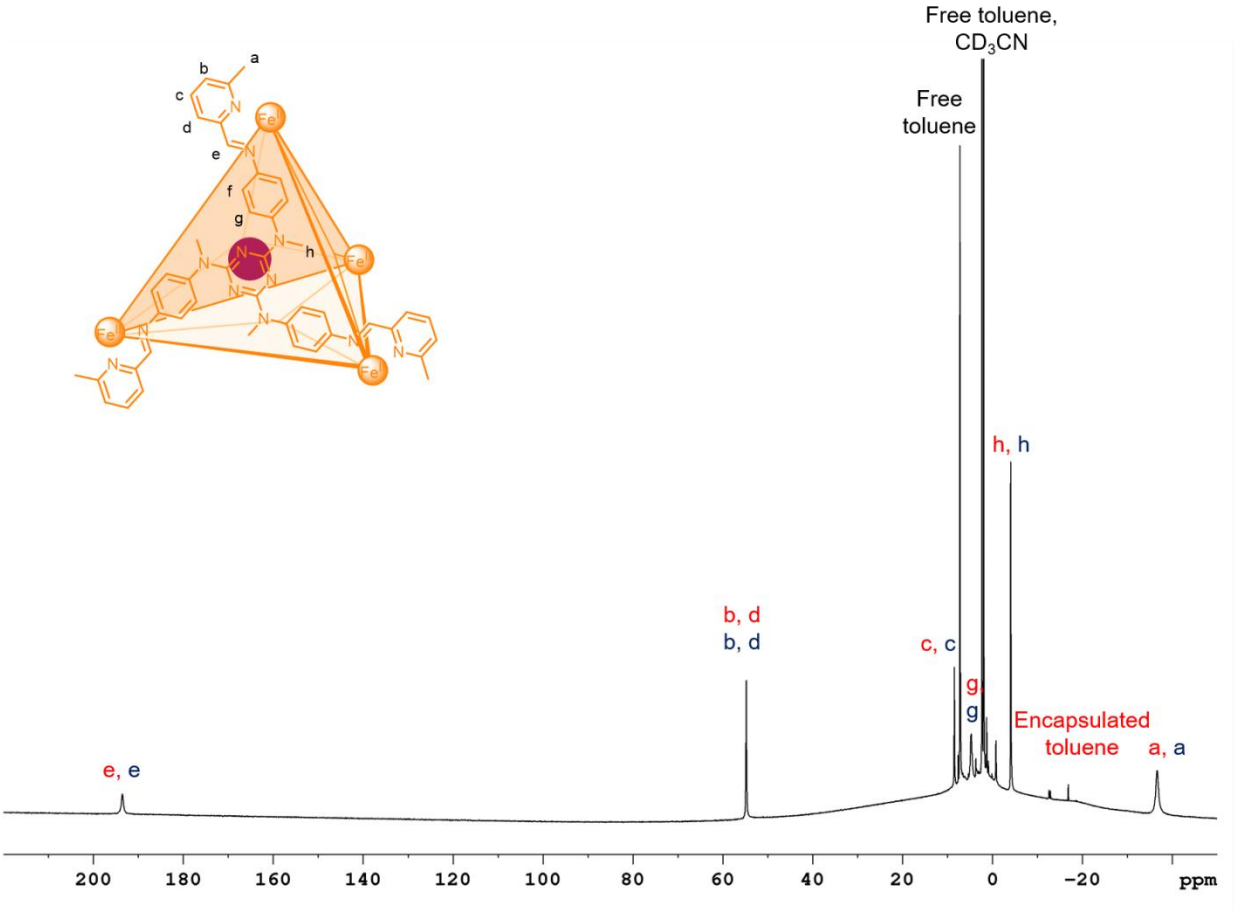

Figure S42. Paramagnetic ^{1}H NMR spectrum of [toluene ⊂ **1**](OTf)$_8$ in CD_3CN at 298 K. Red labels refer to [toluene ⊂ **1**](OTf)$_8$ and blue labels refer to empty cage **1**.

3.11 *R*-Limonene

^{1}H NMR (400 MHz, CD_3CN, 298 K) δ (ppm): 193.6 (H_e), 55.0 ($H_{b/d}$), 54.5 ($H_{b/d}$), 8.5 (H_c), -3.5 (H_h), -14.0 – -19.3 (encapsulated *R*-limonene), -36.0 (H_a)

ESI-MS *m/z*: 610.3 [*R*-limonene ⊂ **1** + 2OTf]$^{6+}$

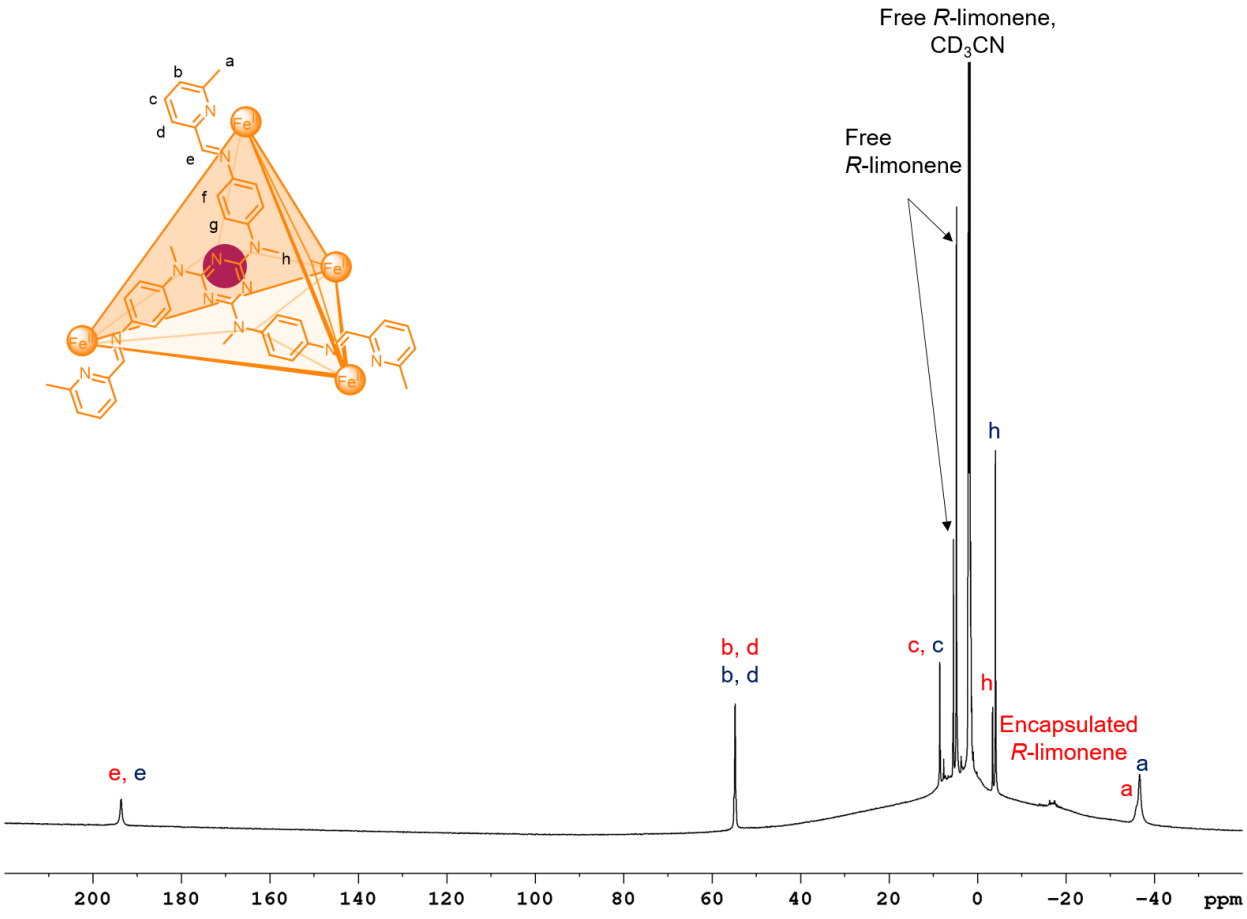

Figure S43. Paramagnetic ^{1}H NMR spectrum of [*R*-limonene ⊂ **1**](OTf)$_8$ in CD_3CN at 298 K. Red labels refer to [*R*-limonene ⊂ **1**](OTf)$_8$, blue labels refer to empty cage **1**.

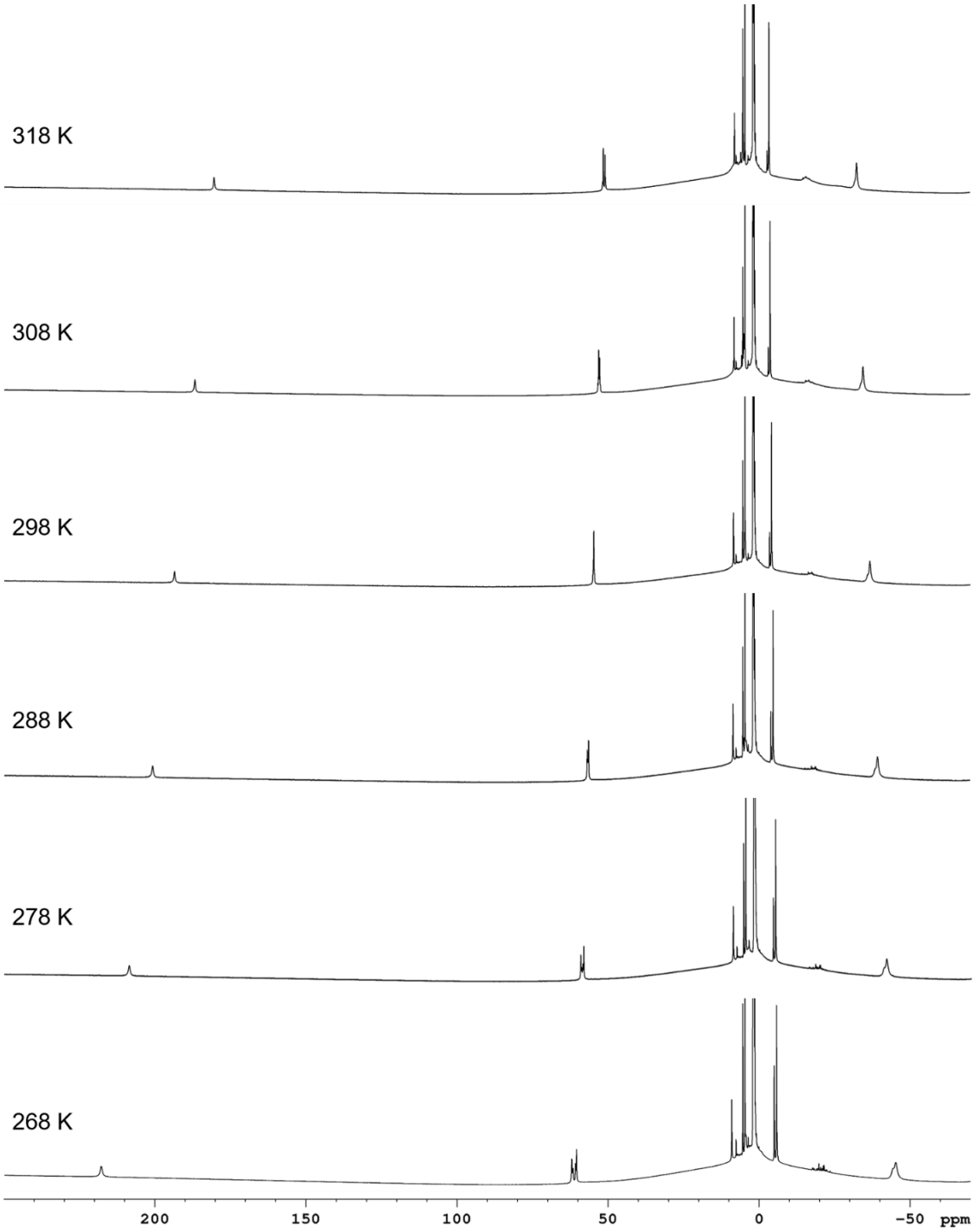

Figure S44. Variable temperature paramagnetic ^{1}H NMR spectra of [*R*-limonene ⊂ **1**](OTf)$_8$ in CD_3CN.

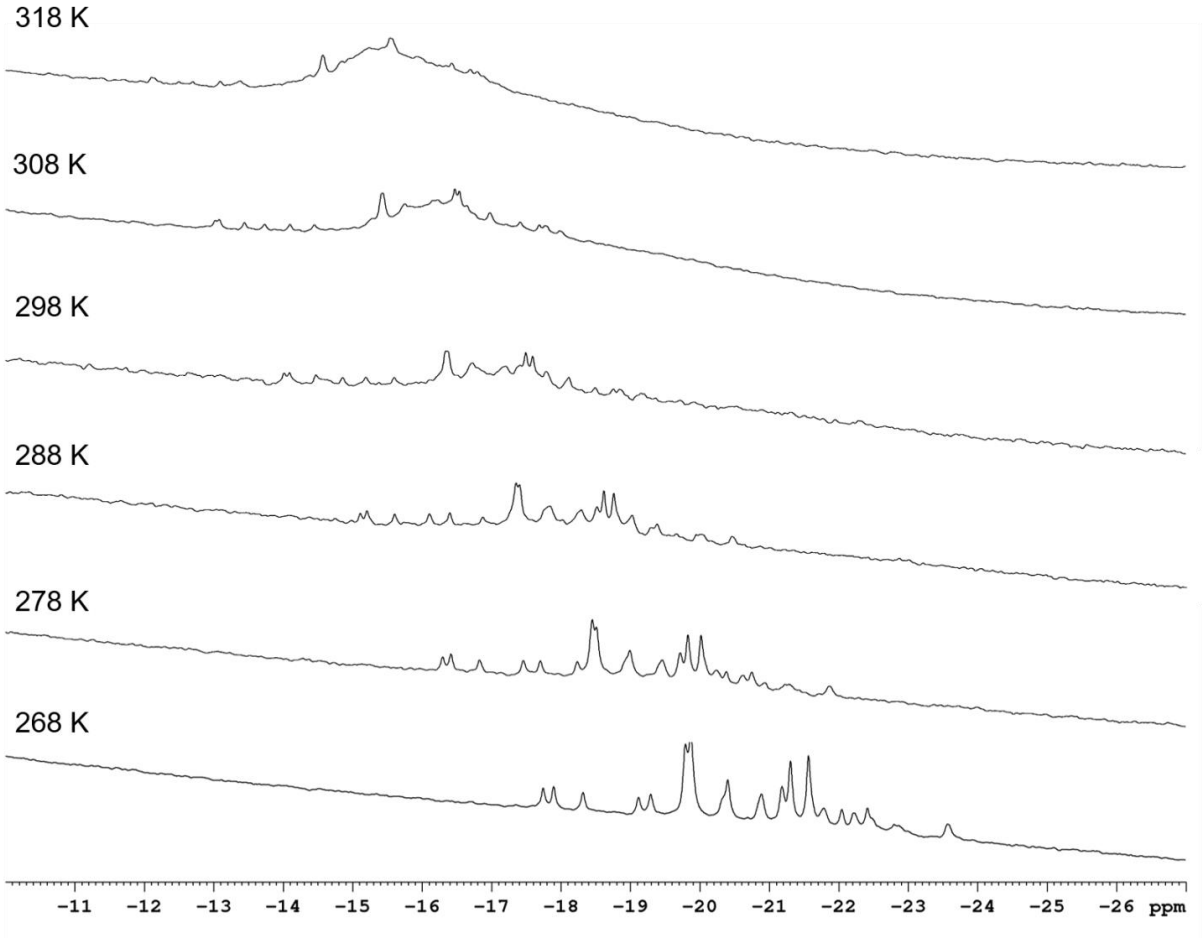

Figure S45. Variable temperature paramagnetic ^{1}H NMR spectra of [*R*-limonene ⊂ **1**](OTf)$_8$ in CD_3CN showing the *R*-limonene guest signals.

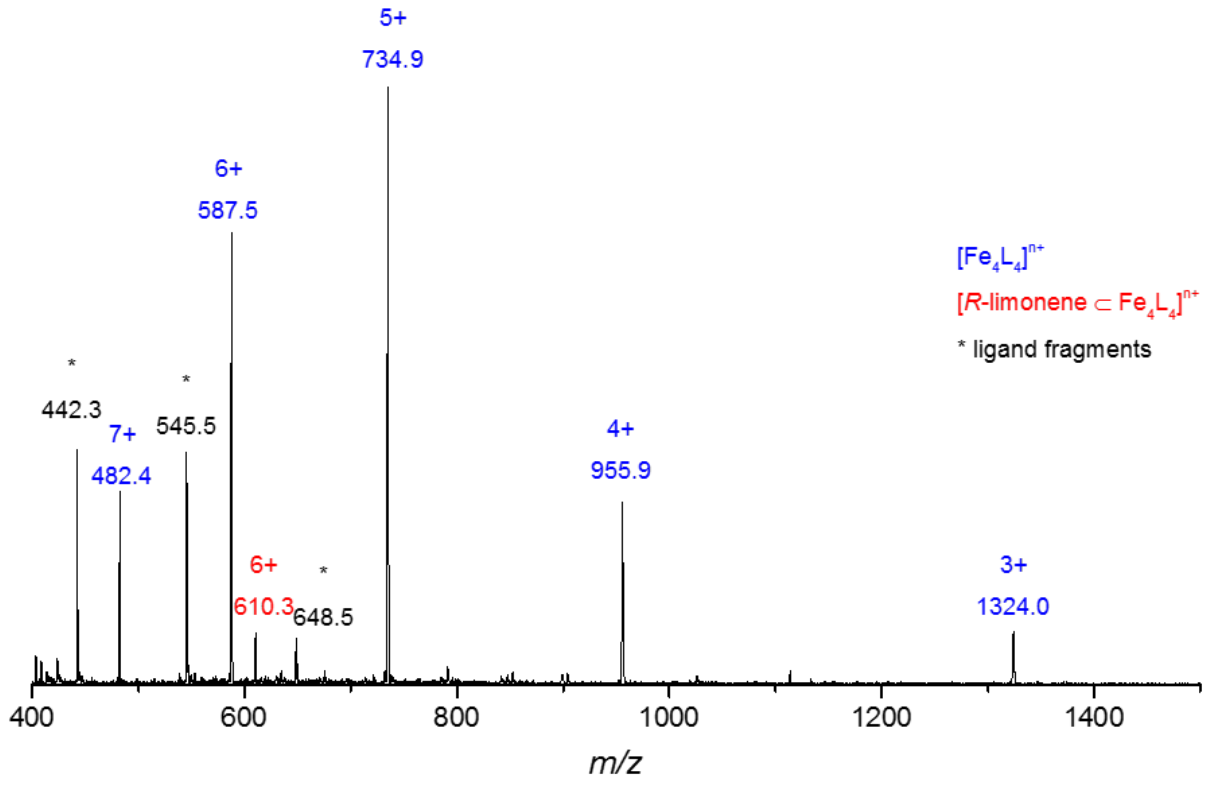

Figure S46. Low resolution ESI-mass spectrum of [*R*-limonene ⊂ **1**](OTf)$_8$.

3.12 *S*-Limonene

^{1}H NMR (400 MHz, CD_3CN, 298 K) δ (ppm): 193.6 (H_e), 55.0 ($H_{b/d}$), 54.6 ($H_{b/d}$), 8.5 (H_c), -3.5 (H_h), -14.0 – -19.3 (encapsulated *S*-limonene), -36.0 (H_a)

ESI-MS *m/z*: 610.3 [*S*-limonene ⊂ **1** + 2OTf]$^{6+}$

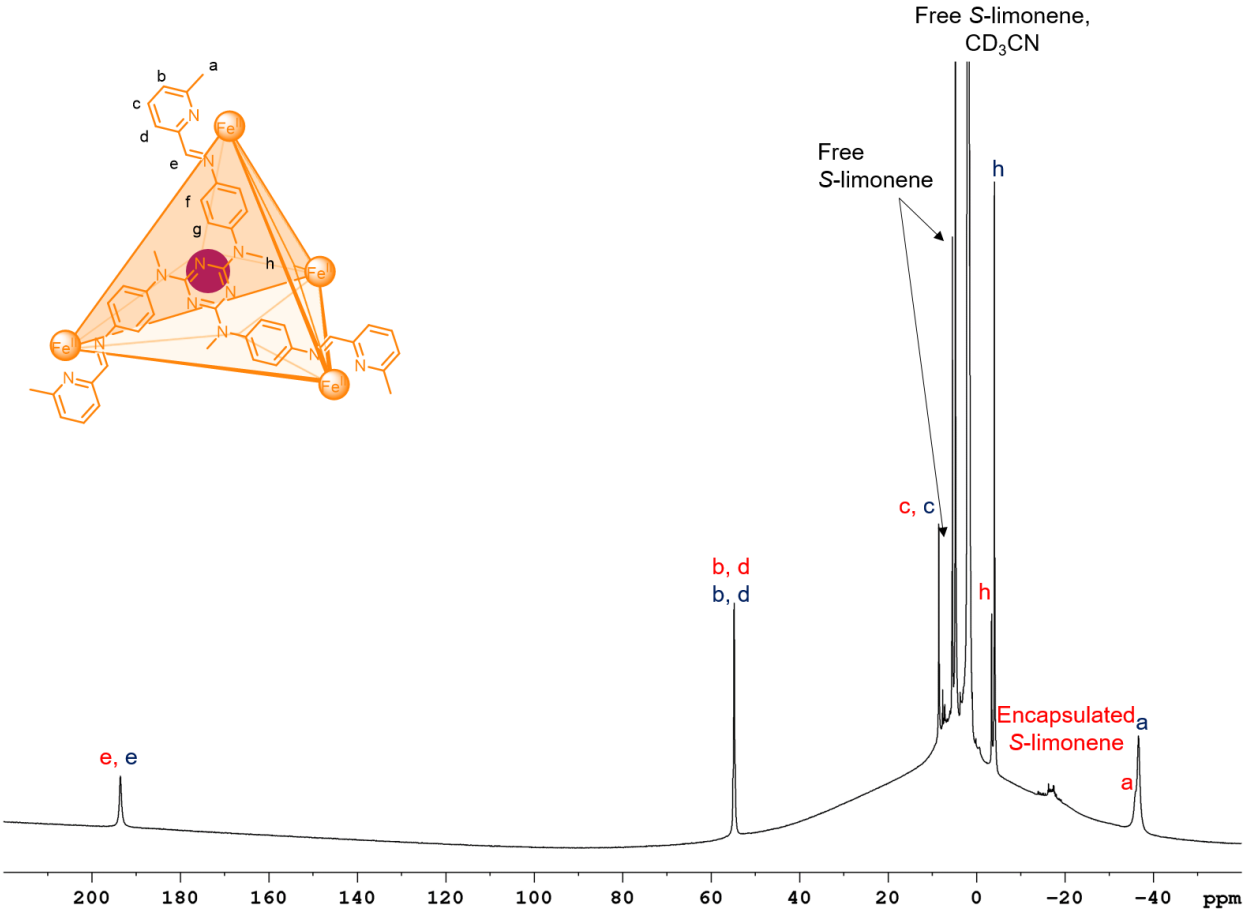

Figure S47. Paramagnetic ^{1}H NMR spectrum of [*S*-limonene ⊂ **1**](OTf)$_8$ in CD_3CN at 298 K. Red labels refer to [*S*-limonene ⊂ **1**](OTf)$_8$, blue labels refer to empty cage **1**.

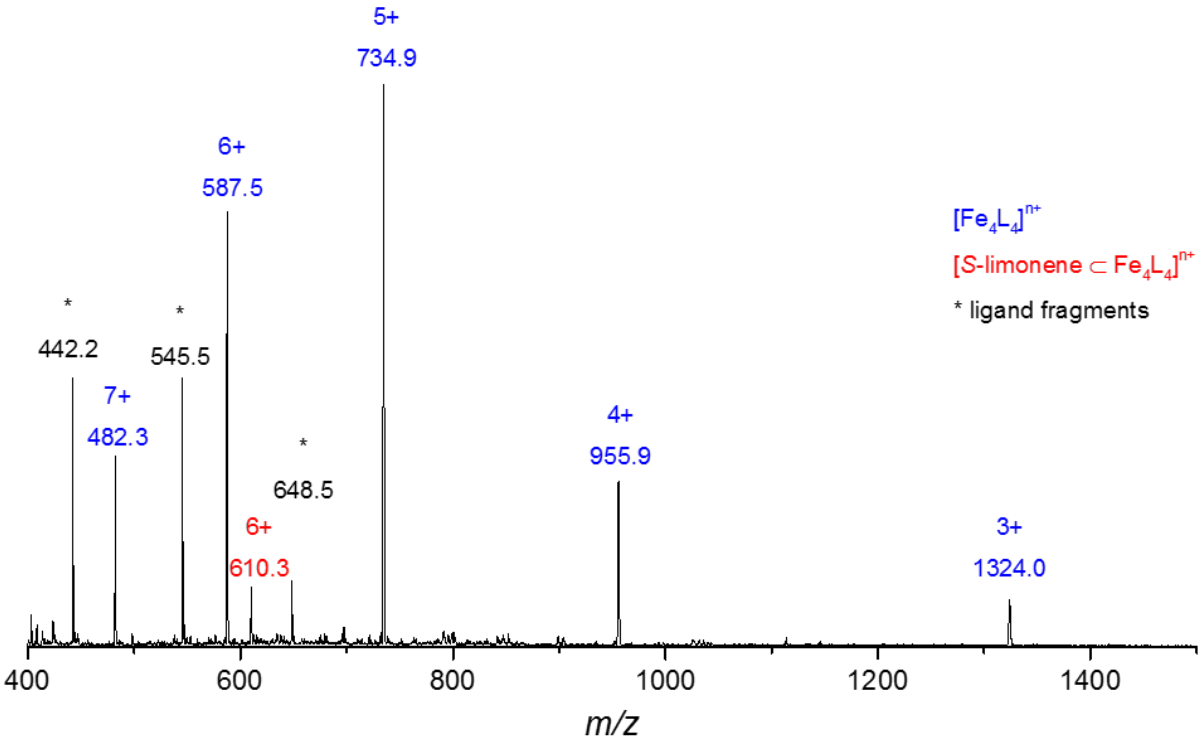

Figure S48. Low resolution ESI-mass spectrum of [*S*-limonene ⊂ **1**](OTf)$_8$.

3.13 *m*-Xylene

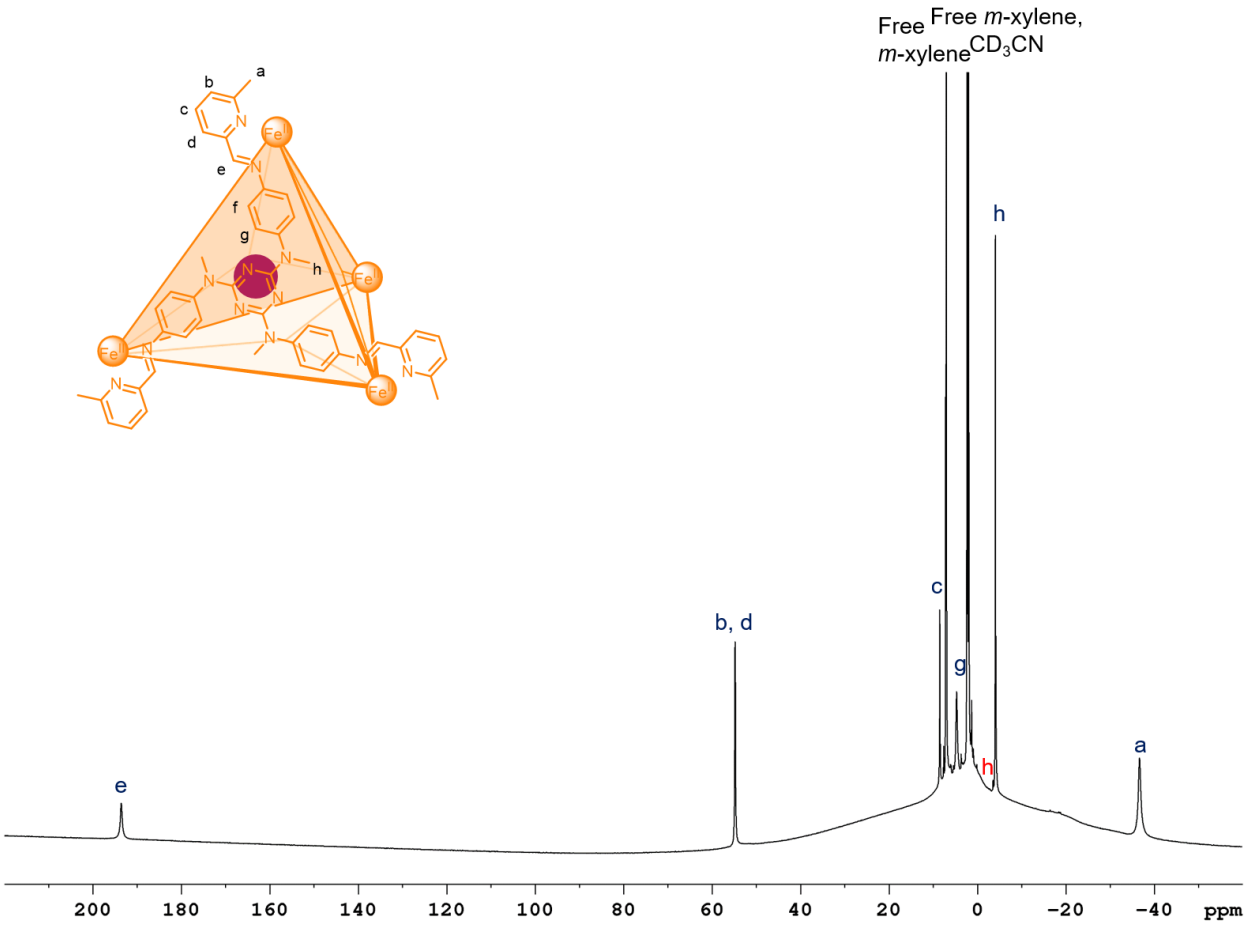

Figure S49. Paramagnetic ^{1}H NMR spectrum of [*m*-xylene ⊂ **1**](OTf)$_8$ in CD_3CN at 298 K. Red labels refer to [*m*-xylene ⊂ **1**](OTf)$_8$ and blue labels refer to empty cage **1**.

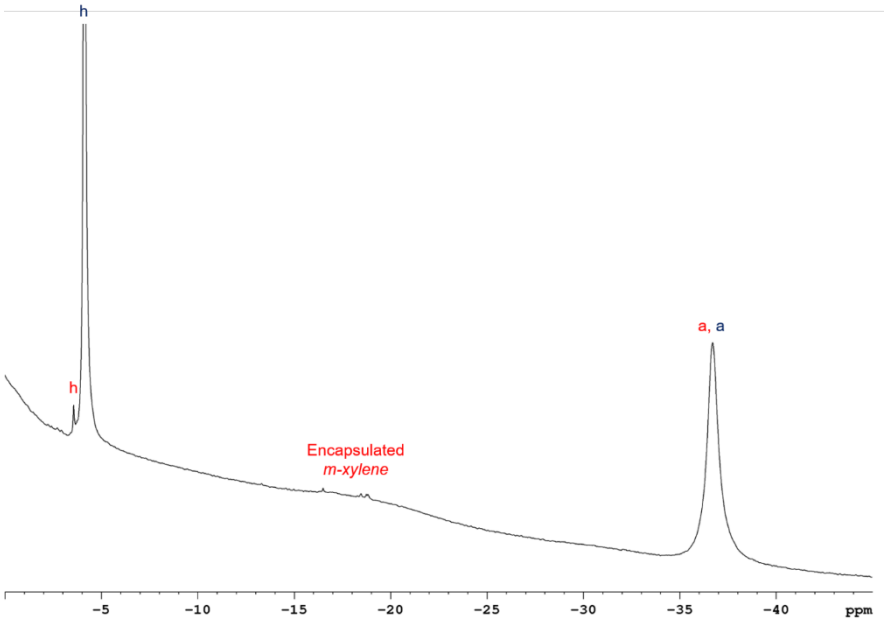

Figure S50. Zoomed inset of paramagnetic ^{1}H NMR spectrum of [*m*-xylene ⊂ **1**](OTf)$_8$ in CD_3CN at 298 K. Red labels refer to [*m*-xylene ⊂ **1**](OTf)$_8$ and blue labels refer to empty cage **1**.

3.14 *p*-Xylene

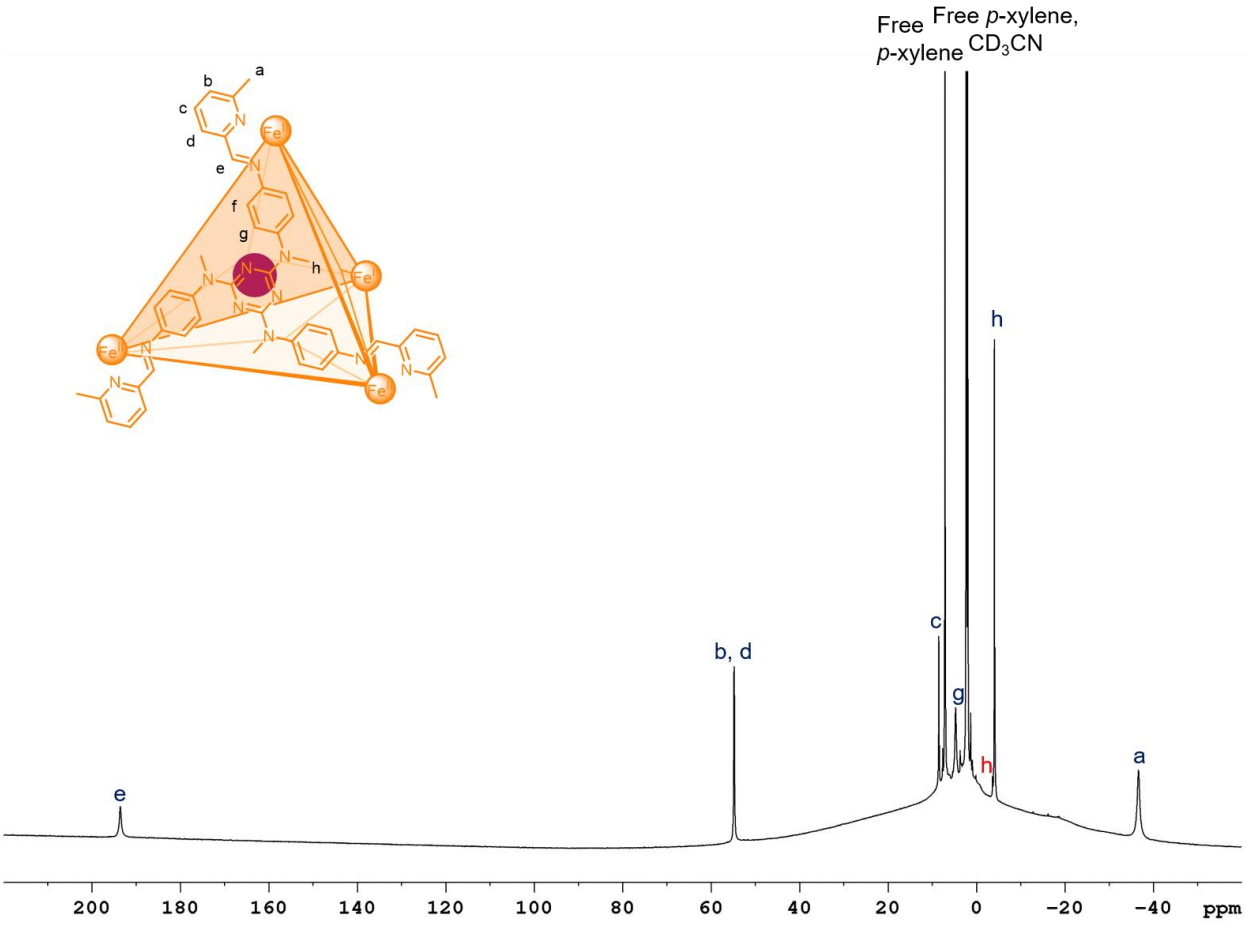

Figure S51. Paramagnetic ^{1}H NMR spectrum of [*p*-xylene ⊂ **1**](OTf)$_8$ in CD_3CN at 298 K. Red labels refer to [*p*-xylene ⊂ **1**](OTf)$_8$ and blue labels refer to empty cage **1**.

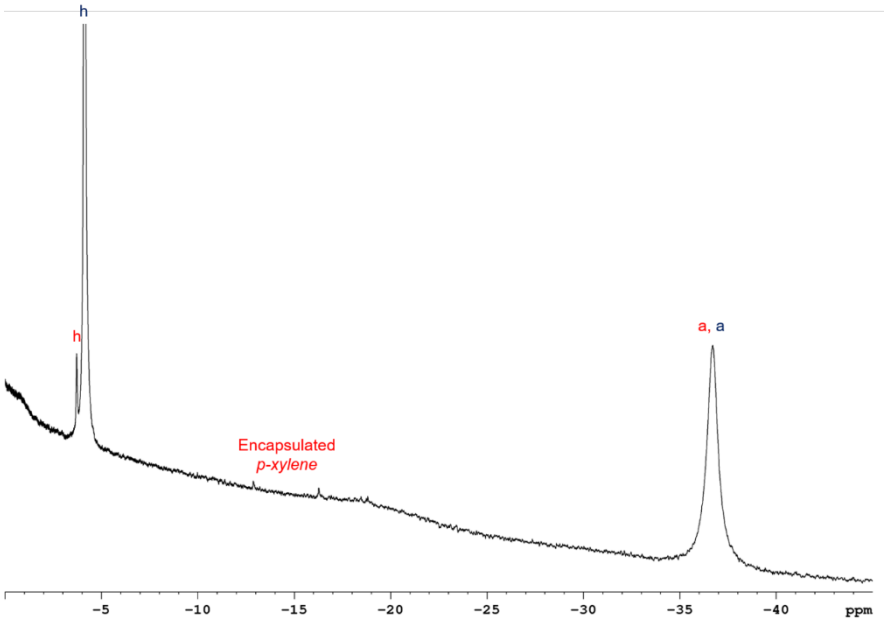

Figure S52. Zoomed inset of paramagnetic ^{1}H NMR spectrum of [*p*-xylene ⊂ **1**](OTf)$_8$ in CD_3CN at 298 K. Red labels refer to [*p*-xylene ⊂ **1**](OTf)$_8$ and blue labels refer to empty cage **1**.

4 Competition Host-Guest Studies

In a glovebox, a competing guest (10-15 equivalents) was added to a solution of the host-guest complexes prepared in Section 3. The J Young NMR tube was sealed and left to equilibrate at 298 K. Paramagnetic ^{1}H NMR spectra were recorded over time and generally equilibration times were several hours.

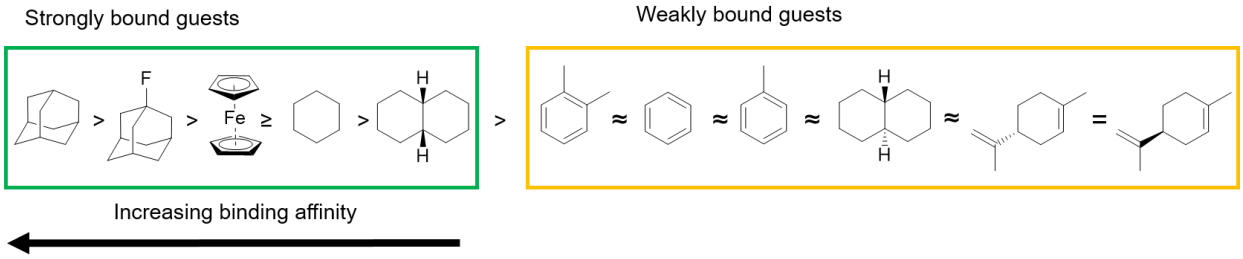

Figure S53. Relative binding affinity of guests for cage **1** determined by competition experiments.

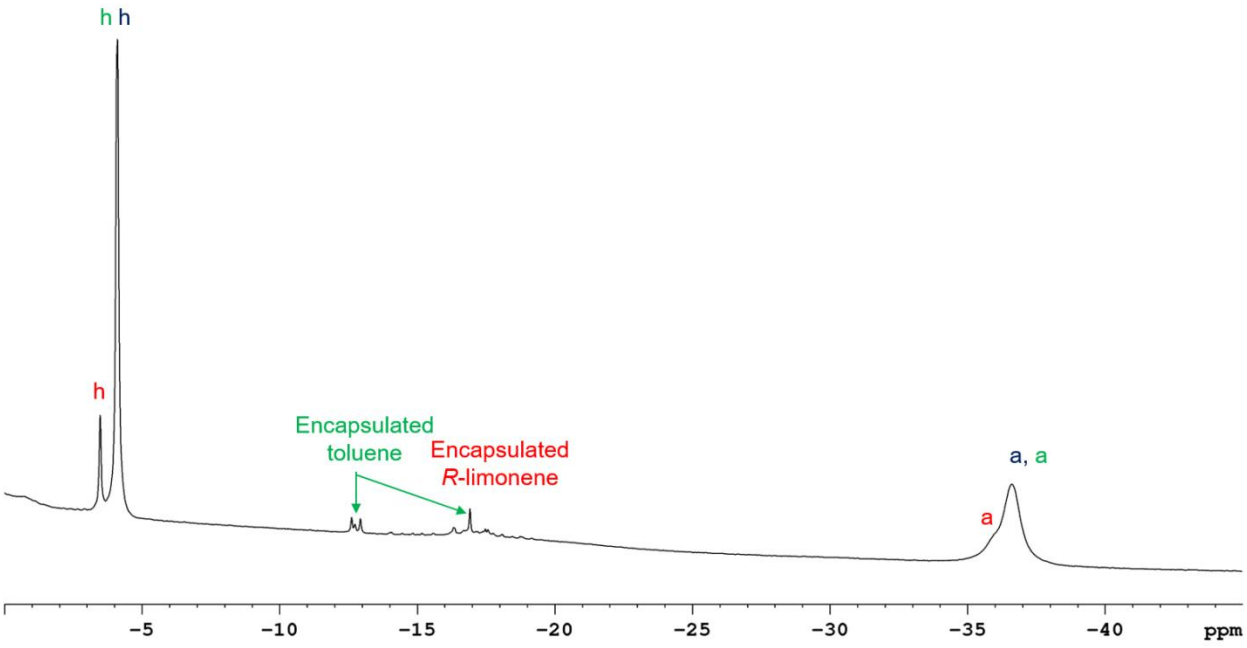

Figure S54. Paramagnetic ^{1}H NMR spectrum of [*R*-limonene ⊂ **1**](OTf)$_8$ in the presence of a competing guest, toluene, in CD_3CN at 298 K. Red labels refer to [*R*-limonene ⊂ **1**](OTf)$_8$, green labels refer to [toluene ⊂ **1**](OTf)$_8$ and blue labels refer to empty cage **1**.

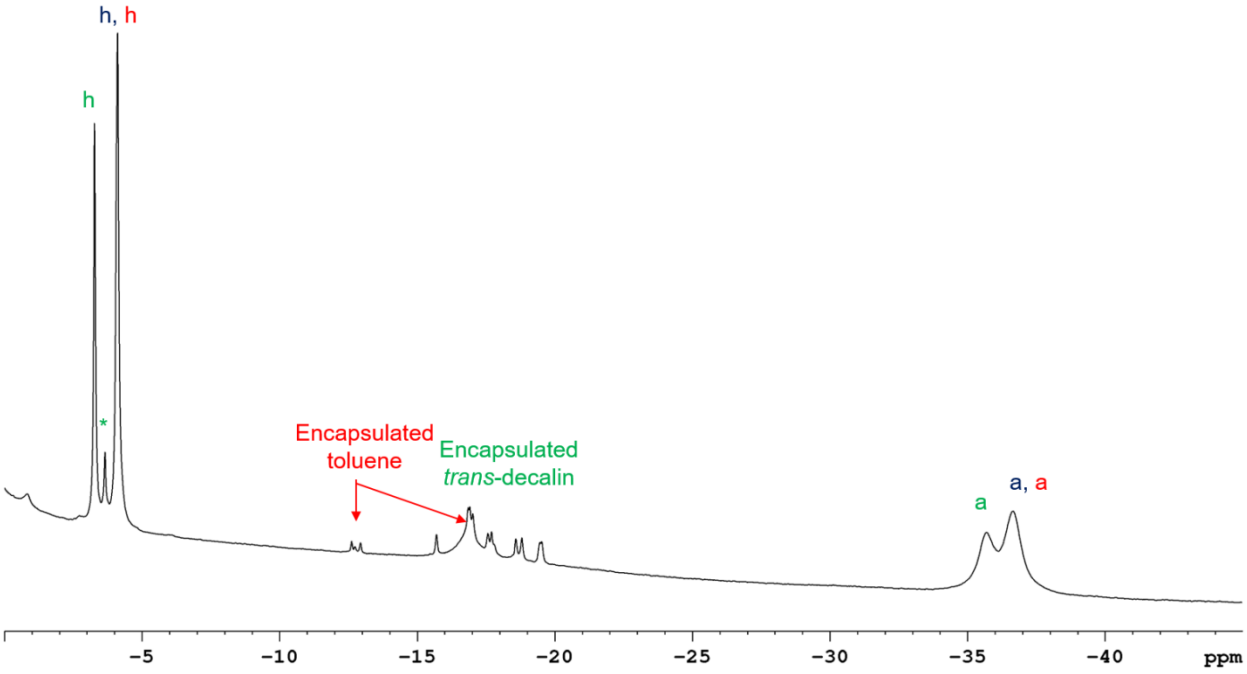

Figure S55. Paramagnetic ^{1}H NMR spectrum of [toluene ⊂ **1**](OTf)$_8$ in the presence of a competing guest, *trans*-decalin, in CD_3CN at 298 K. Red labels refer to [toluene ⊂ **1**](OTf)$_8$, green labels refer to [*trans*-decalin ⊂ **1**](OTf)$_8$, * refers to [*cis*-decalin ⊂ **1**](OTf)$_8$ and blue labels refer to empty cage **1**.

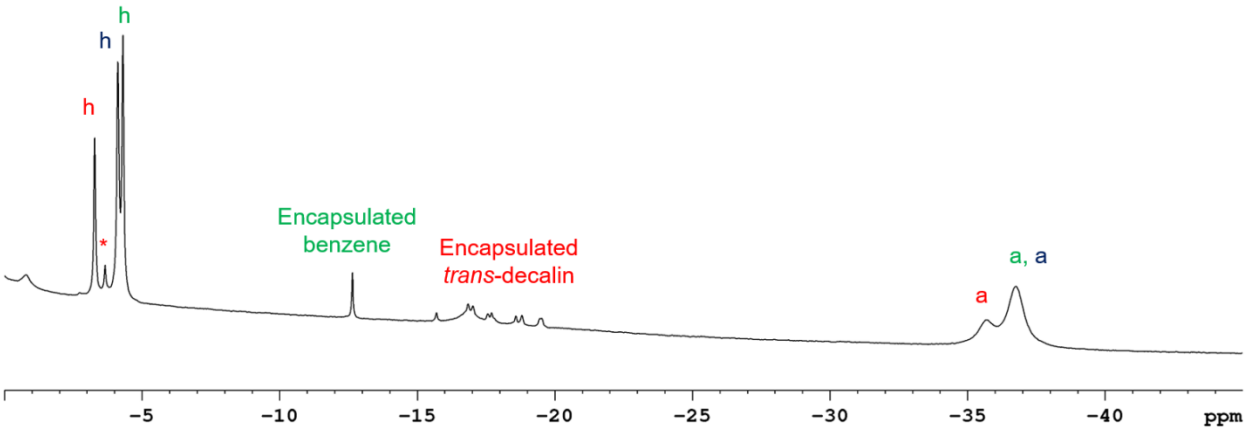

Figure S56. Paramagnetic ^{1}H NMR spectrum of [*trans*-decalin ⊂ **1**](OTf)$_8$ in the presence of a competing guest, benzene, in CD_3CN at 298 K. Red labels refer to [*trans*-decalin ⊂ **1**](OTf)$_8$, * refers to [*cis*-decalin ⊂ **1**](OTf)$_8$, green labels refer to [benzene ⊂ **1**](OTf)$_8$ and blue labels refer to empty cage **1**.

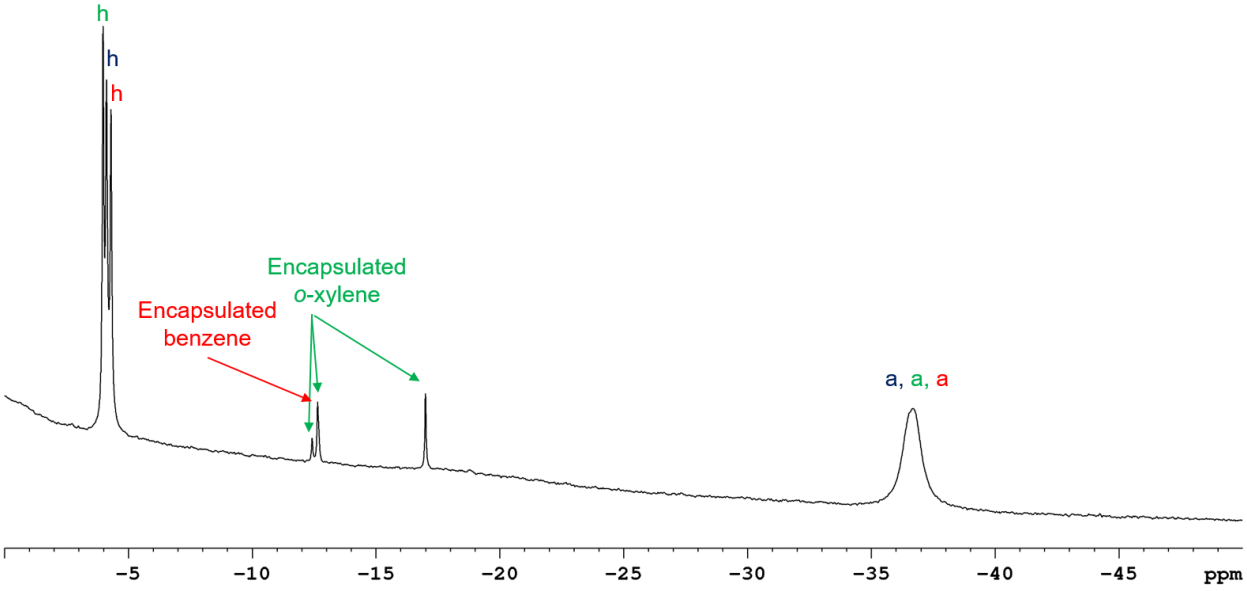

Figure S57. Paramagnetic ^{1}H NMR spectrum of [benzene ⊂ **1**](OTf)$_8$ in the presence of a competing guest, *o*-xylene, in CD_3CN at 298 K. Red labels refer to [benzene ⊂ **1**](OTf)$_8$, green labels refer to [*o*-xylene ⊂ **1**](OTf)$_8$ and blue labels refer to empty cage **1**.

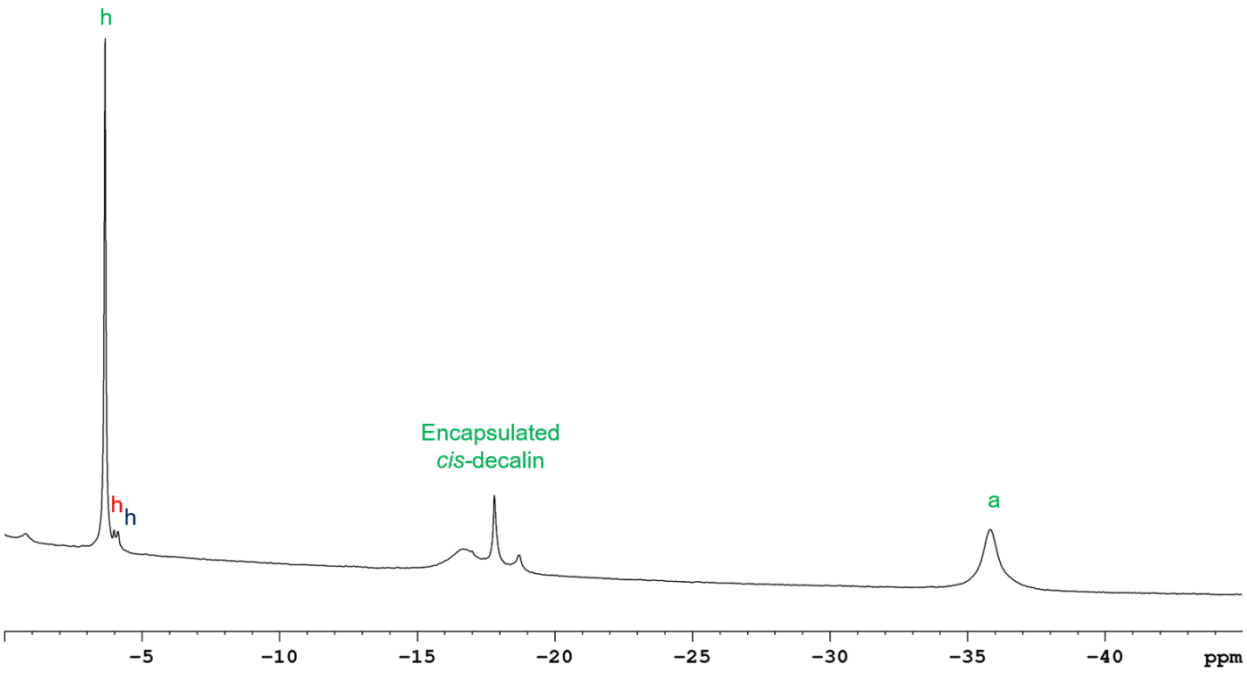

Figure S58. Paramagnetic ^{1}H NMR spectrum of [*o*-xylene ⊂ **1**](OTf)$_8$ in the presence of a competing guest, *cis*-decalin, in CD_3CN at 298 K. Red labels refer to [*o*-xylene ⊂ **1**](OTf)$_8$, green labels refer to [*cis*-decalin ⊂ **1**](OTf)$_8$ and blue labels refer to empty cage **1**.

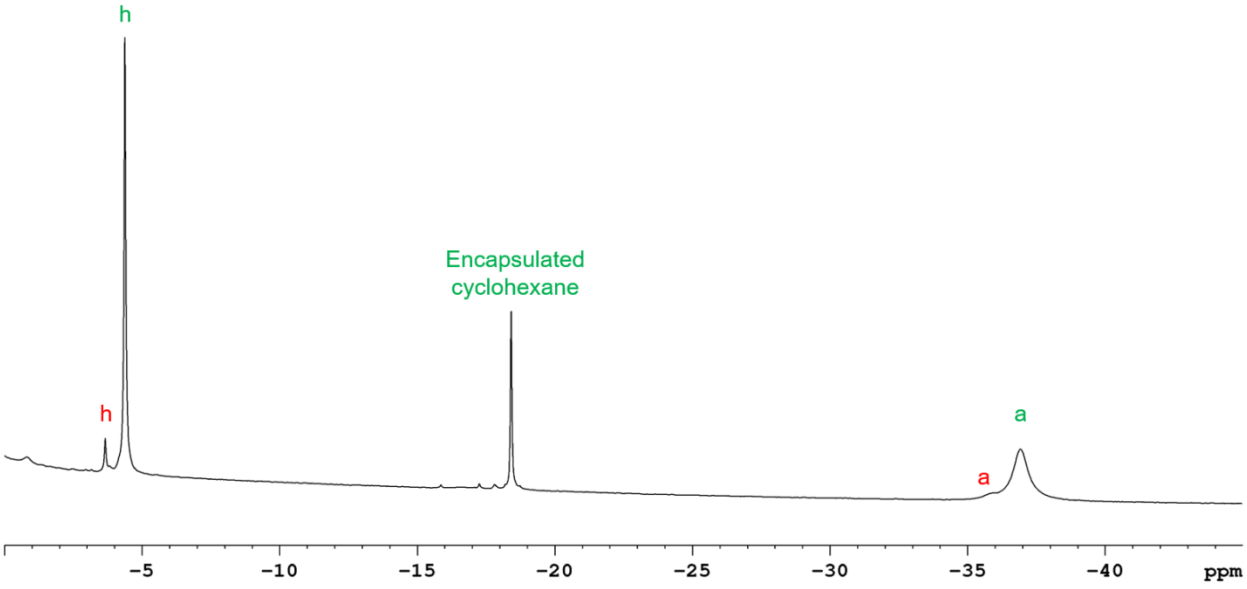

Figure S59. Paramagnetic ^{1}H NMR spectrum of [*cis*-decalin ⊂ **1**](OTf)$_8$ in the presence of a competing guest, cyclohexane, in CD_3CN at 298 K. Red labels refer to [*cis*-decalin ⊂ **1**](OTf)$_8$ and green labels refer to [cyclohexane ⊂ **1**](OTf)$_8$.

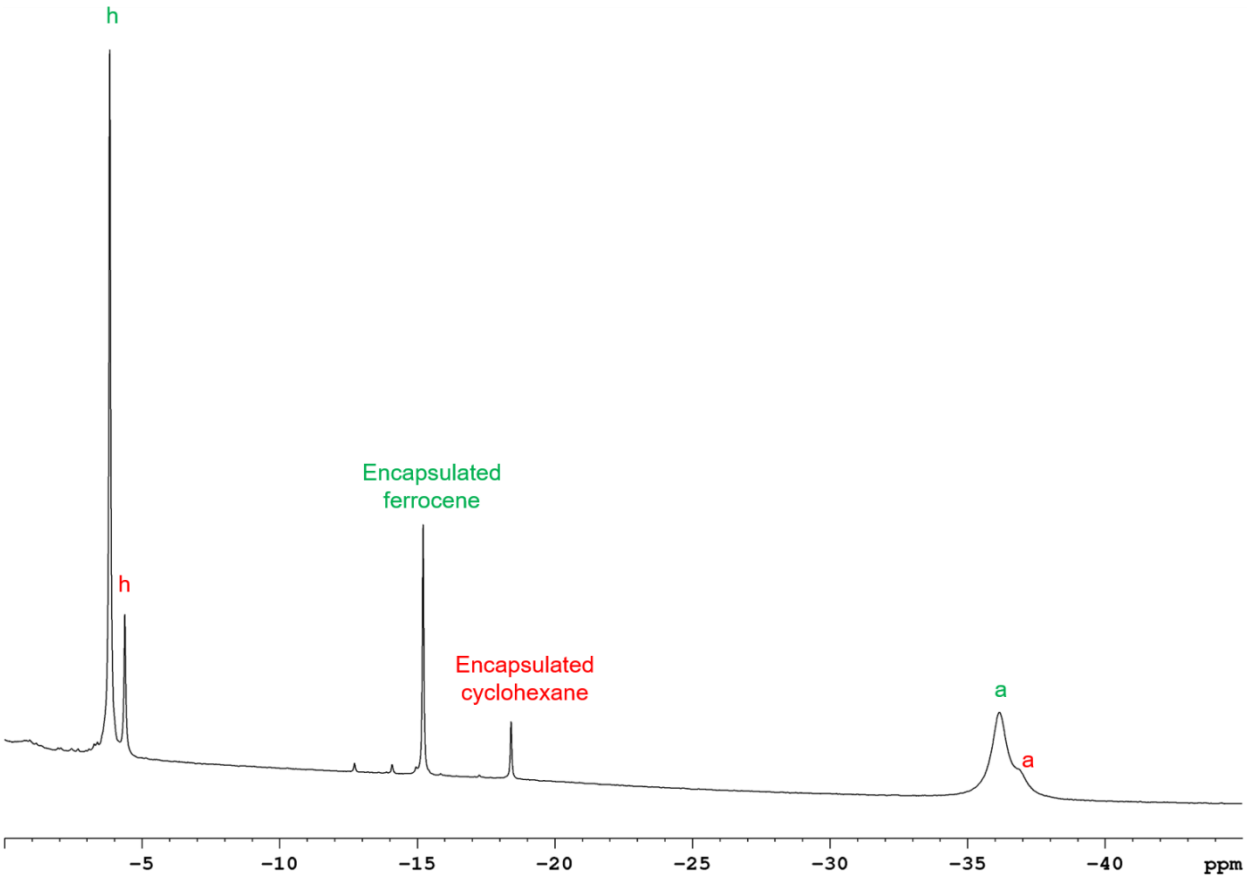

Figure S60. Paramagnetic ^{1}H NMR spectrum of [cyclohexane ⊂ **1**](OTf)$_8$ in the presence of a competing guest, ferrocene, in CD_3CN at 298 K. Red labels refer to [cyclohexane ⊂ **1**](OTf)$_8$ and green labels refer to [ferrocene ⊂ **1**](OTf)$_8$.

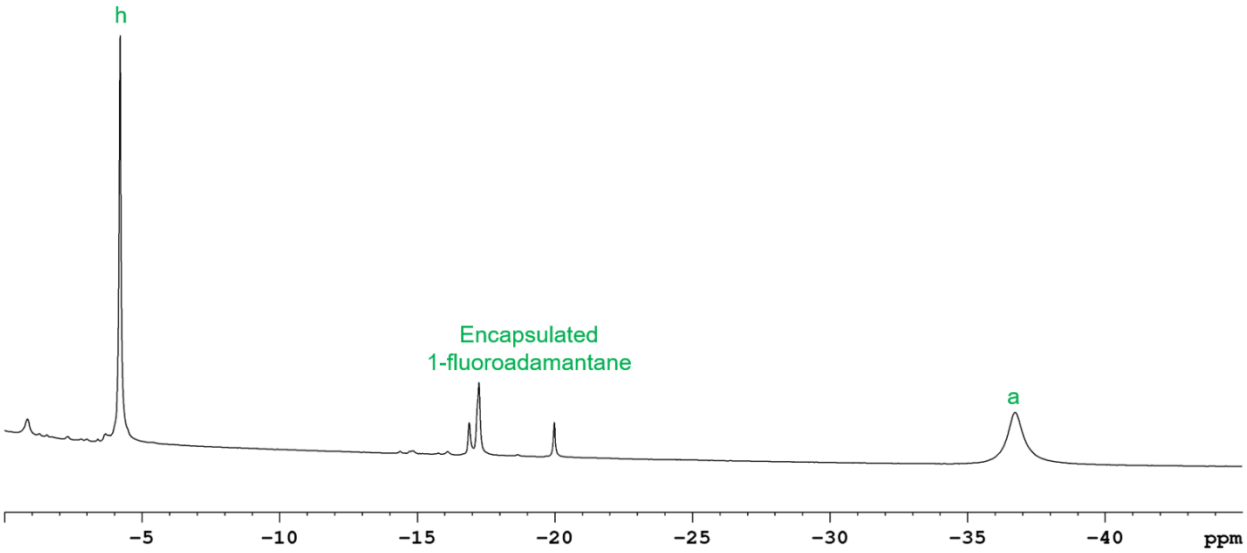

Figure S61. Paramagnetic ^{1}H NMR spectrum of [ferrocene ⊂ **1**](OTf)$_8$ in the presence of a competing guest, 1-fluoroadamantane, in CD_3CN at 298 K. Green labels refer to [1-fluoroadamantane ⊂ **1**](OTf)$_8$.

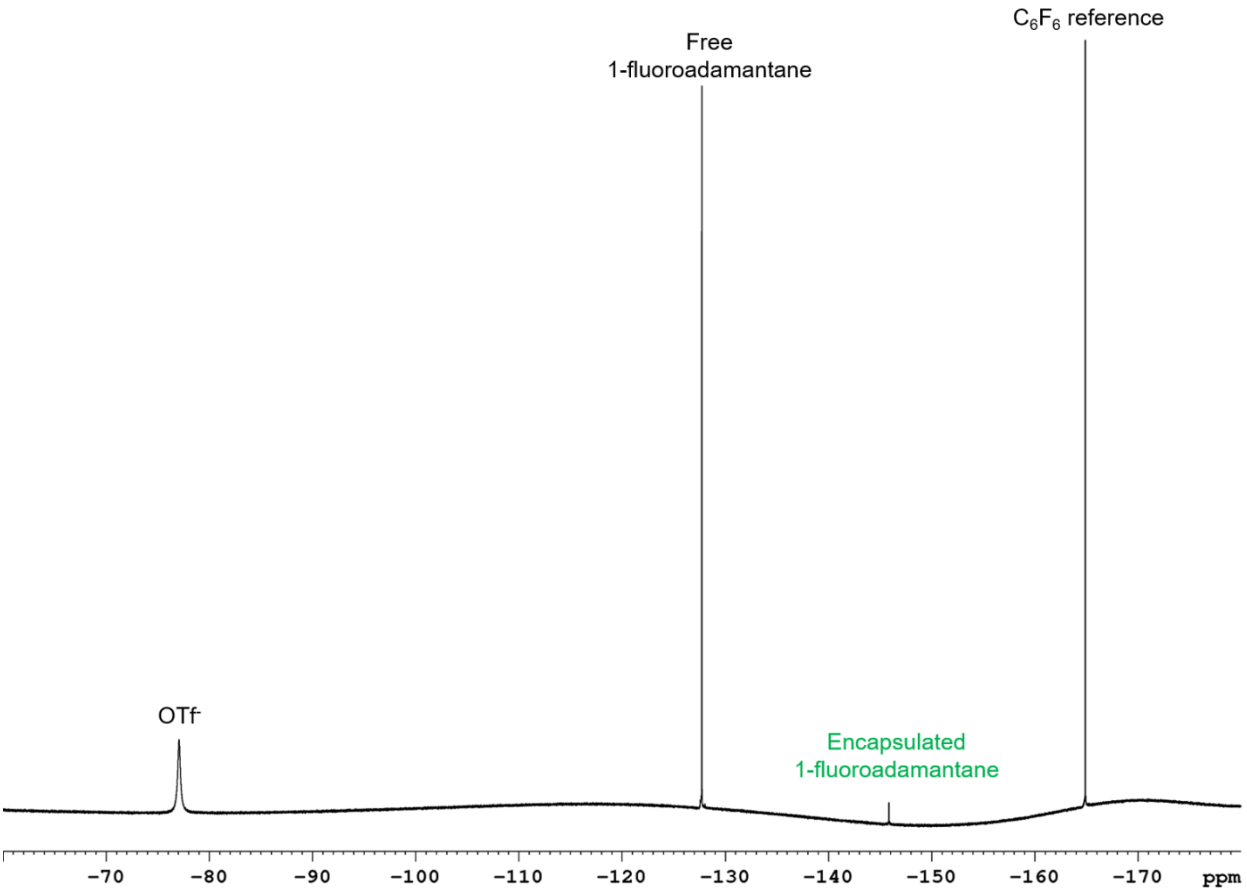

Figure S62. ^{19}F NMR spectrum of [ferrocene ⊂ **1**](OTf)$_8$ in the presence of a competing guest, 1-fluoroadamantane, in CD_3CN at 298 K. Green labels refer to [1-fluoroadamantane ⊂ **1**](OTf)$_8$.

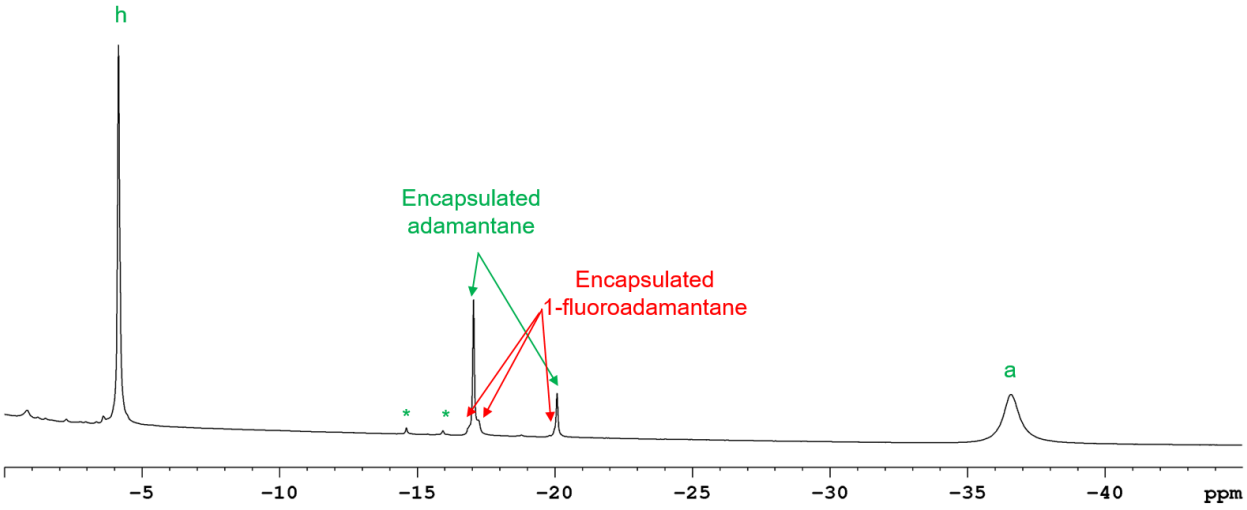

Figure S63. Paramagnetic ^{1}H NMR spectrum of [1-fluoroadamantane ⊂ **1**](OTf)$_8$ in the presence of a competing guest, adamantane, in CD_3CN at 298 K. Green labels refer to [adamantane ⊂ **1**](OTf)$_8$, * refers to encapsulation of impurities in adamantane and red labels refer to [1-fluoroadamantane ⊂ **1**](OTf)$_8$.

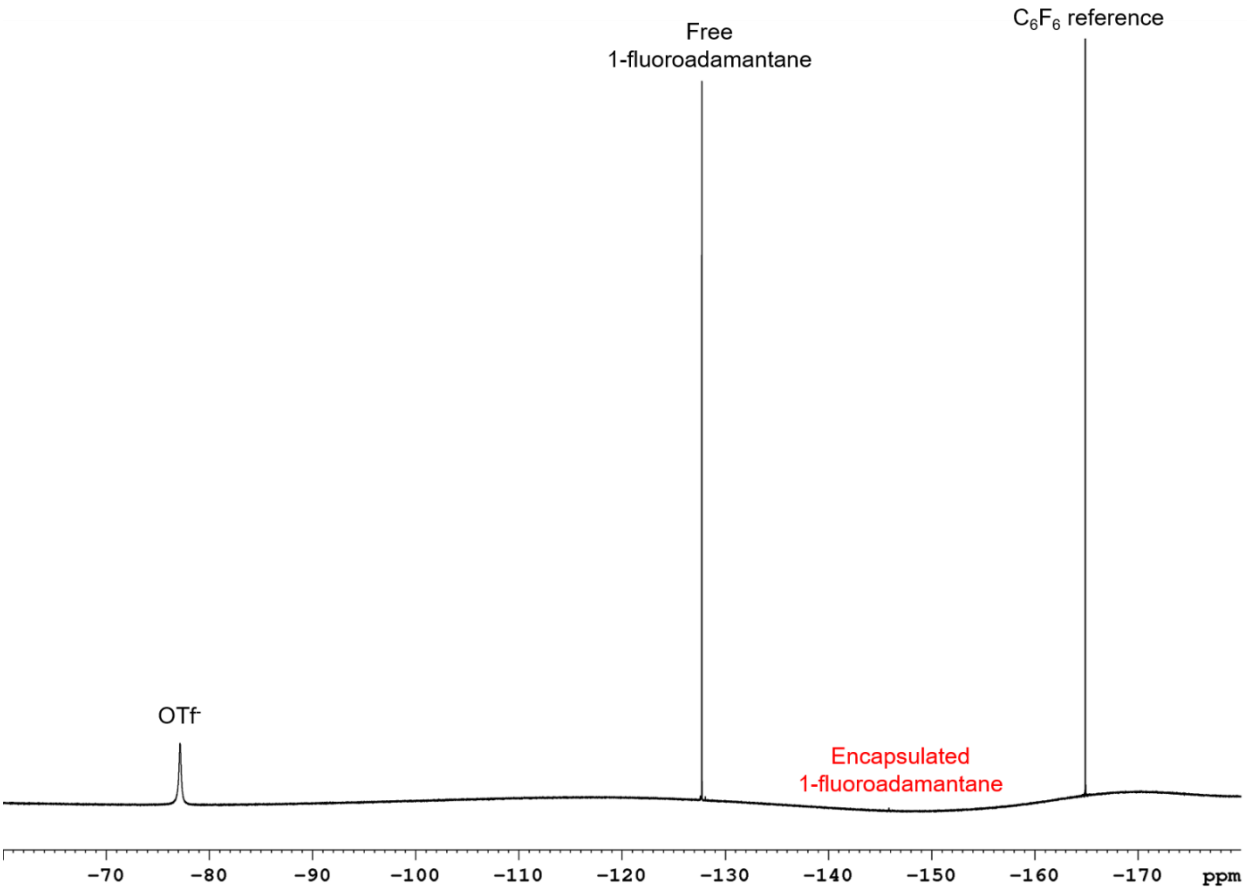

Figure S64. ^{19}F NMR spectrum of [1-fluoroadamantane $\subset$ **1**](OTf)$_8$ in the presence of a competing guest, adamantane, in CD_3CN at 298 K.

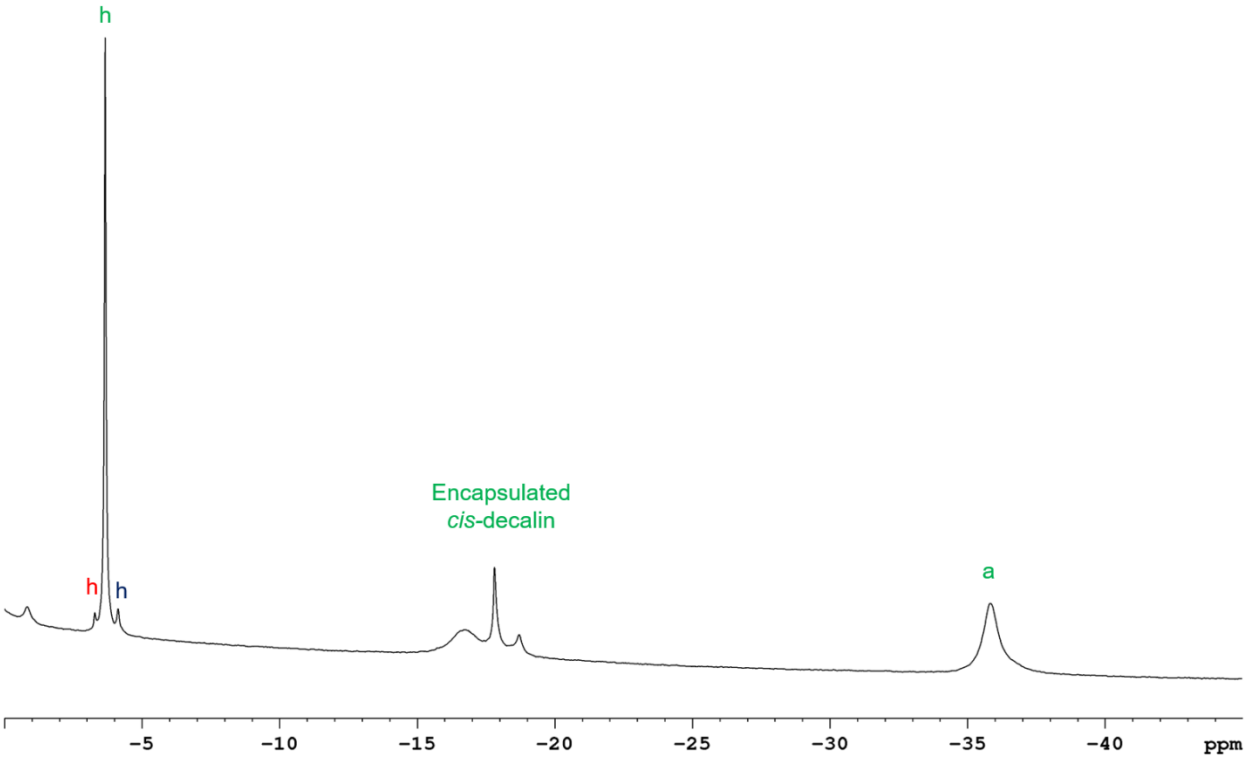

Figure S65. Paramagnetic ^{1}H NMR spectrum of [*trans*-decalin ⊂ **1**](OTf)$_8$ in the presence of a competing guest, *cis*-decalin, in CD_3CN at 298 K. Red labels refer to [*trans*-decalin ⊂ **1**](OTf)$_8$, green labels refer to [*cis*-decalin ⊂ **1**](OTf)$_8$ and blue labels refer to empty cage **1**.

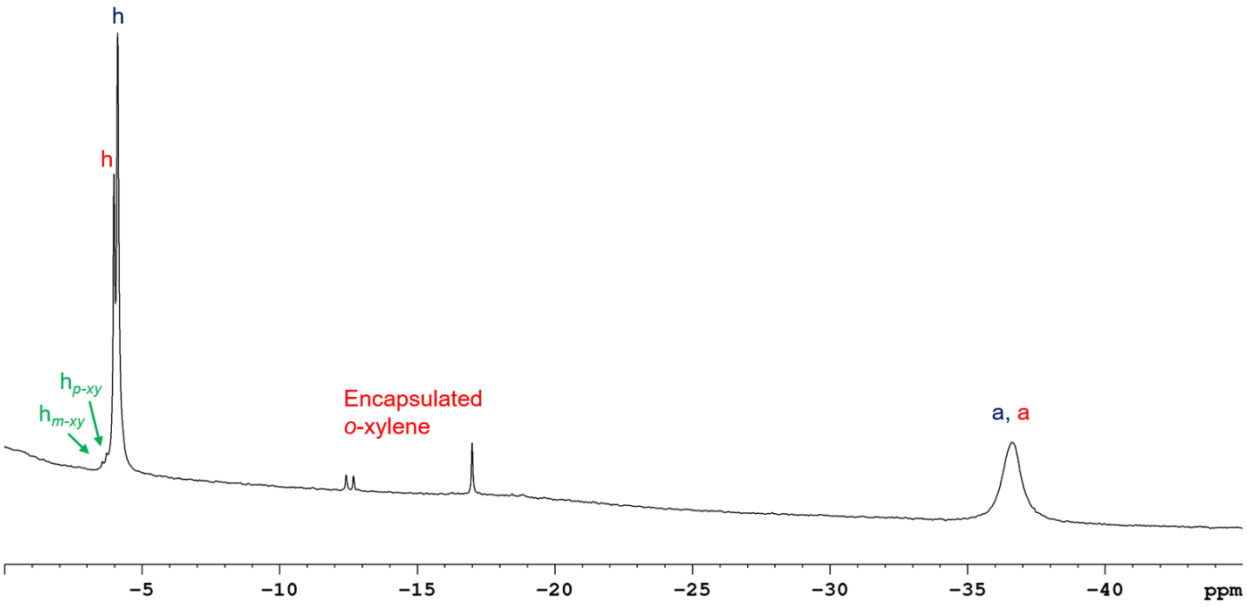

Figure S66. Paramagnetic ^{1}H NMR spectrum of cage **1** equilibrated with a 1:1:1 mixture of *m*-, *o*-, and *p*-xylene showing the selective binding of *o*-xylene (red labels) with trace binding of *m*- and *p*-xylene (green labels) and empty cage (blue labels) in CD_3CN at 298 K.

5 Transformation from Cage 1 to Cage 2

5.1 In the Absence of a Guest

In a glovebox, 24 equivalents of 2-formylpyridine (2.28 µL) was added to a 2 mM solution of cage **1** in CD_3CN (0.5 mL) in a J Young NMR tube. The NMR tube was sealed and left to equilibrate for 16 h at 323 K and a colour change from orange to red-purple was observed. ^1H, paramagnetic ^1H and ^{19}F NMR spectra were recorded. In a glovebox, D_2O (25 µL, 5% v/v) was added to the solution, the J Young tube was sealed and left to equilibrate at 323 K for 1 day. NMR spectra were recorded periodically to monitor the equilibration process.

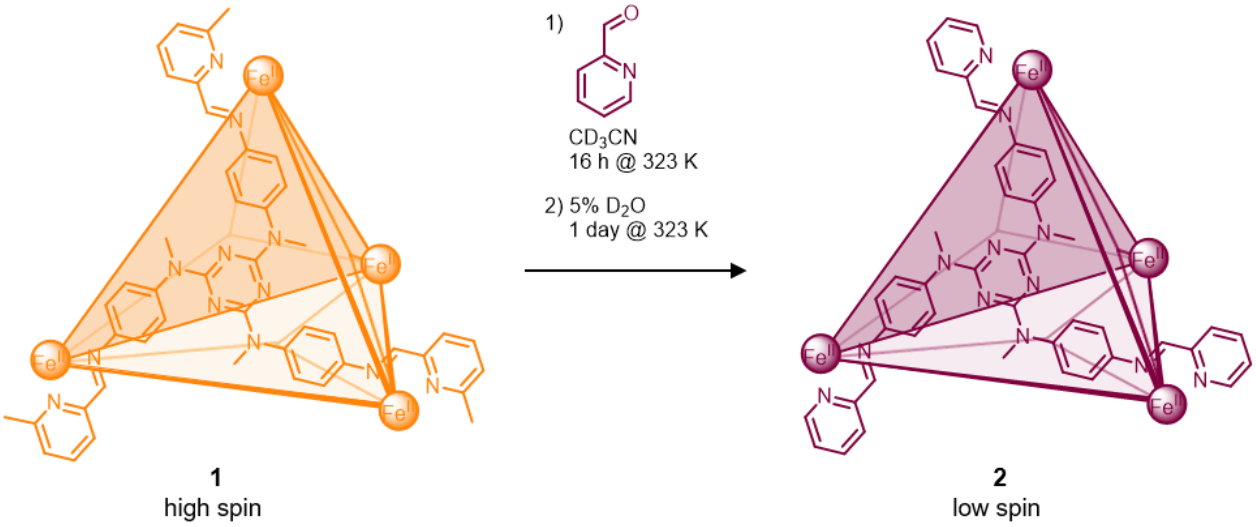

Scheme S2. Transformation from **1** to **2** induced by aldehyde exchange of 2-formyl-6-methylpyridine for 2-formylpyridine.

Figure S67. High spin cage **1** (left) and transformation to low spin cage **2** (right) after addition of 2-formylpyridine and D_2O to cage **1**.

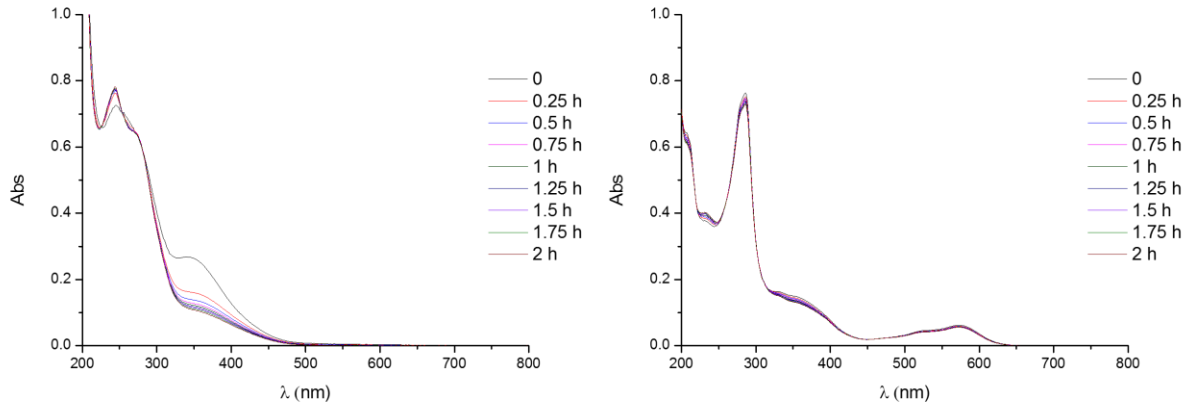

Figure S68. UV/visible spectra of cage **1** (left) and cage **2** (right) showing the stability of the cages over 2 hours at a concentration of 3 μM in CH_3CN at 298 K. The sample of cage **1** was prepared using anhydrous CH_3CN in a glovebox.

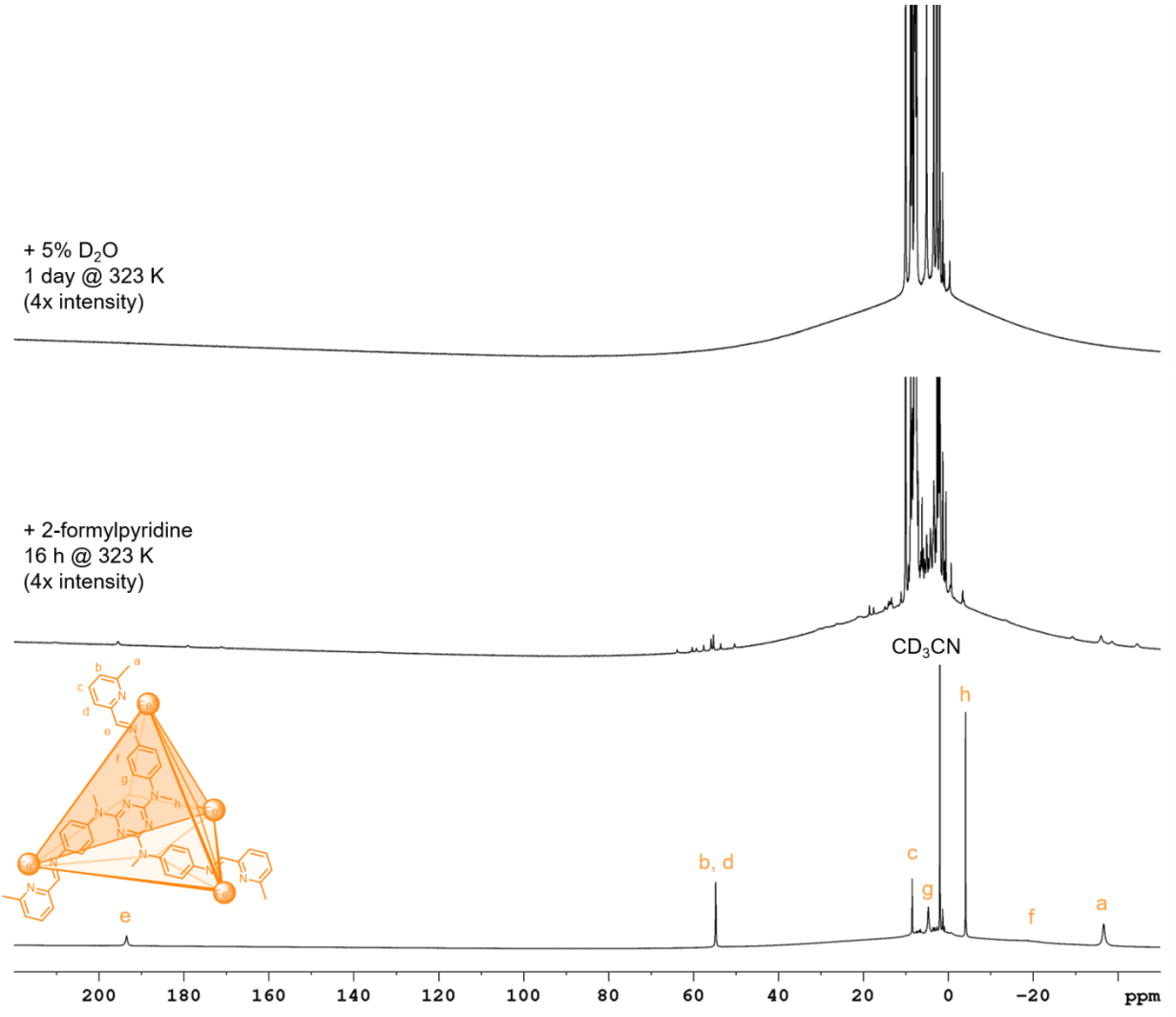

Figure S69. Paramagnetic ^{1}H NMR spectra of the transformation from cage **1** (orange labels) to cage **2** upon sequential addition of 24 eq. of 2-formylpyridine and 5% D_2O and heating at 323 K in CD_3CN.

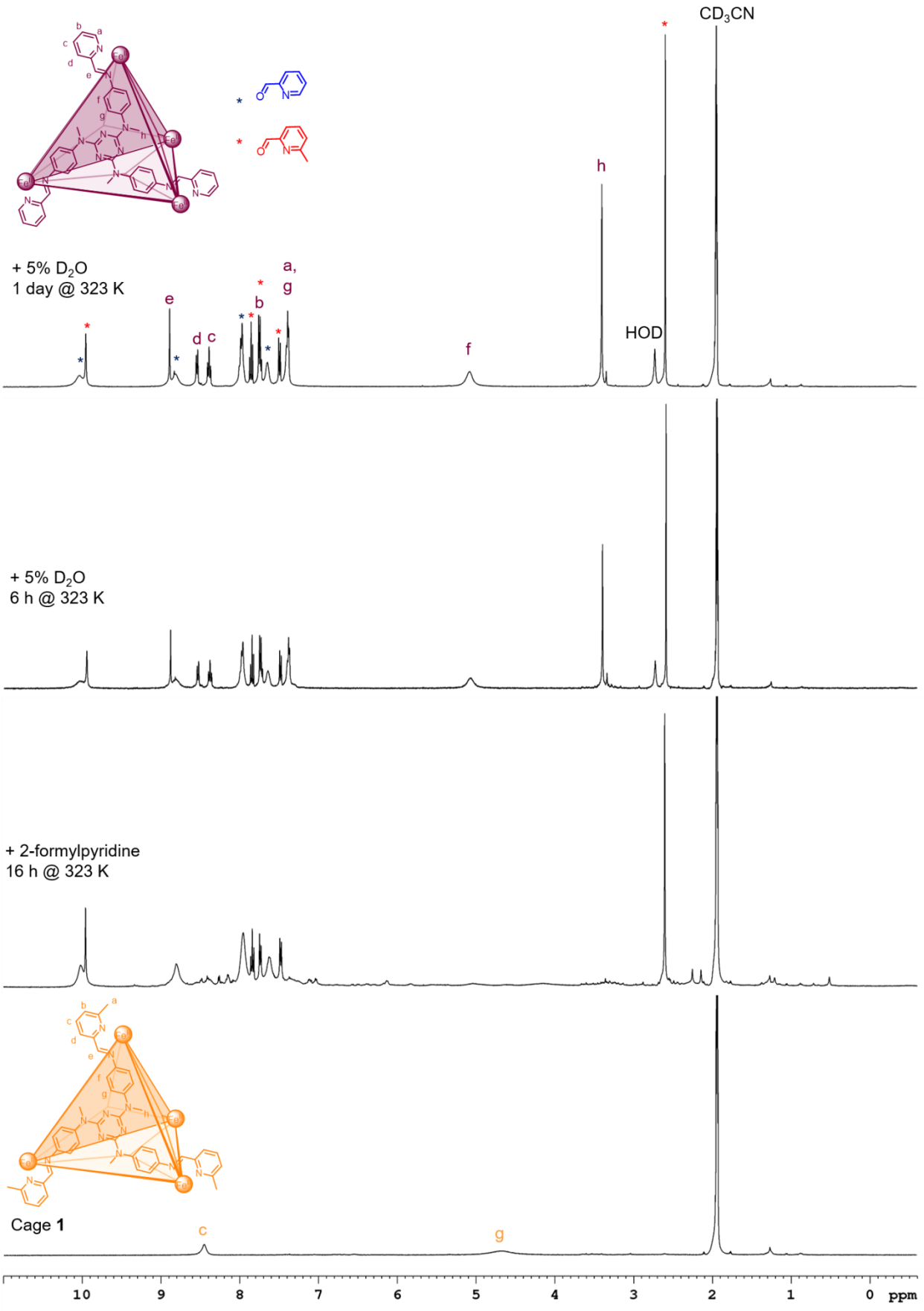

Figure S70. ^{1}H NMR spectra for the transformation from cage **1** (orange labels) to cage **2** (purple labels) upon sequential addition of 24 eq. of 2-formylpyridine and 5% D_2O and heating at 323 K in CD_3CN.

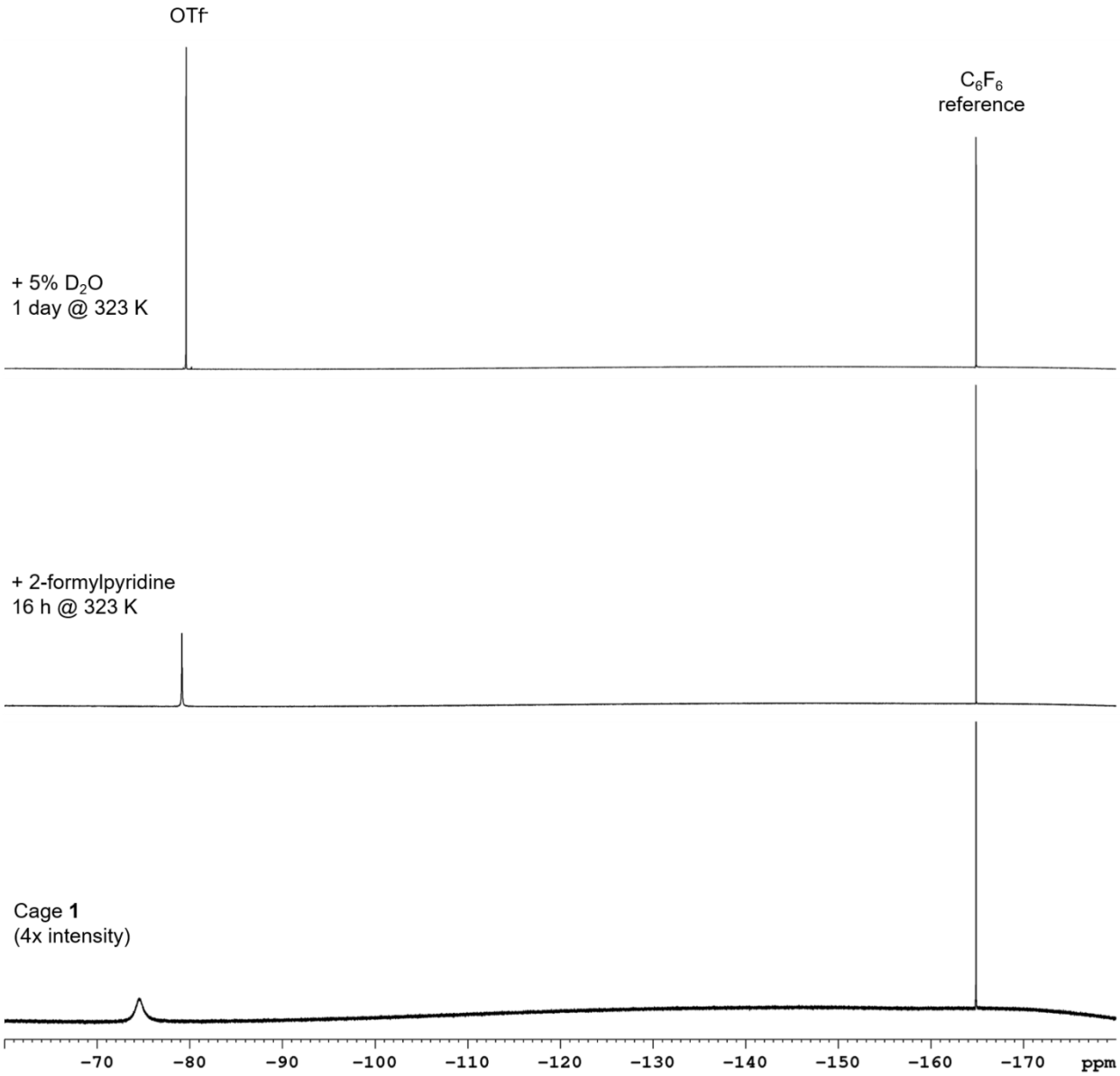

Figure S71. ^{19}F NMR spectra of the transformation from cage **1** to cage **2** upon sequential addition of 24 eq. of 2-formylpyridine and 5% D_2O and heating at 323 K in CD_3CN.

5.2 In the Presence of a Guest, 1-Fluoroadamantane

In a glovebox, 1-fluoroadamantane (1.55 mg, 0.01 mmol) was added to a 2 mM solution of cage **1** (4.42 mg, 0.001 mmol) in CD_3CN (0.5 mL) and the mixture was left to equilibrate at room temperature for at least 4 hours. 2-Formylpyridine (24 eq., 2.28 µL) was added to the host-guest complex and the mixture was left to equilibrate for 16 h at 323 K. D_2O (25 µL, 5% v/v) was then added to the solution and the solution was left to equilibrate at 323 K for several days. NMR spectra were recorded periodically to monitor the equilibration process.

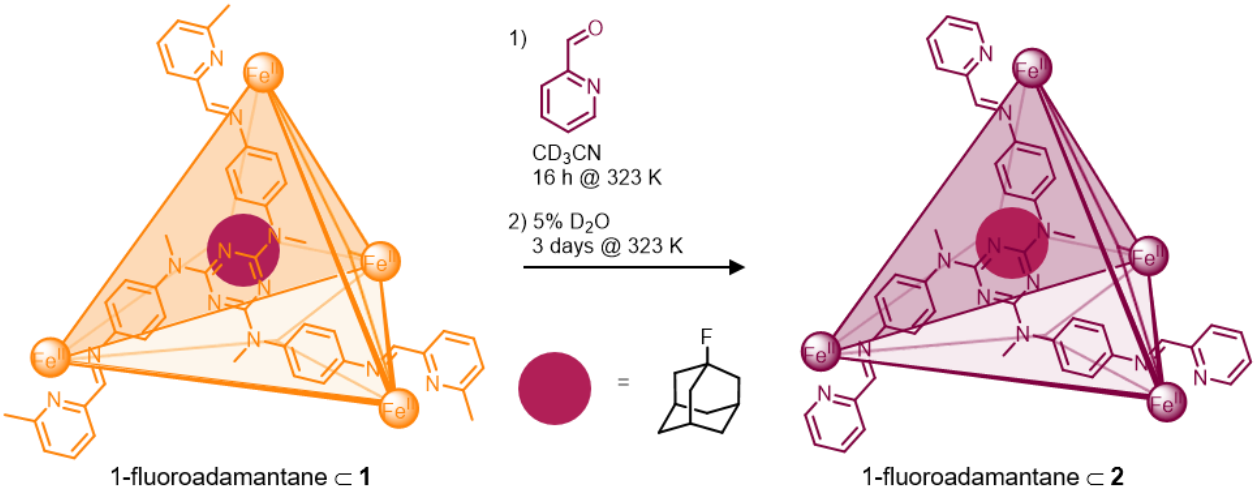

Scheme S3. Transformation from **1** to **2** in the presence of a guest, 1-fluoroadamantane, induced by aldehyde exchange of 2-formyl-6-methylpyridine for 2-formylpyridine.

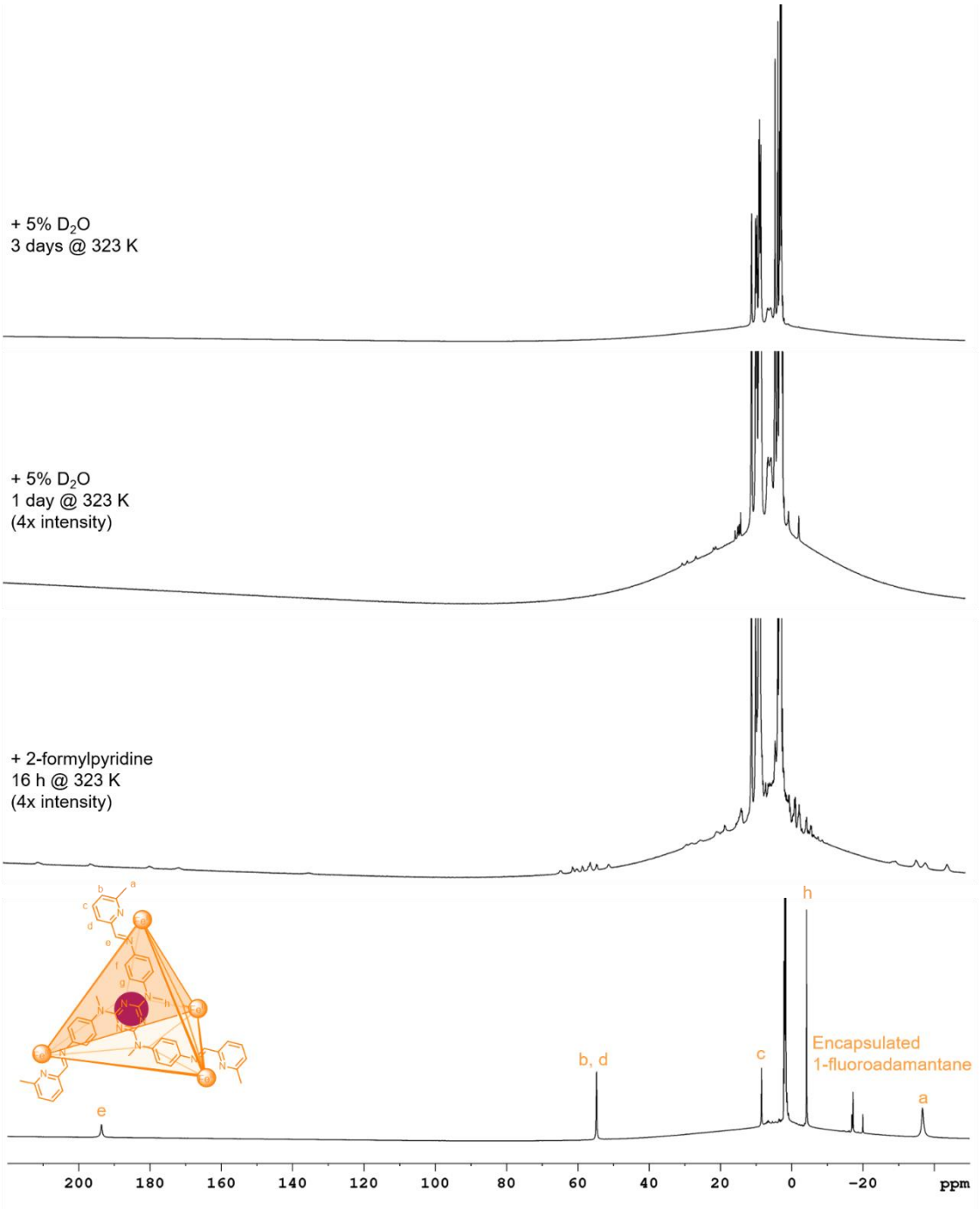

Figure S72. Paramagnetic ^{1}H NMR spectra of the transformation from [1-fluoroadamantane ⊂ **1**]$^{8+}$ (orange labels) to [1-fluoroadamantane ⊂ **2**]$^{8+}$ upon sequential addition of 24 eq. of 2-formylpyridine and 5% D_2O and heating at 323 K in CD_3CN.

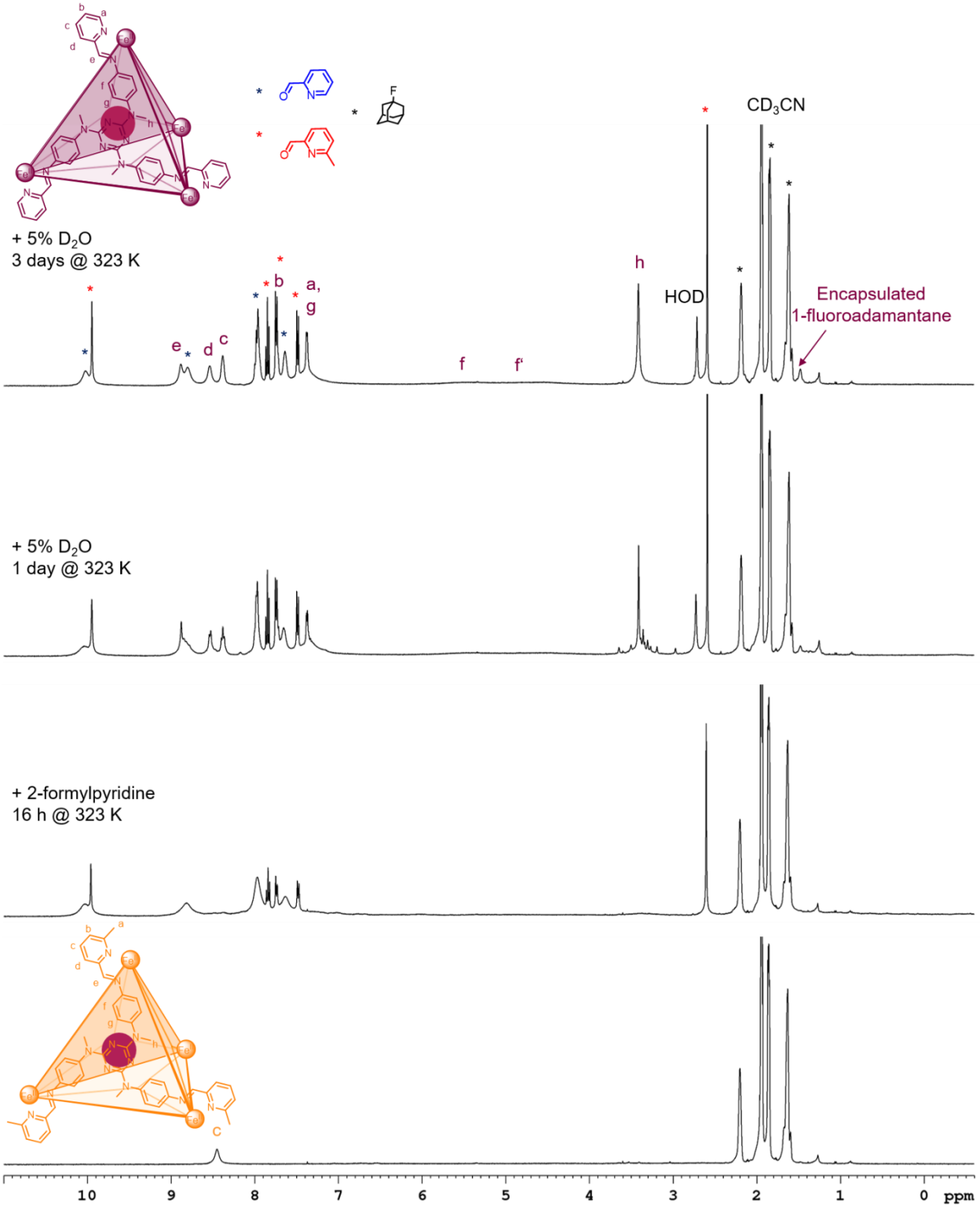

Figure S73. ^{1}H NMR spectra for the transformation from [1-fluoroadamantane ⊂ **1**]$^{8+}$ (orange labels) to [1-fluoroadamantane ⊂ **2**]$^{8+}$ (purple labels) upon sequential addition of 24 eq. of 2-formylpyridine and 5% D_2O and heating at 323 K in CD_3CN.

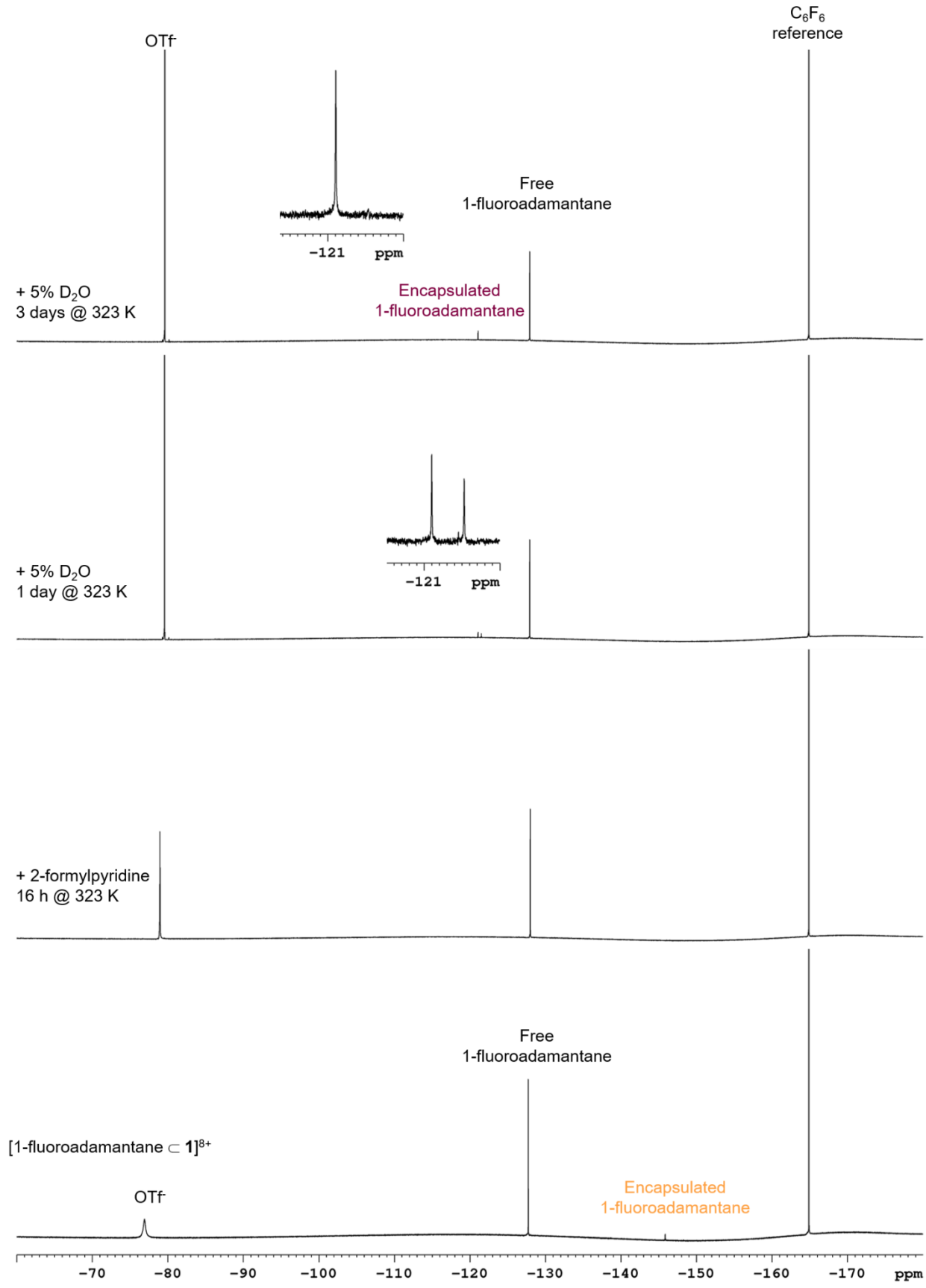

Figure S74. ^{19}F NMR spectra of the transformation from [1-fluoroadamantane ⊂ **1**]$^{8+}$ (orange labels) to [1-fluoroadamantane ⊂ **2**]$^{8+}$ (purple labels) upon sequential addition of 24 eq. of 2-formylpyridine and 5% D_2O and heating at 323 K in CD_3CN.

The equilibration process was slower for the full than for the empty cage, with kinetics depending on the amount of water added: equilibration approached completion on a time scale of more than 10 days for 2% D_2O, 3 days for 5% D_2O and 1 day for 10% D_2O (Figure S75).

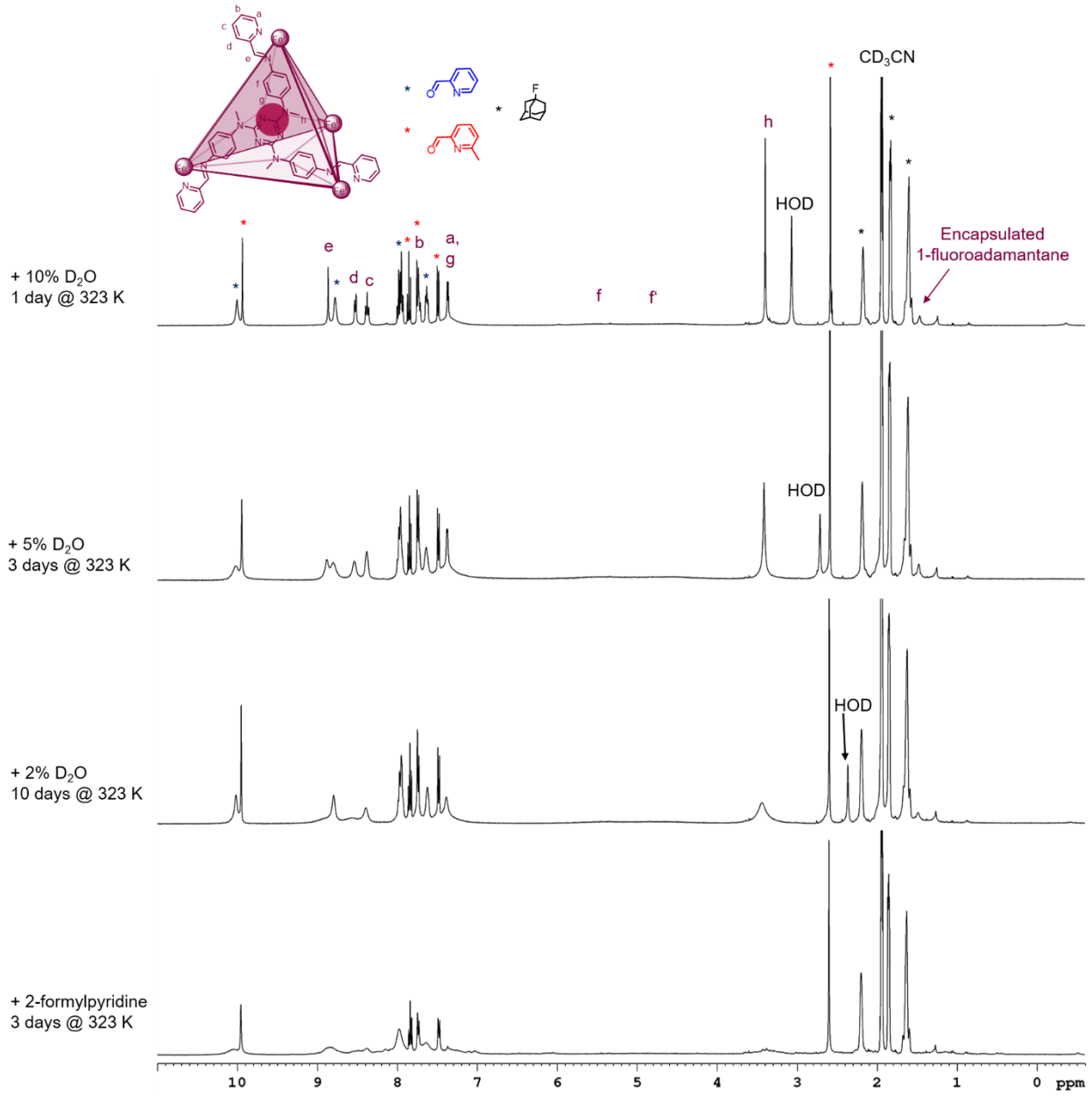

Figure S75. ^{1}H NMR spectra for the transformation from [1-fluoroadamantane ⊂ **1**]$^{8+}$ to [1-fluoroadamantane ⊂ **2**]$^{8+}$ upon heating at 323 K following addition of 24 eq. of 2-formylpyridine then addition of 2, 5 or 10% D_2O in CD_3CN.

6 Cage 2

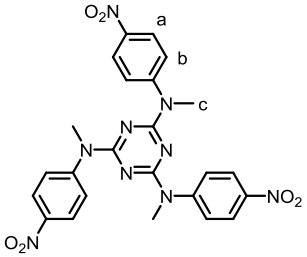

Ligand **A** and cage **2** were prepared according to literature procedures, which were modified as specified below.[2]

6.1 *N*2,*N*4,*N*6-Trimethyl-*N*2,*N*4,*N*6-tris(4-nitrophenyl)-1,3,5-triazine-2,4,6-triamine

Modified literature procedure:[2] Cyanuric chloride (0.369 g, 2.00 mmol), *N*-methyl-4-nitroaniline (1.07 g, 7.00 mmol), and dioxane (10 mL) were combined in a microwave vial. The reaction mixture was

microwaved for 20 minutes at 120 °C. The resulting off-white solid was washed with water (100 mL), methanol (300 mL), and diethyl ether (70 mL) to give the desired product in 78% yield (0.832 g, 1.57 mmol).

Spectroscopic data were consistent with those reported in the literature.[2]

^{1}H NMR (500 MHz, CD_2Cl_2, 298 K) δ (ppm): 8.14 (d, ^{3}J = 9.1 Hz, 6H, H_a), 7.50 (d, ^{3}J = 9.1 Hz, 6H, H_b), 3.47 (s, 9H, H_c)

^{13}C NMR (125 MHz, CD_2Cl_2, 298 K) δ (ppm): 165.5, 150.6, 144.5, 126.3, 124.0, 37.3

6.2 Cage 2 Synthesis

Modified literature procedure:[2] In a glovebox, $Fe(OTf)_2$ (28.3 mg, 0.08 mmol), ligand **A** (35.3 mg, 0.08 mmol) and 2-formylpyridine (22.8 µL, 0.24 mmol) were combined with degassed MeCN (10 mL). The mixture was stirred at room temperature for 21 h. The reaction mixture was added dropwise to diethyl ether (60 mL) to precipitate **2** and the mixture was centrifuged, the supernatant decanted and the solid was washed with diethyl ether two times. The purple solid was dried *in vacuo* to give **2** (60.3 mg, 82%).

^{1}H NMR (400 MHz, CD_3CN, 298 K) δ (ppm): 8.91 (s, 12H, H_f), 8.55 (d, ^{3}J = 7.44 Hz, 12H, H_d), 8.39 (unresolved dd, 12H, H_c), 7.74 (unresolved dd, 12H H_b), 7.45 – 7.36 (m, 36H, H_a, H_i), 5.08 (bs, 24H, H_h), 3.41 (s, 36H, H_k)

^{13}C NMR (125 MHz, CD_3CN, 298 K) δ (ppm): 175.9 (C_f), 165.5 (C_l), 159.4 (C_e), 156.8 (C_a), 146.4 (C_g), 145.3 (C_j), 140.6 (C_c), 132.0 (C_d), 130.5 (C_b), 126.1 (C_i), 122.0 (C_h), 38.1 (C_k)

6.3 NMR Spectra

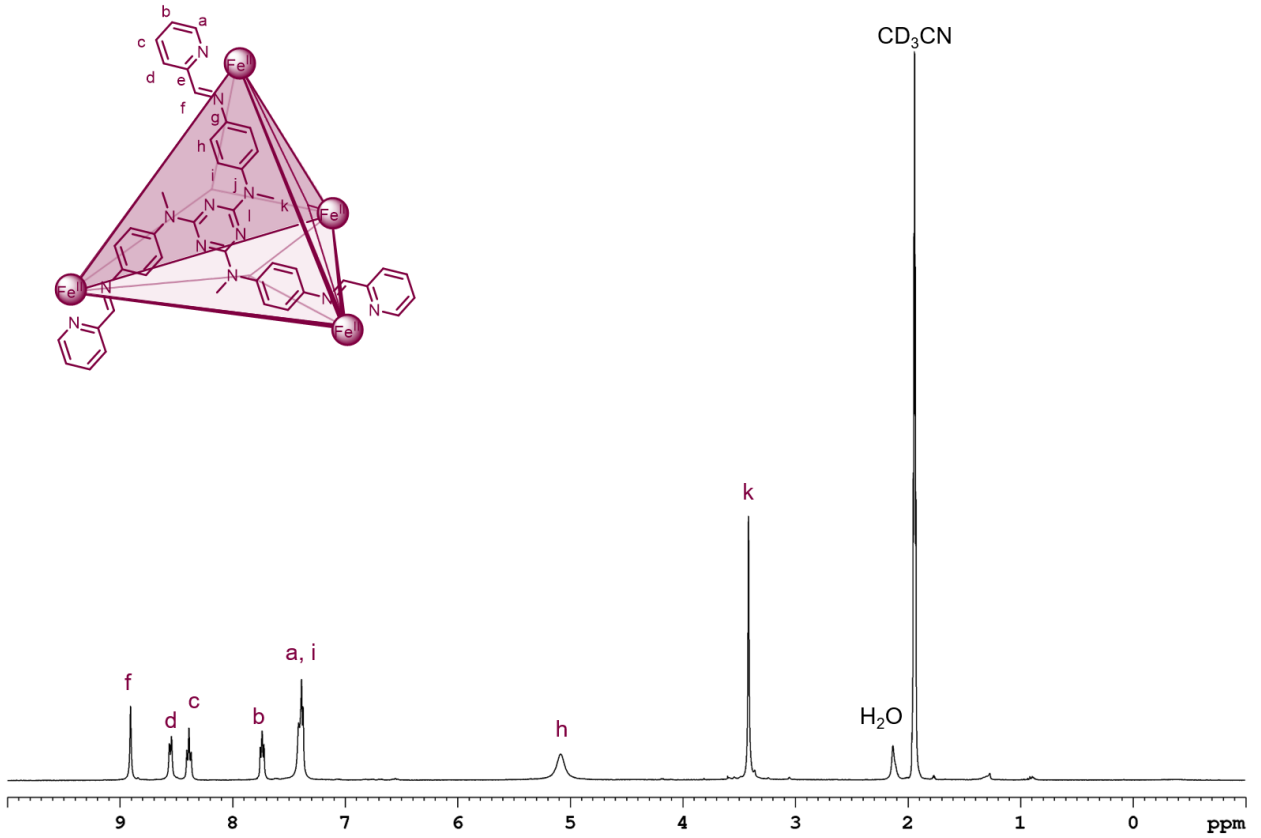

Figure S76. ^{1}H NMR spectrum of [**2**](OTf)$_8$ in CD_3CN at 298 K.

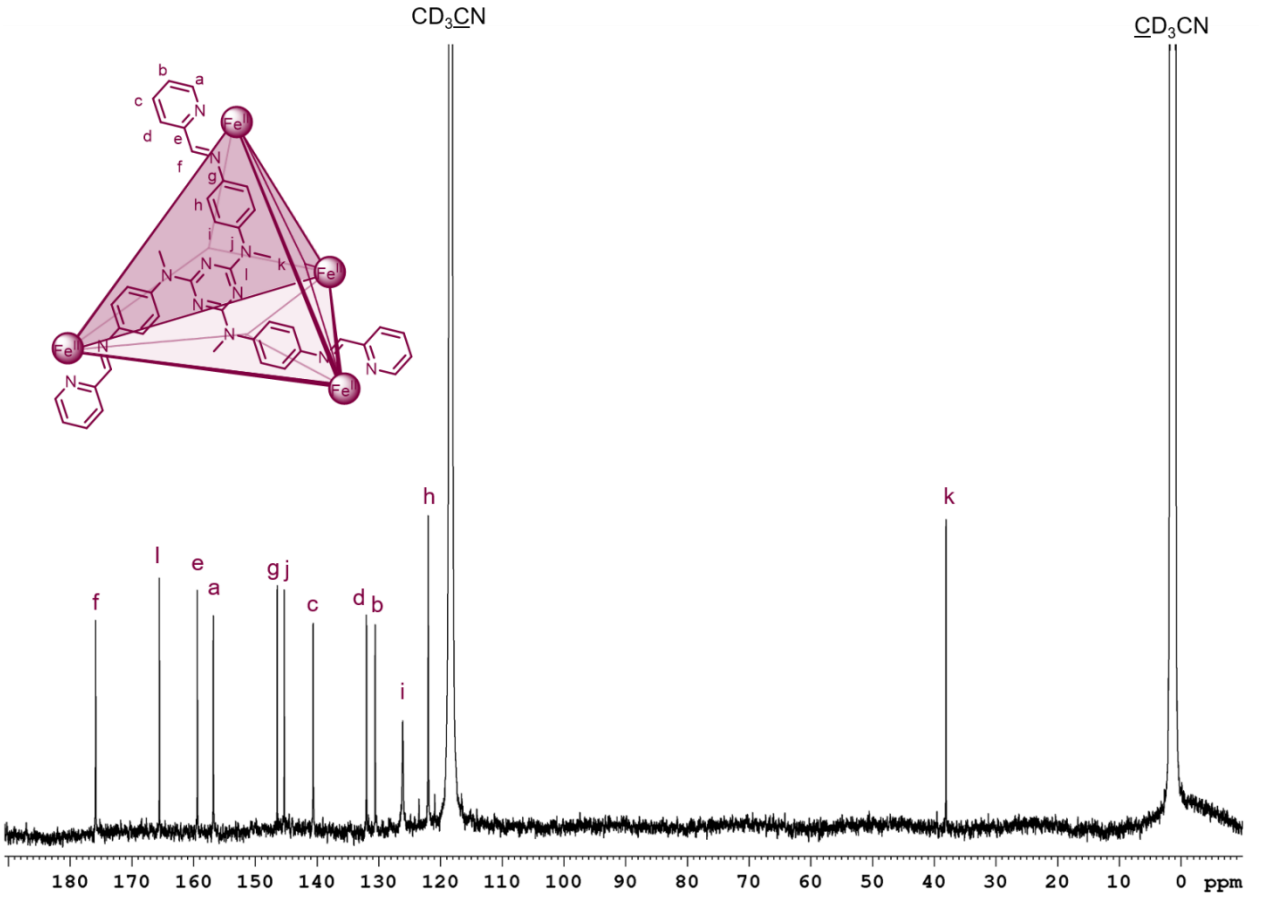

Figure S77. ^{13}C NMR spectrum of [**2**](OTf)$_8$ in CD_3CN at 298 K.

6.4 Host-Guest Complex with 1-Fluoroadamantane

10-15 equivalents of the guest were added to a 2 mM solution of cage **2** in CD_3CN (0.5 mL) and the solution was left to equilibrate at 298 K for at least 3 days.

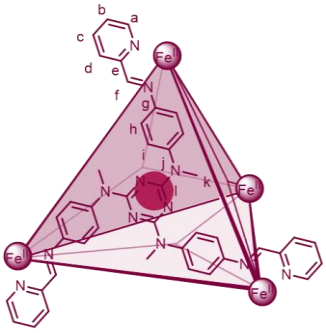

^{1}H NMR (400 MHz, CD_3CN, 298 K) δ (ppm): 8.91 (bs, 12H, H_f), 8.56 (b, 12H, H_d), 8.39 (b, 12H, H_c), 7.74 (bt, 12H, H_b), 7.51 – 7.21 (m, 36H, H_a, H_i), 5.45 (b, 12H, H_h), 4.58 (b, 12H, $H_{h'}$), 3.44 (b, 36H, H_k), 2.16 (b, 3H, encapsulated 1-fluoroadamantane overlapped with free 1-fluoroadamantane and H_2O), 1.89 – 1.58 (b, 6H, encapsulated 1-fluoroadamantane overlapped with free 1-fluoroadamantane), 1.49 (b, 6H, encapsulated 1-fluoroadamantane)

^{13}C NMR (125 MHz, CD_3CN, 298 K) δ (ppm): 176.0 (C_f), 165.5 (C_l), 159.4 (C_e), 156.8 (C_a), 146.5 (C_g), 145.1 (C_j), 140.7 (C_c), 132.0 (C_d), 130.5 (C_b), 126.0 (C_i), 121.9 (C_h), 43.3 (encapsulated 1-fluoroadamantane), 38.3 (C_k), 35.4 (encapsulated 1-fluoroadamantane), 32.2 (encapsulated 1-fluoroadamantane)

Assignments of quaternary cage carbons are based on assignments for other host-guest complexes for cage **2**[2] since cross-peaks in the HMBC were not observed, most likely due to the broadness of the signals in the ^{1}H NMR spectrum. For this reason, it was also not possible to assign the quaternary carbon signals for the encapsulated 1-fluoroadamantane guest.

^{19}F NMR (376 MHz, CD_3CN, 298 K, referenced to C_6F_6) δ (ppm): -79.6 (OTf^-), -121.1 (encapsulated 1-fluoroadamantane), -128.2 (free 1-fluoroadamantane)

ESI-MS *m/z*: 480.3 [1-fluoroadamantane ⊂ **2** + OTf]$^{7+}$, 585.1 [1-fluoroadamantane ⊂ **2** + 2OTf]$^{6+}$, 731.9 [1-fluoroadamantane ⊂ **2** + 3OTf]$^{5+}$, 952.2 [1-fluoroadamantane ⊂ **2** + 4OTf]$^{4+}$, 1319.3 [1-fluoroadamantane ⊂ **2** + 5OTf]$^{3+}$

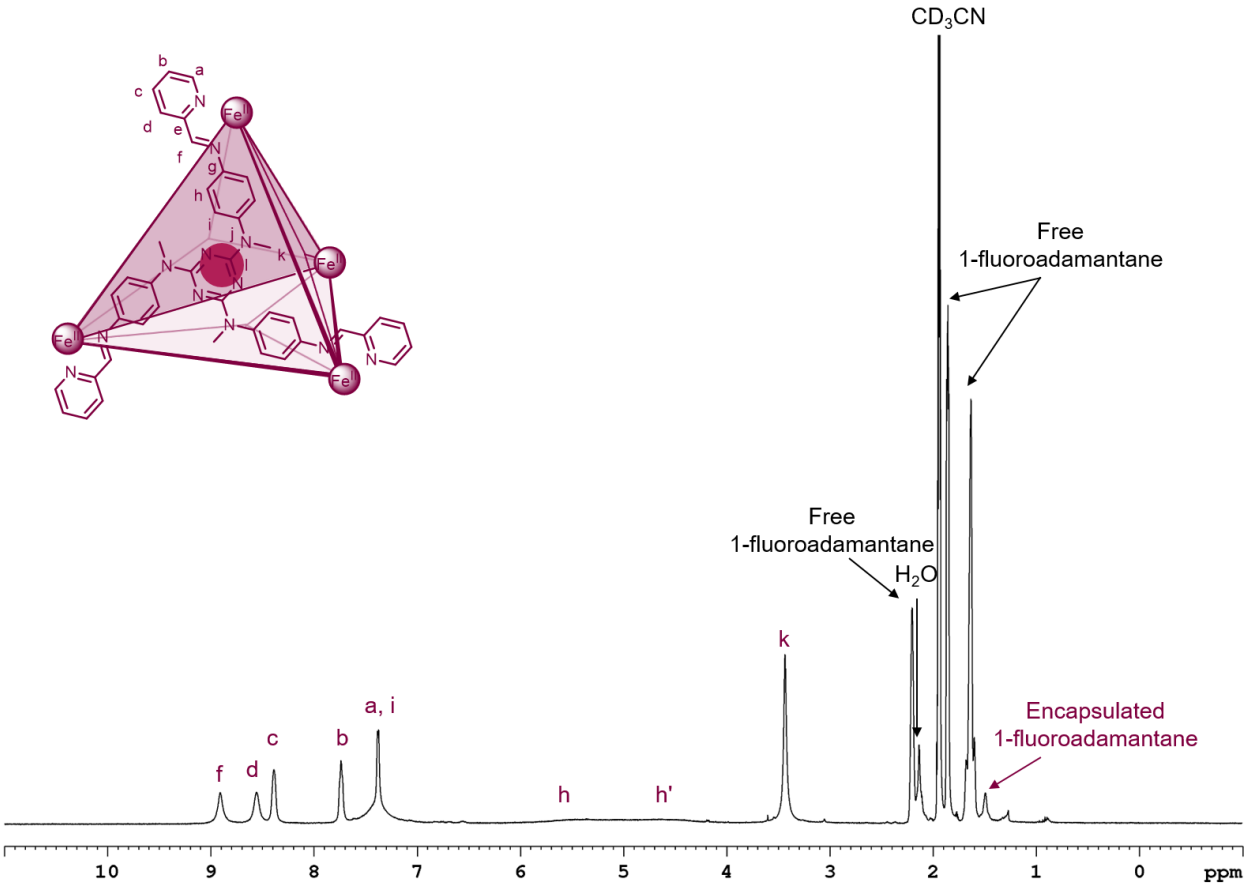

Figure S78. ^{1}H NMR spectrum of [1-fluoroadamantane ⊂ **2**](OTf)$_8$ in CD_3CN at 298 K.

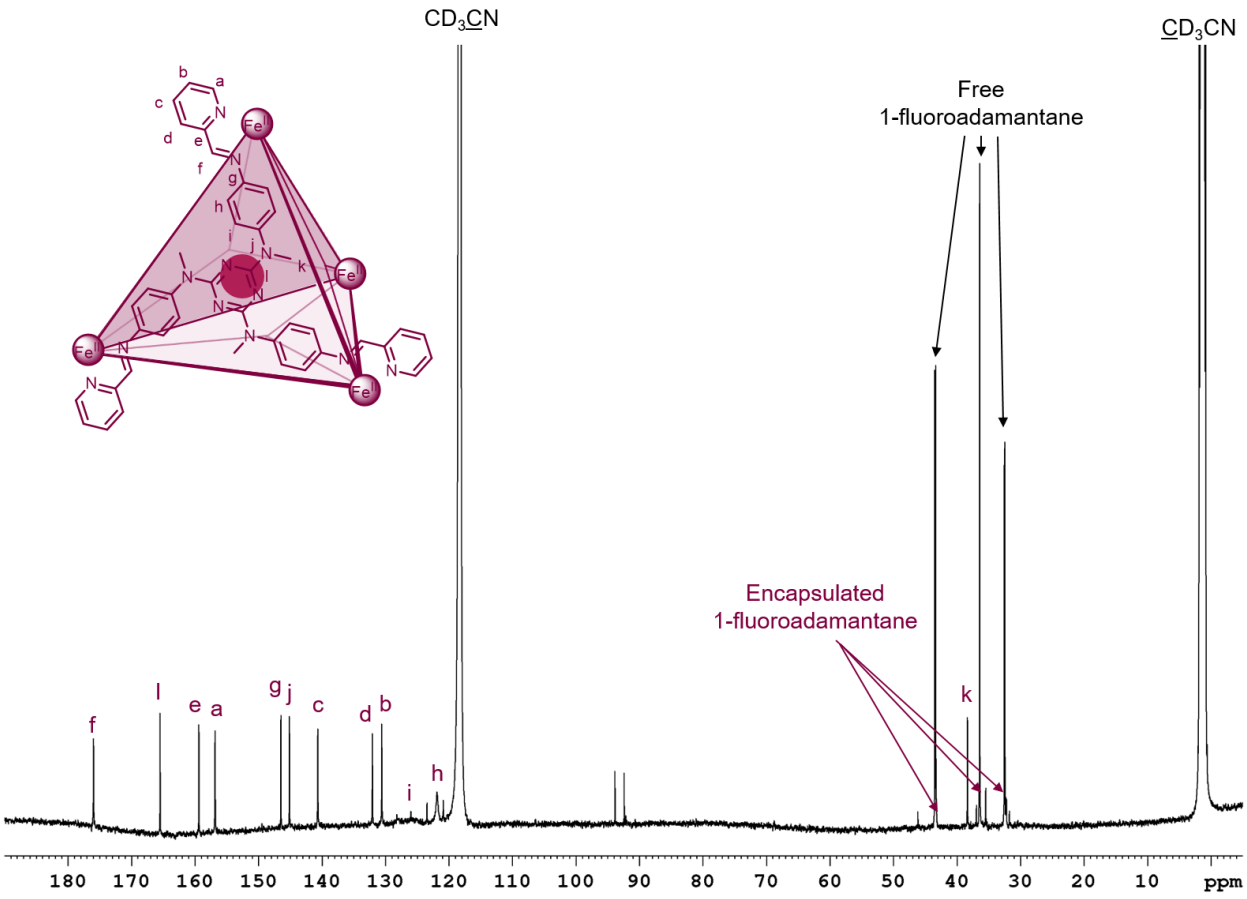

Figure S79. ^{13}C NMR spectrum of [1-fluoroadamantane ⊂ **2**](OTf)$_8$ in CD_3CN at 298 K.

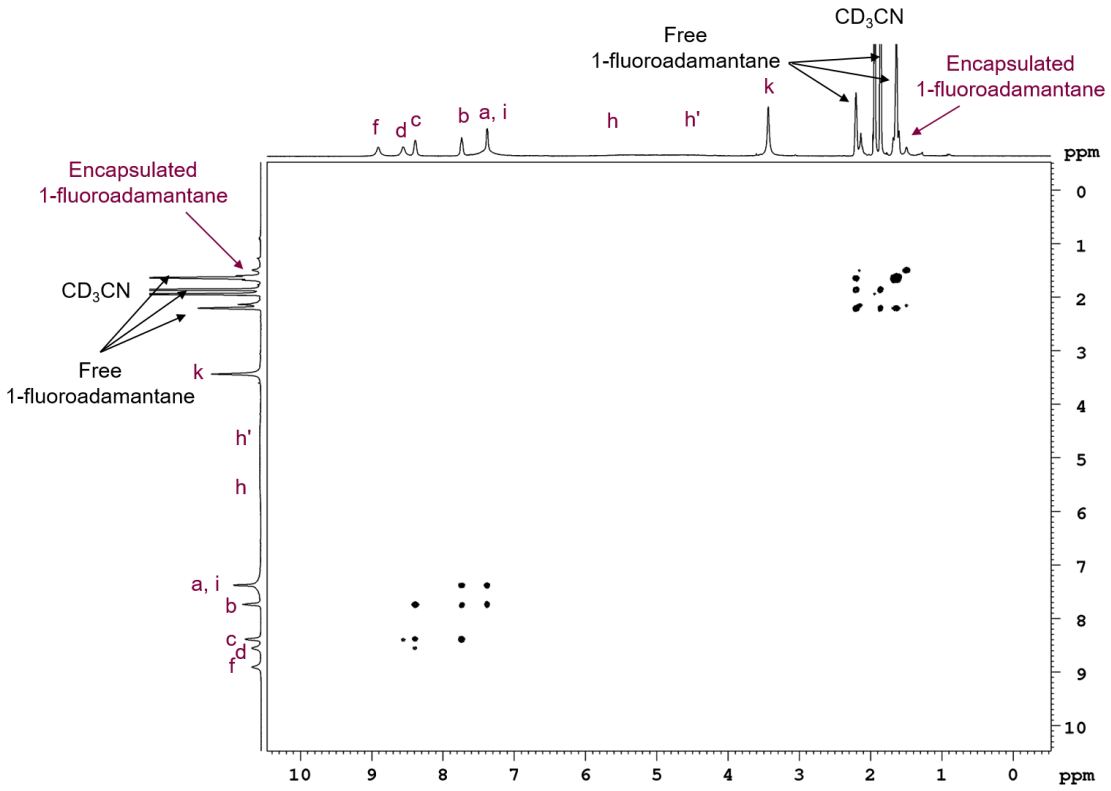

Figure S80. COSY NMR spectrum of [1-fluoroadamantane ⊂ **2**](OTf)$_8$ in CD_3CN at 298 K.

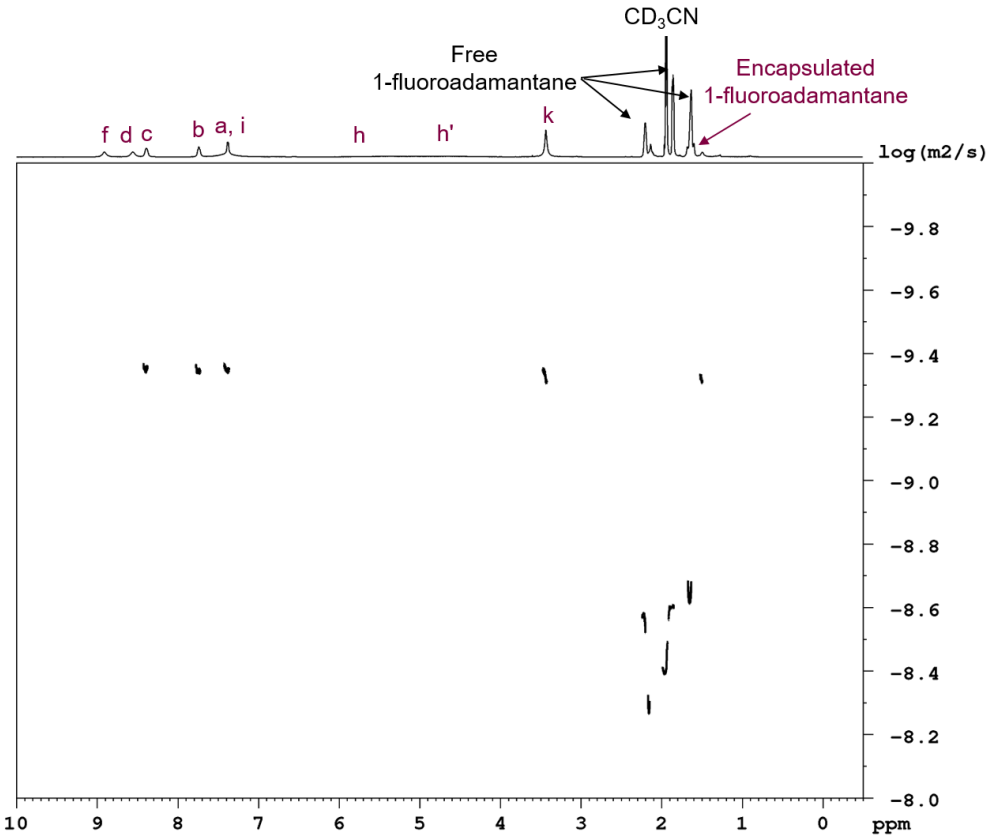

Figure S81. DOSY NMR spectrum of [1-fluoroadamantane ⊂ **2**](OTf)$_8$ in CD_3CN at 298 K.

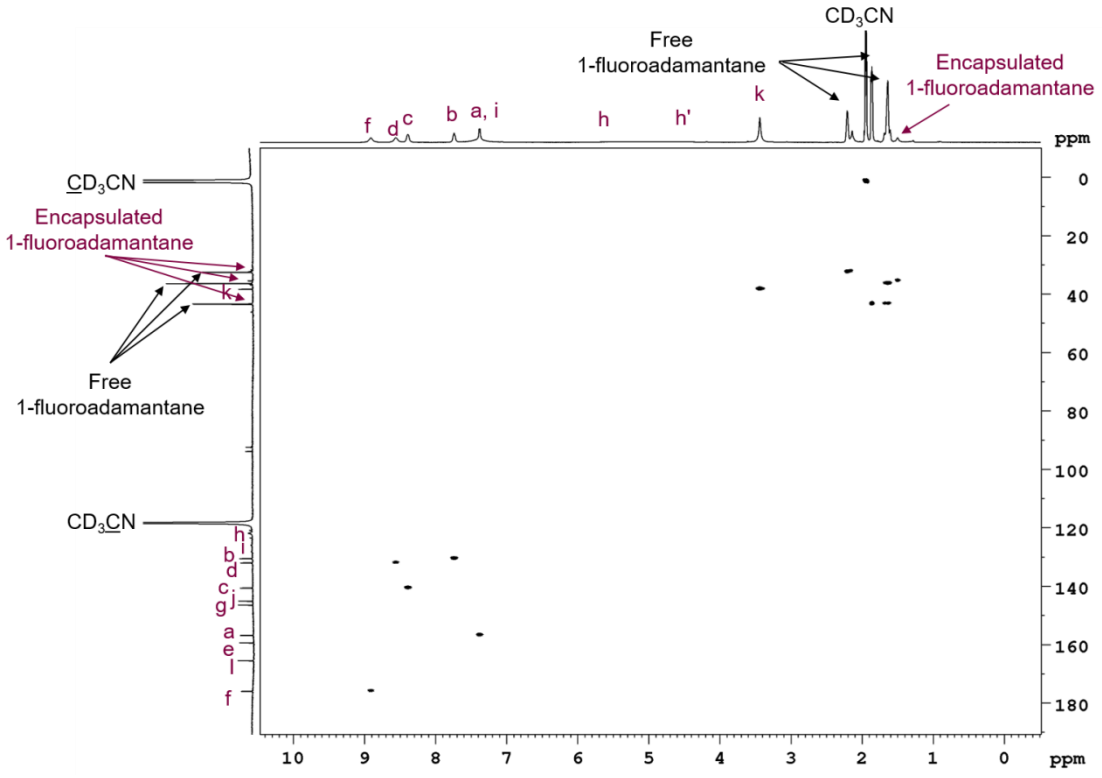

Figure S82. HSQC NMR spectrum of [1-fluoroadamantane ⊂ **2**](OTf)$_8$ in CD_3CN at 298 K.

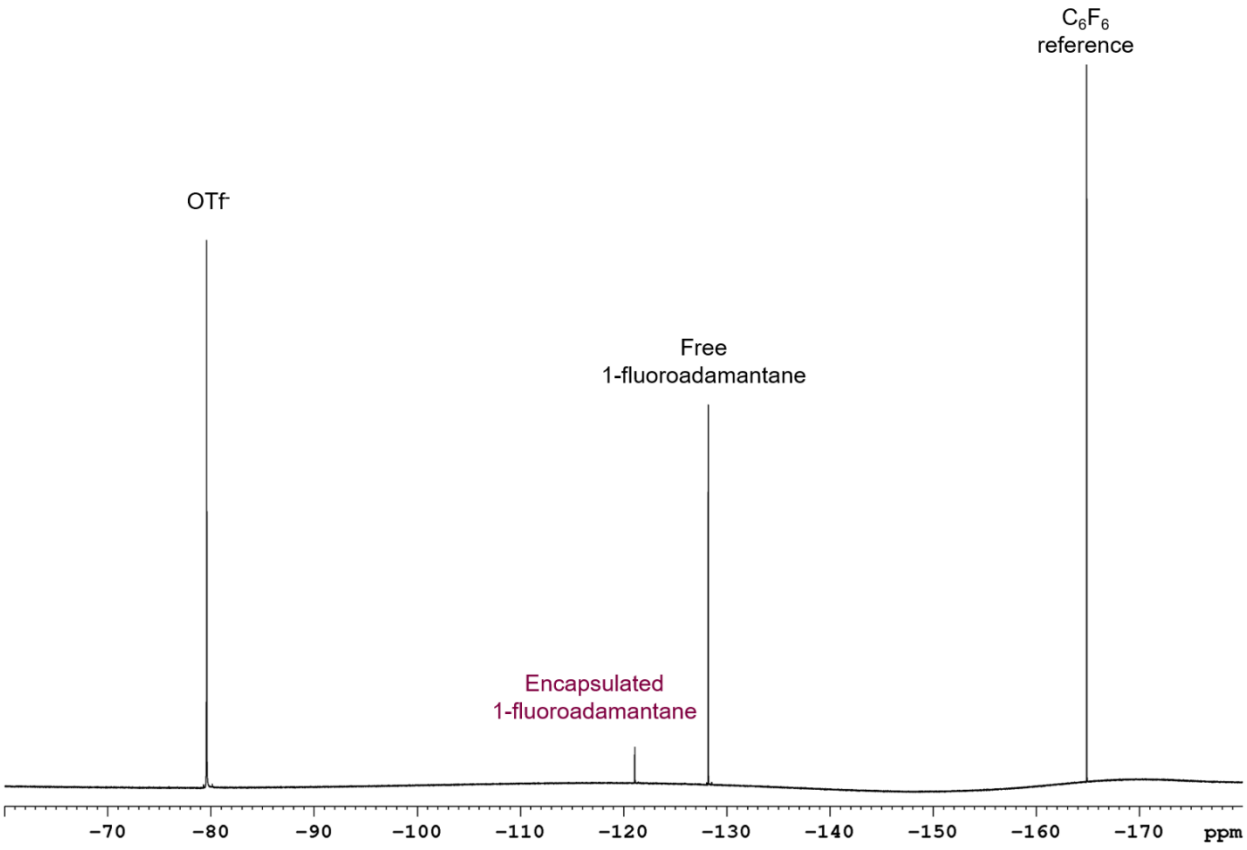

Figure S83. ^{19}F NMR spectrum of [1-fluoroadamantane ⊂ **2**](OTf)$_8$ in CD_3CN at 298 K.

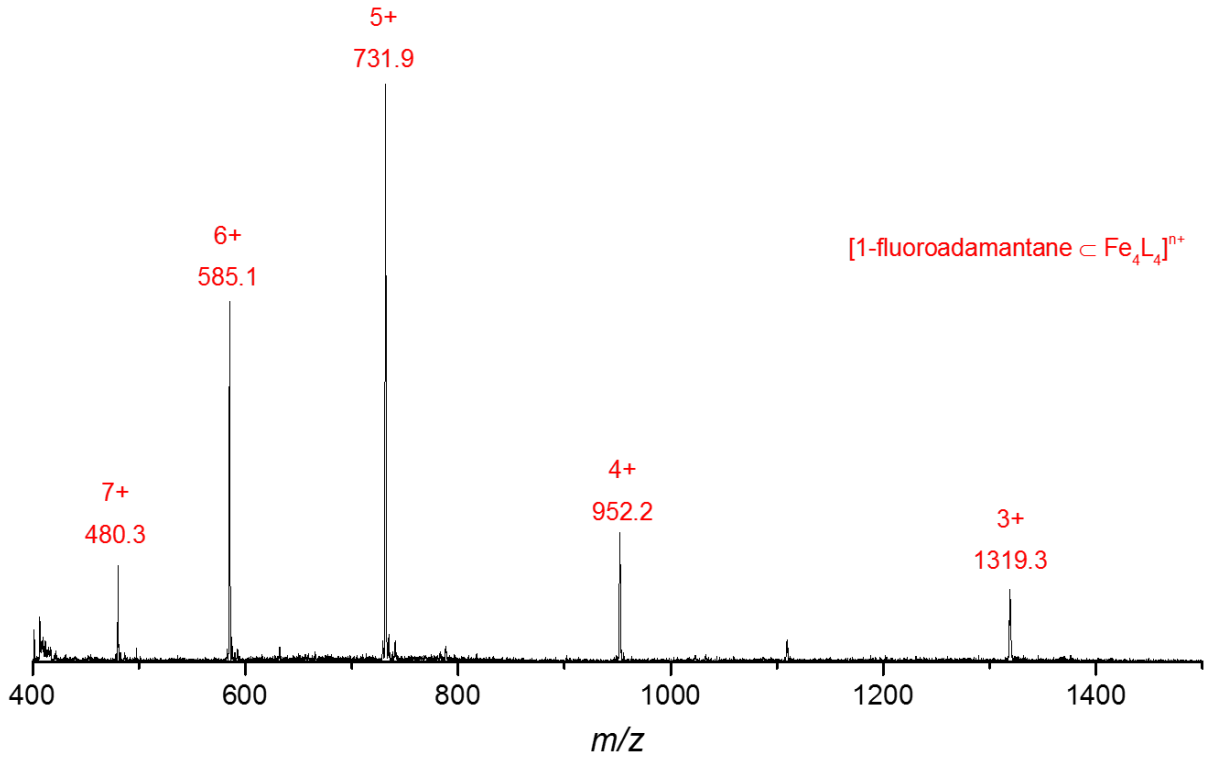

Figure S84. Low resolution ESI-mass spectrum of [1-fluoroadamantane ⊂ **2**](OTf)$_8$.

7 Cage 3

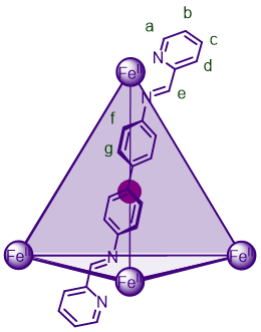

[$BF_4 \subset$ **3**]$(BF_4)_7$ was prepared according to a modified literature procedure[9] where the cage was isolated by precipitation or trituration with diethyl ether.

Spectroscopic data (Figures S93 and S94) were consistent with those reported in the literature.[9] The BF_4^- anion templates the formation of the *T*-symmetric diastereomer. Small peaks in the ^{19}F NMR spectra are attributed to encapsulation of BF_4^- within trace amounts of other diastereomers.

^{1}H NMR (400 MHz, CD_3CN, 298 K) δ (ppm): 8.69 (s, 12H, H_e), 8.39 (d, ^3J = 7.6 Hz, 12H, H_d), 8.35 (t, ^3J = 7.4 Hz, 12H, H_c), 7.78 (unresolved d, 24H, H_g), 7.73 (t, ^3J = 6.4 Hz, 12H, H_b), 7.42 (d, ^3J = 5.4 Hz, 12H, H_a) 5.46 (d, ^3J = 8.2 Hz, 24H, H_f)

^{19}F NMR (376 MHz, CD_3CN, 298 K, referenced to C_6F_6) δ (ppm): -142.33 (encapsulated $^{10}BF_4^-$), -142.39 (encapsulated $^{11}BF_4^-$), -151.89 (free $^{10}BF_4^-$), -151.94 (free $^{11}BF_4^-$)

8 Disassembly of Cages

8.1 Disassembly of [1-Fluoroadamantane ⊂ 1]$^{8+}$ in the Presence of [$BF_4 \subset$ 3]$^{8+}$

In a glovebox, 1-fluoroadamantane (0.79 mg, 0.005 mmol, 10 eq.) was added to a mixture of cage **1** (2.19 mg, 0.0005 mmol) and [$BF_4 \subset$ **3**]$^{8+}$ (1.55 mg, 0.0005 mmol) in CD_3CN (0.5 mL) and the mixture was left to equilibrate at room temperature for 5 hours. *p*-Anisidine (1.47 mg, 0.012 mmol, 24 eq.) was added and the mixture was left to equilibrate at room temperature for 3 days.

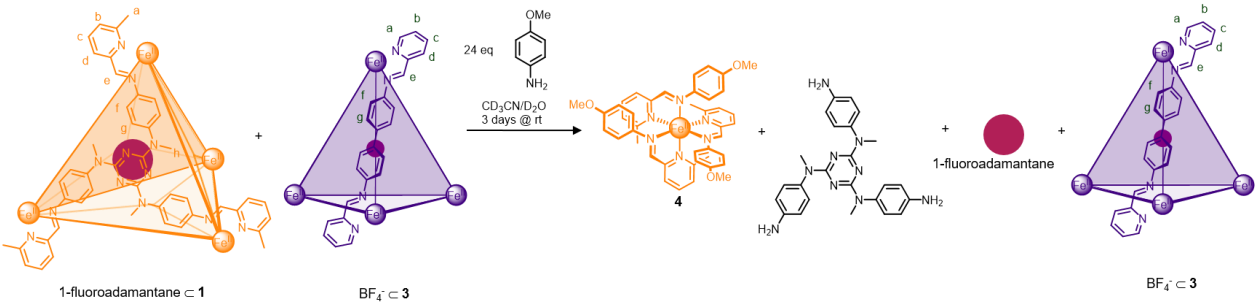

Scheme S4. Disassembly of [1-fluoroadamantane ⊂ **1**]$^{8+}$ in the presence of [$BF_4^- \subset$ **3**]$^{8+}$ triggered by the chemical stimulus, *p*-anisidine.

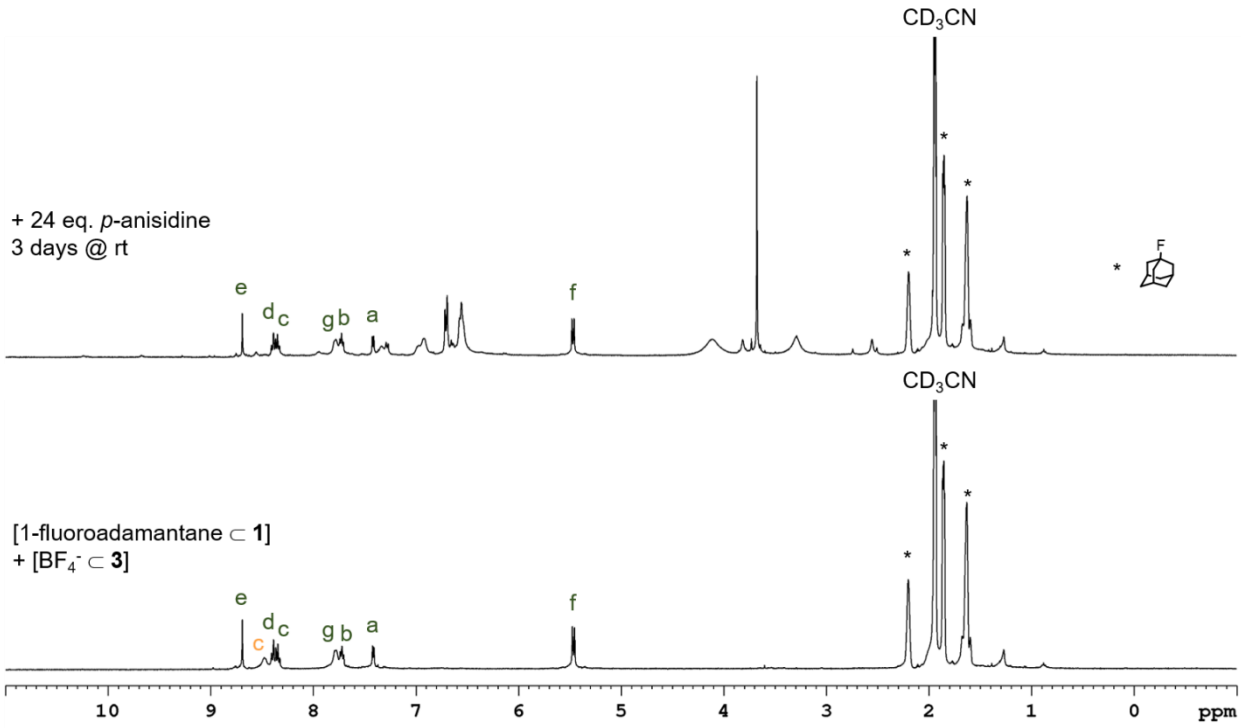

Figure S85. ^{1}H NMR spectra for the disassembly of [1-fluoroadamantane ⊂ **1**]$^{8+}$ (orange labels) in the presence of [BF_4^- ⊂ **3**]$^{8+}$ (green labels) in CD_3CN following the addition of 24 eq. *p*-anisidine and equilibration at room temperature for 3 days. See Scheme S4 for proton assignments and signals marked with * correspond to free 1-fluoroadamantane.

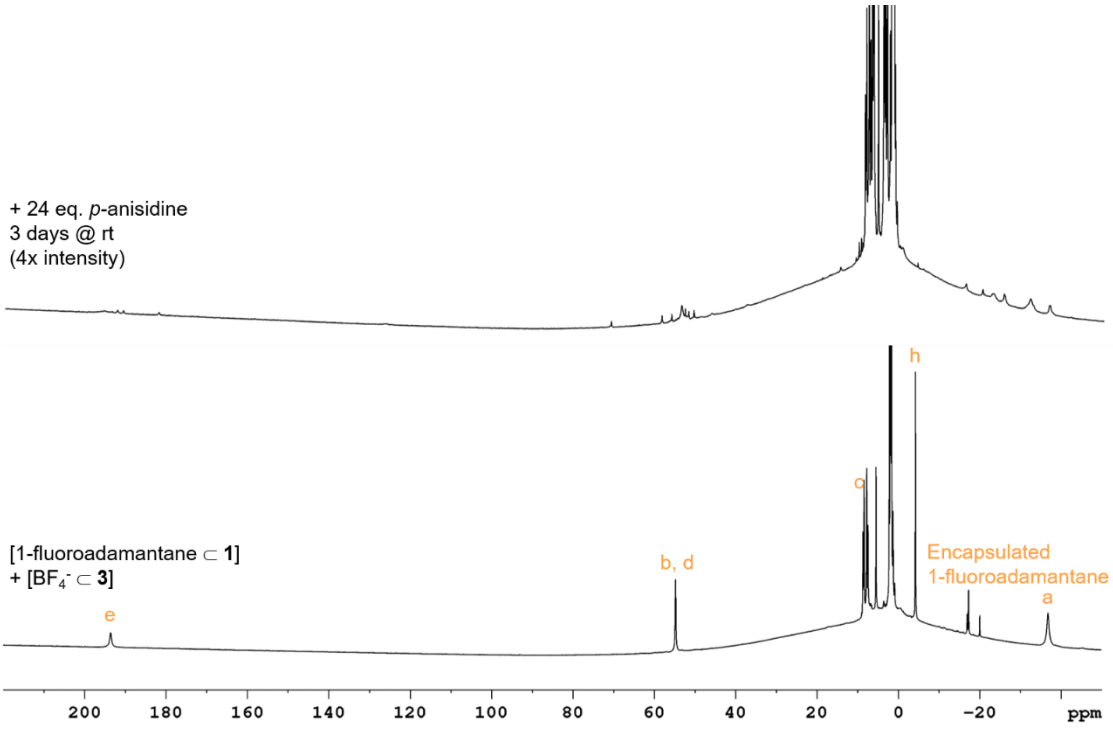

Figure S86. Paramagnetic ^{1}H NMR spectra for the disassembly of [1-fluoroadamantane ⊂ **1**]$^{8+}$ (orange labels) in the presence of [BF_4^- ⊂ **3**]$^{8+}$ (green labels) in CD_3CN following the addition of 24 eq. *p*-anisidine and equilibration at room temperature for 3 days. See Scheme S4 for proton assignments.

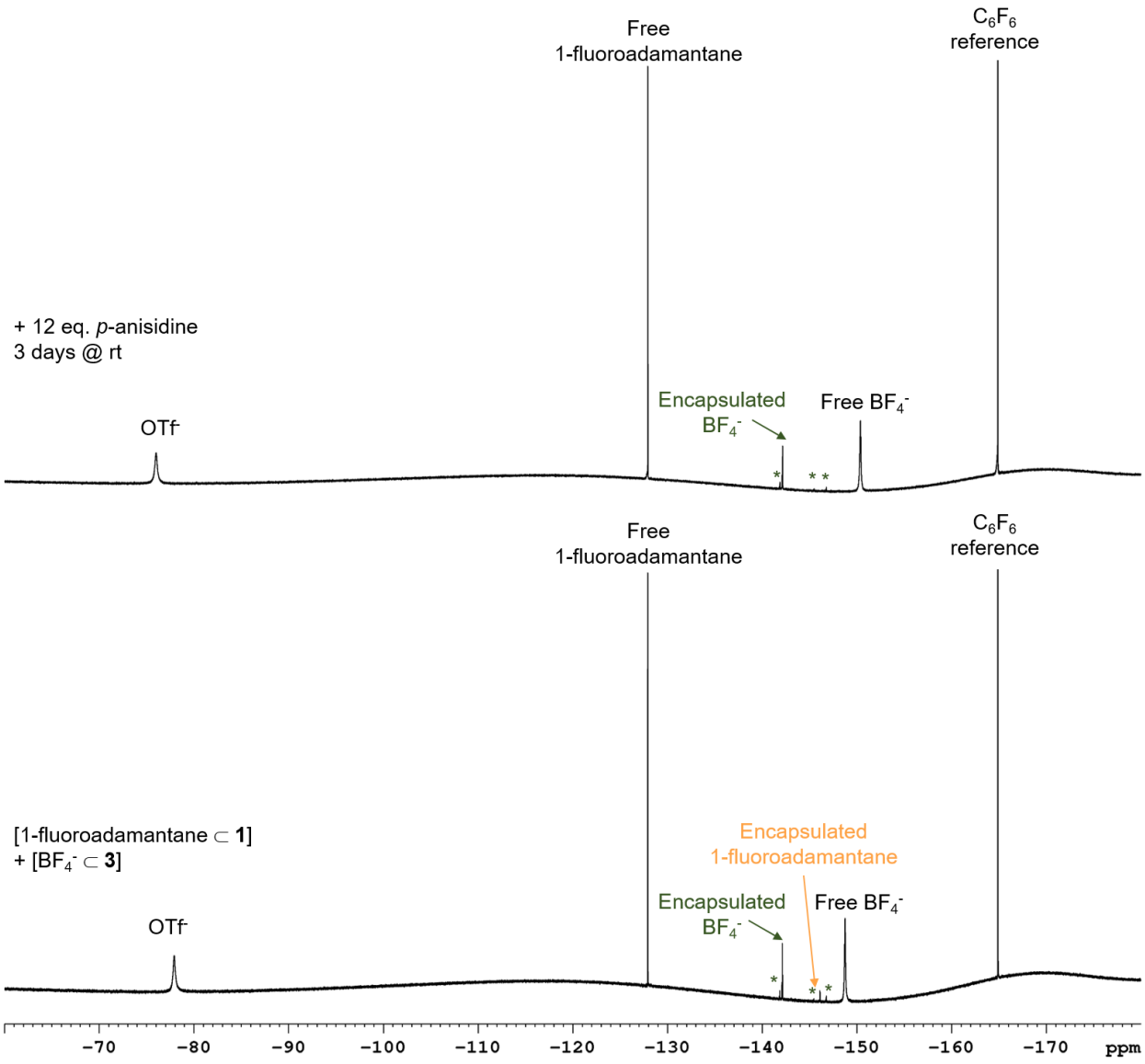

Figure S87. ^{19}F NMR spectra for the disassembly of [1-fluoroadamantane ⊂ **1**]$^{8+}$ (orange labels) in the presence of [BF_4^- ⊂ **3**]$^{8+}$ (green labels, * is attributed to encapsulation of BF_4^- within trace amounts of other diastereomers) in CD_3CN following the addition of 24 eq. *p*-anisidine and equilibration at room temperature for 3 days.

8.2 Titrations of Cages 1 and 3

Preparation of [1-Fluoroadamantane ⊂ **1**]$^{8+}$: In a glovebox, 1-fluoroadamantane (0.79 mg, 0.005 mmol) was added to cage **1** (2.21 mg, 0.0005 mmol) in CD_3CN (0.5 mL) and the mixture was left to equilibrate at room temperature for at least 3 hours.

Titration: To a solution of [1-fluoroadamantane ⊂ **1**]$^{8+}$ (1 mM) and/or [BF_4 ⊂ **3**]$^{8+}$ (1.55 mg, 1 mM) was added aliquots of 6 eq. *p*-anisidine (10 µL, 300 mM). After each addition, the mixture was equilibrated at room temperature for 1 day and NMR spectra were recorded.

8.2.1 Mixture of [1-Fluoroadamantane ⊂ **1**]$^{8+}$ and [BF_4 ⊂ **3**]$^{8+}$

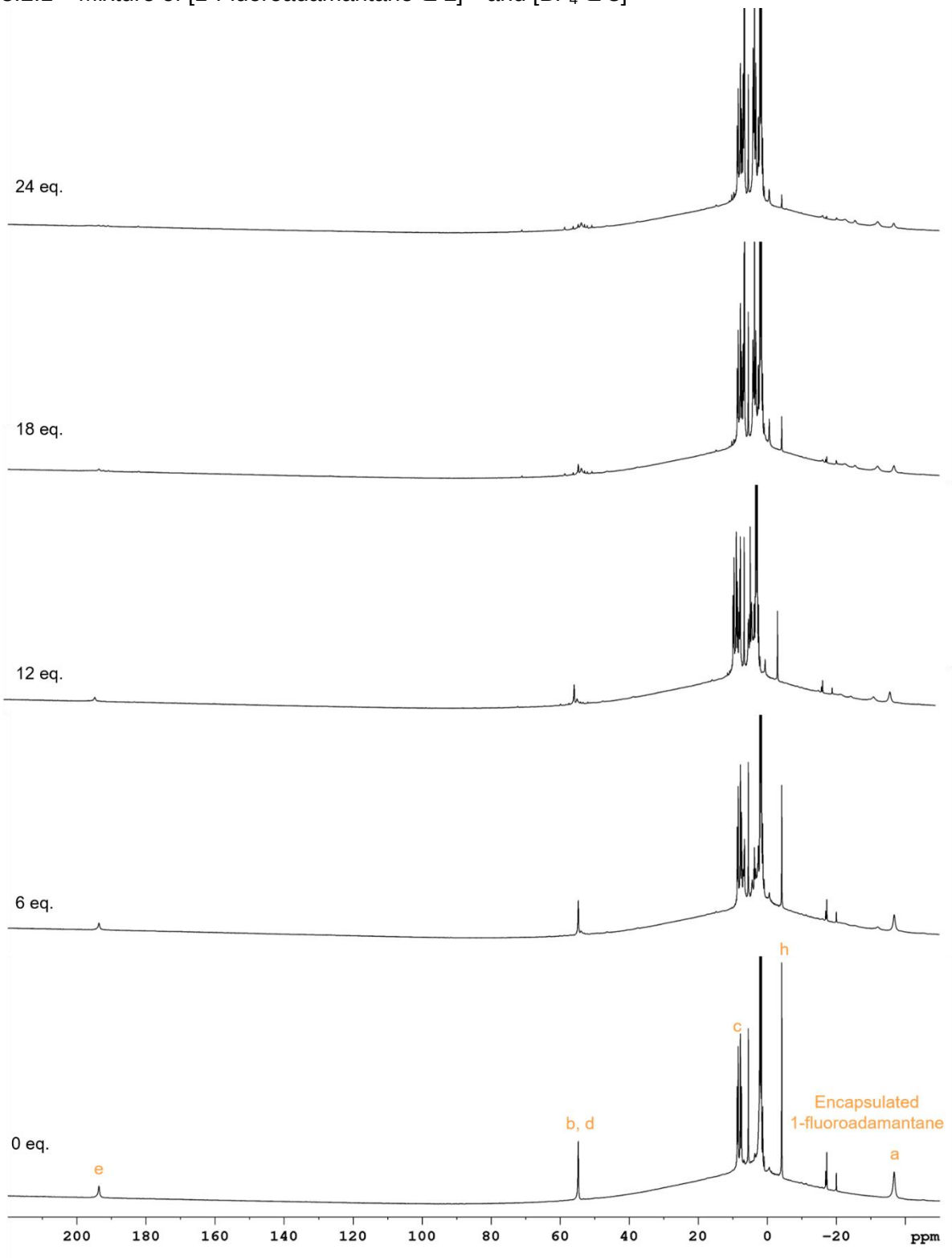

Figure S88. Paramagnetic ^{1}H NMR spectra for the titration of [1-fluoroadamantane ⊂ **1**]$^{8+}$ (orange labels) and [BF_4 ⊂ **3**]$^{8+}$ with 0-24 eq. *p*-anisidine in CD_3CN. See Scheme S4 for proton assignments.

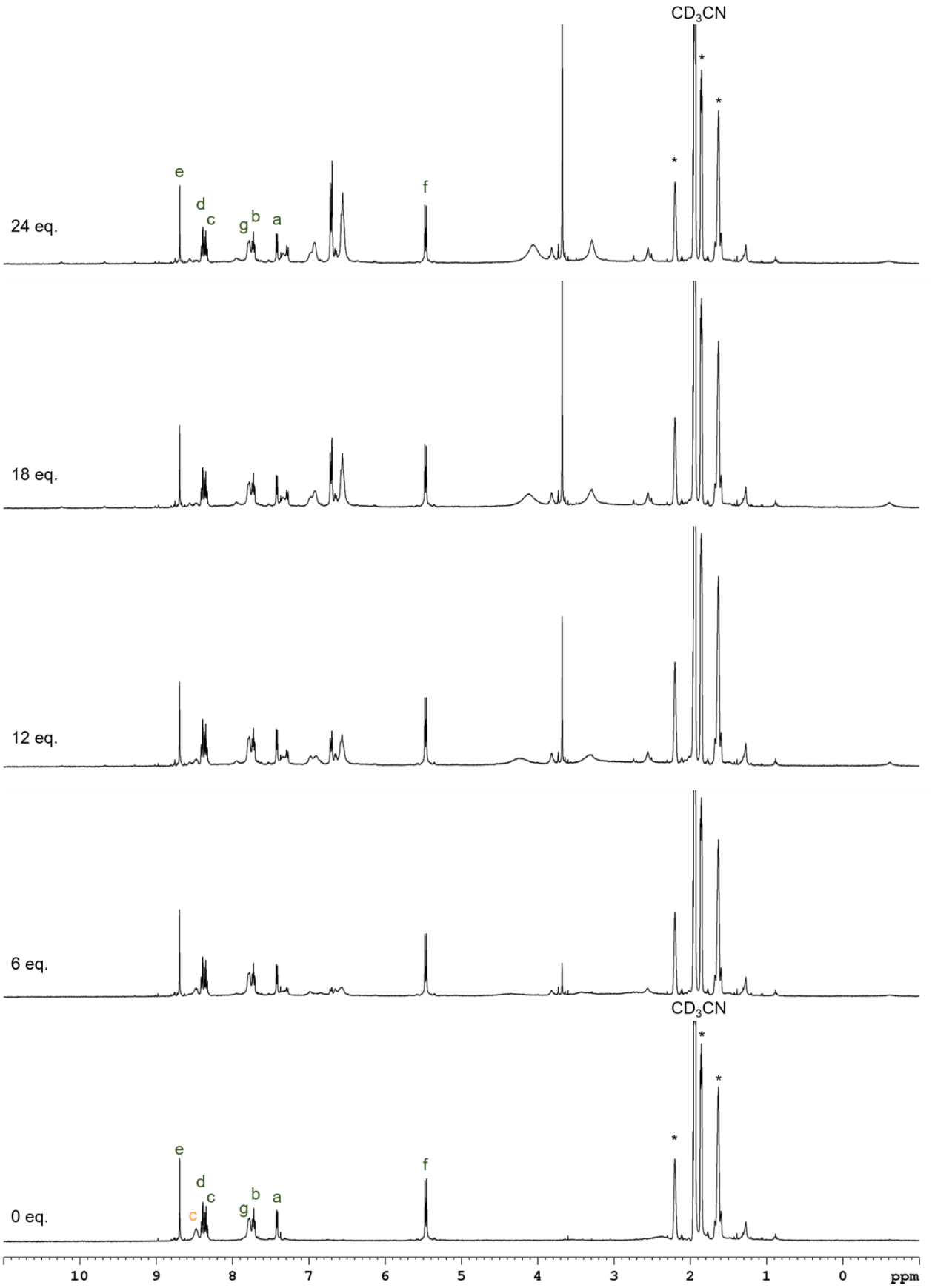

Figure S89. ^{1}H NMR spectra for the titration of [1-fluoroadamantane ⊂ **1**]$^{8+}$ (orange labels) and [BF_4 ⊂ **3**]$^{8+}$ (green labels) with 0-24 eq. *p*-anisidine in CD_3CN. See Scheme S4 for cage proton assignments and signals marked with * correspond to free 1-fluoroadamantane.

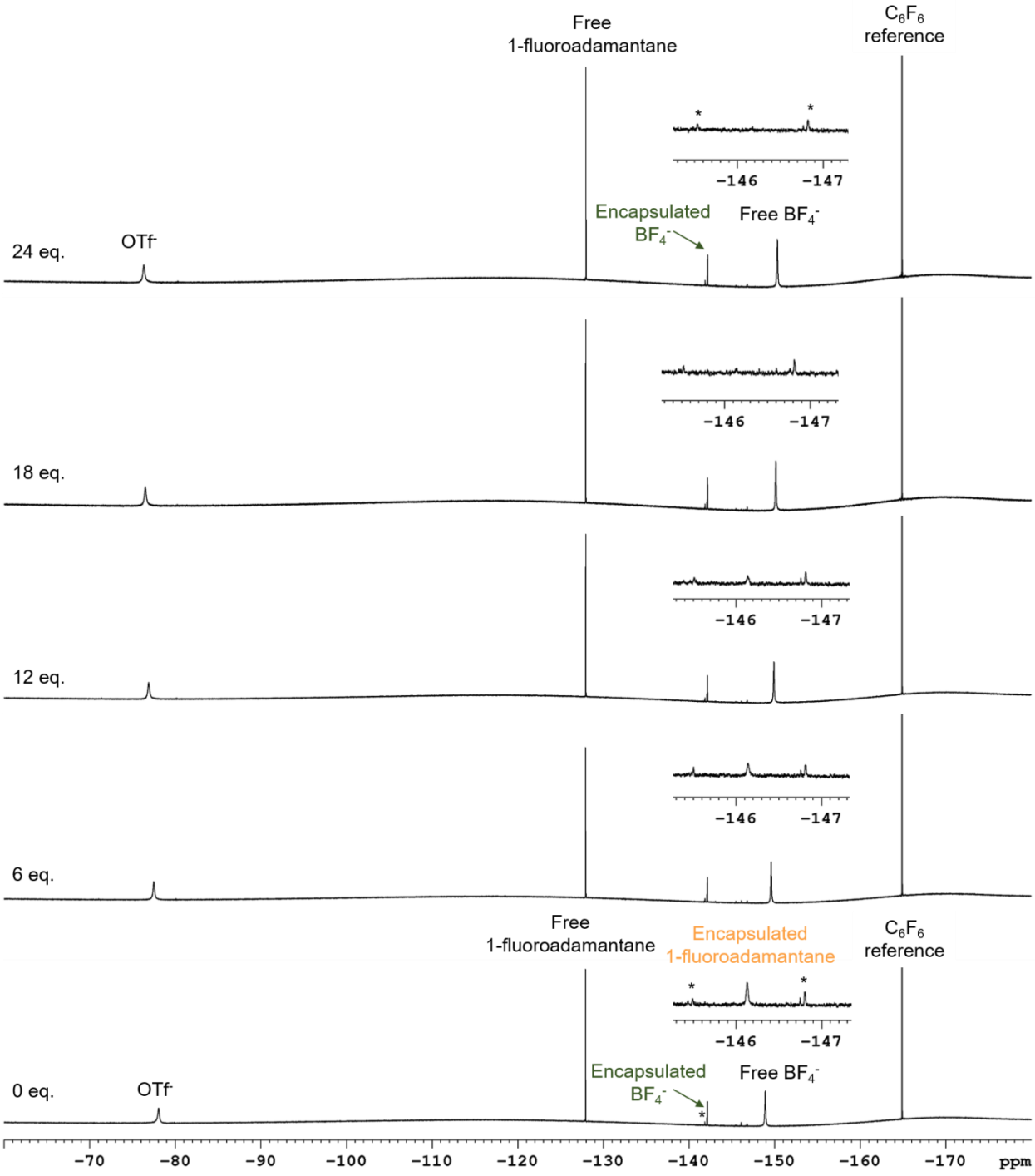

Figure S90. ^{19}F NMR spectra for the titration of [1-fluoroadamantane ⊂ **1**]$^{8+}$ (orange labels) and [BF_4 ⊂ **3**]$^{8+}$ (green labels, * is attributed to encapsulation of BF_4^- within trace amounts of other diastereomers) with 0-24 eq. *p*-anisidine in CD_3CN.

8.2.2 [1-Fluoroadamantane ⊂ **1**]$^{8+}$

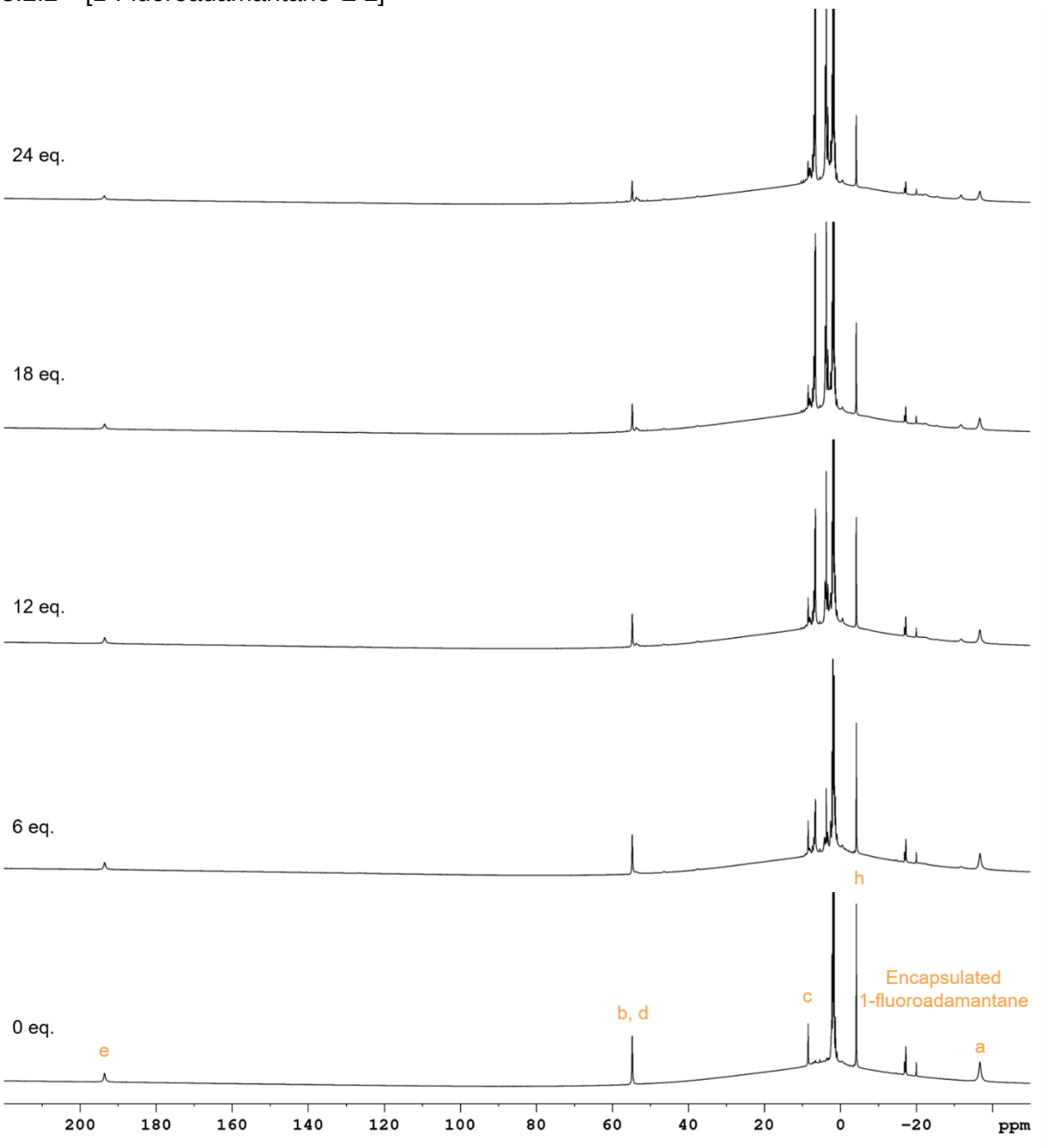

Figure S91. Paramagnetic ^{1}H NMR spectra for the titration of [1-fluoroadamantane ⊂ **1**]$^{8+}$ (orange labels) with 0-24 eq. *p*-anisidine in CD_3CN. See Scheme S4 for proton assignments.

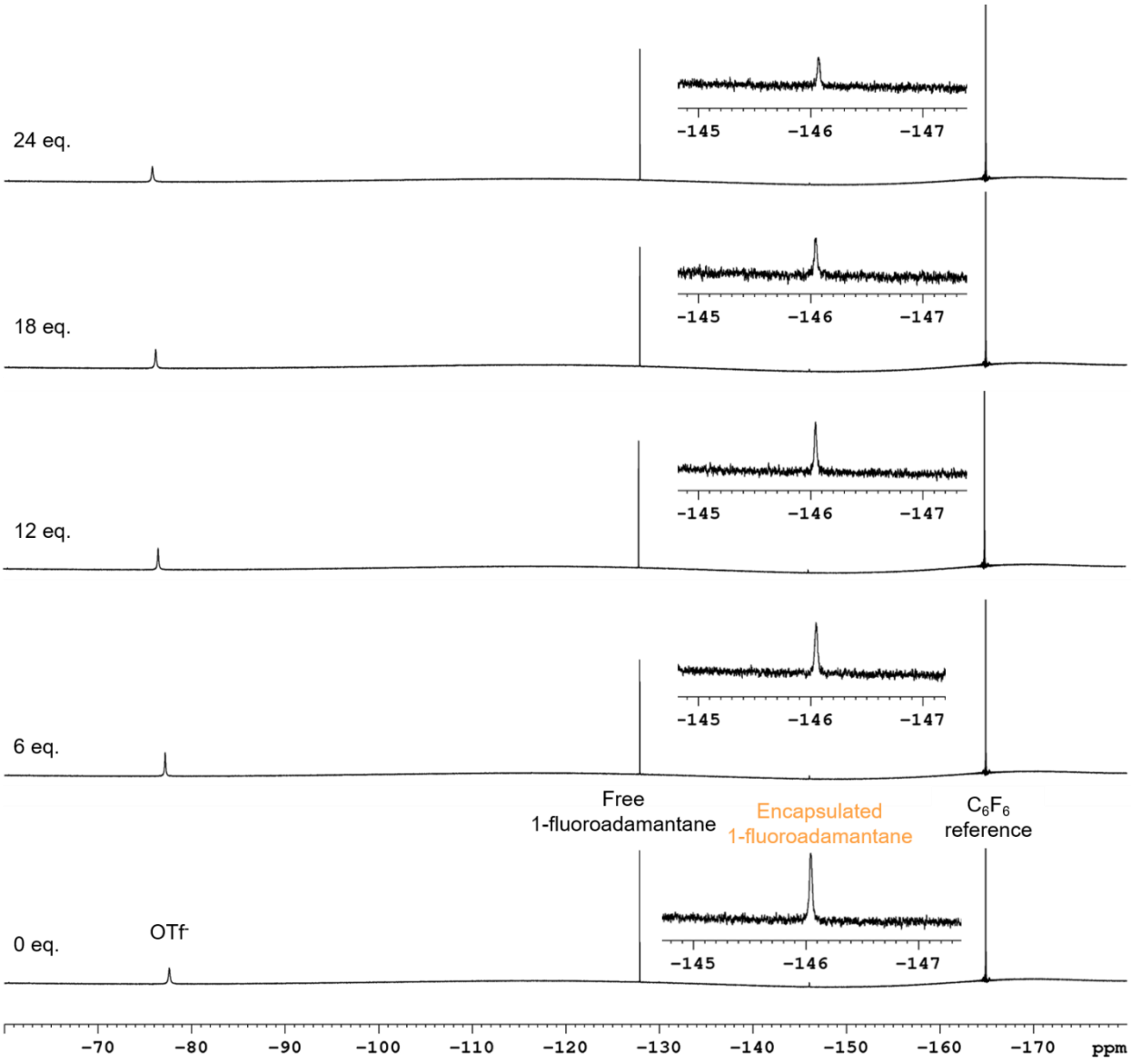

Figure S92. ^{19}F NMR spectra for the titration of [1-fluoroadamantane ⊂ **1**]$^{8+}$ (orange labels) with 0-24 eq. *p*-anisidine in CD_3CN.

8.2.3 $[BF_4 \subset \mathbf{3}]^{8+}$

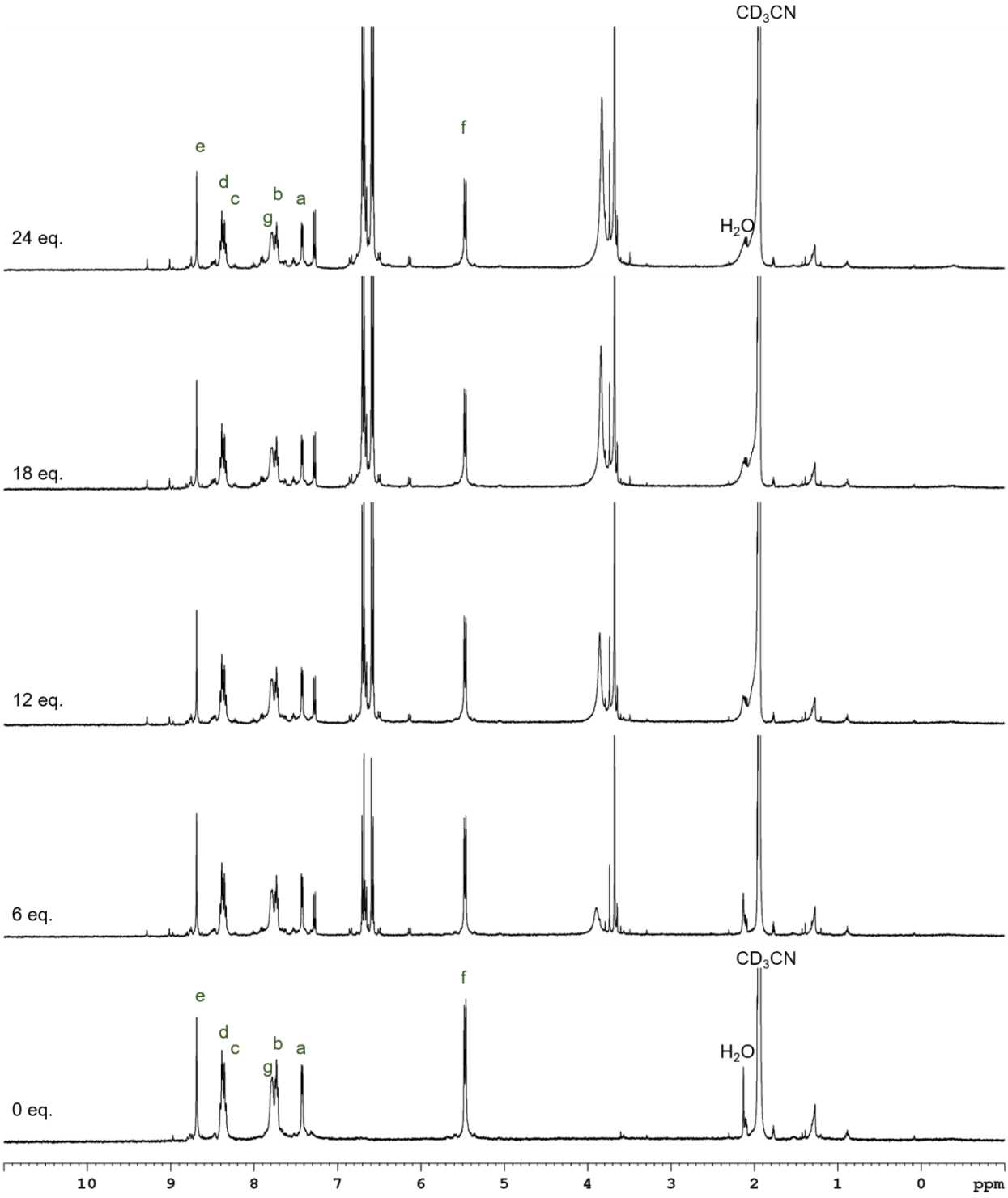

Figure S93. ^{1}H NMR spectra for the titration of $[BF_4 \subset \mathbf{3}]^{8+}$ (green labels) with 0-24 eq. *p*-anisidine in CD_3CN. See Scheme S4 for cage proton assignments.

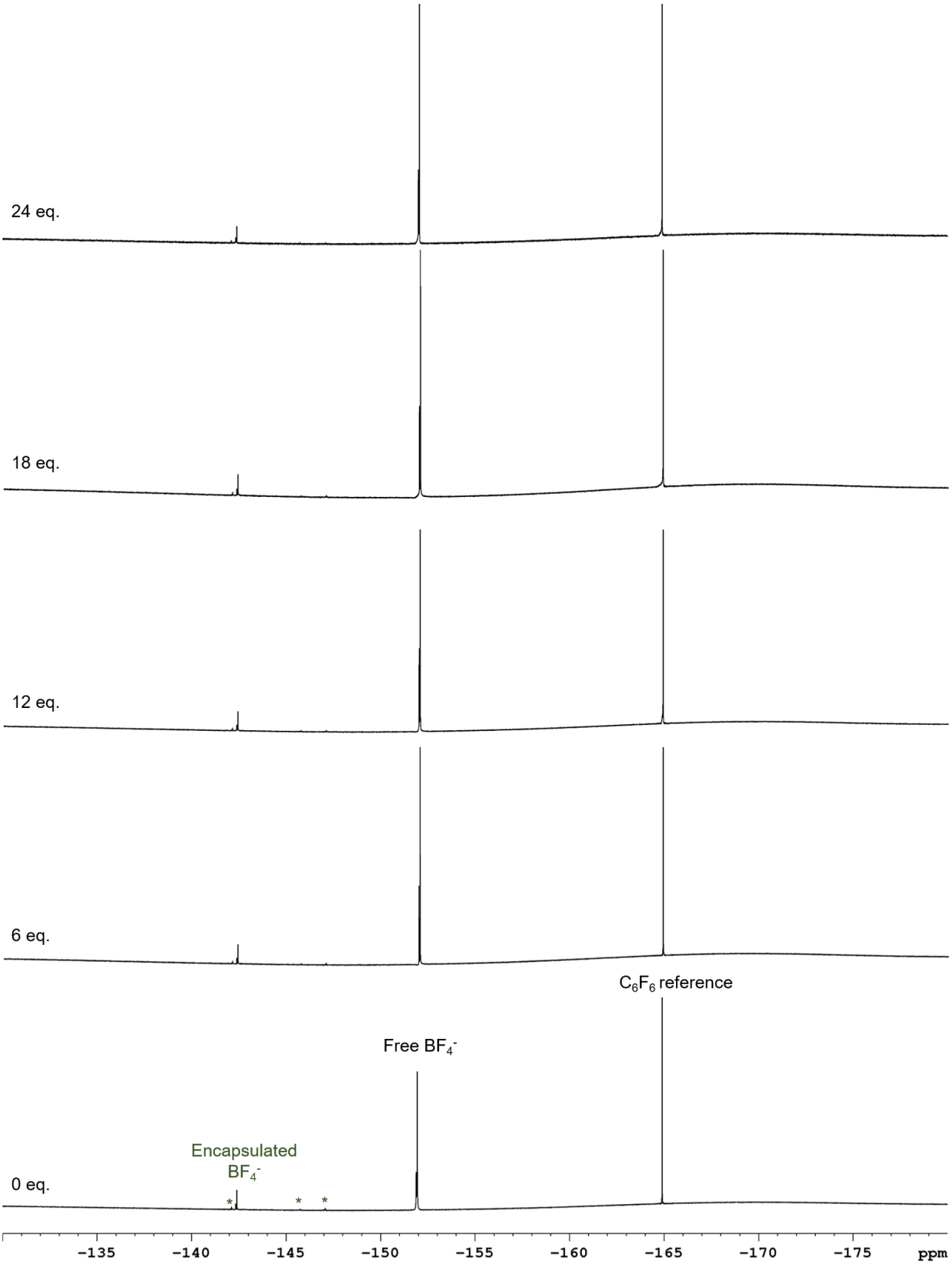

Figure S94. ^{19}F NMR spectra for the titration of $[BF_4 \subset \mathbf{3}]^{8+}$ (green labels) with 0-24 eq. *p*-anisidine in CD_3CN. Signals marked with * are attributed to encapsulation of BF_4^- within trace amounts of other diastereomers.

8.3 Disassembly of [$BF_4 \subset$ **3**]$^{8+}$ in the Presence of [1-Fluoroadamantane $\subset$ **2**]$^{8+}$

8.3.1 Transformation

In a glovebox, 1-fluoroadamantane (0.79 mg, 0.005 mmol) was added to a mixture of cage **1** (2.21 mg, 0.0005 mmol) and [$BF_4 \subset$ **3**]$^{8+}$ (1.55 mg, 0.0005 mmol) in CD_3CN (0.5 mL) and the mixture was left to equilibrate at room temperature for at least 3 hours. 2-Formylpyridine (24 eq., 1.14 µL) was added to the host-guest complexes of the two cages and the mixture was left to equilibrate for 16 h at 323 K. D_2O (25 µL, 5% v/v) was then added to the solution and the solution was left to equilibrate at 323 K for three days. NMR spectra were recorded periodically to monitor the equilibration process.

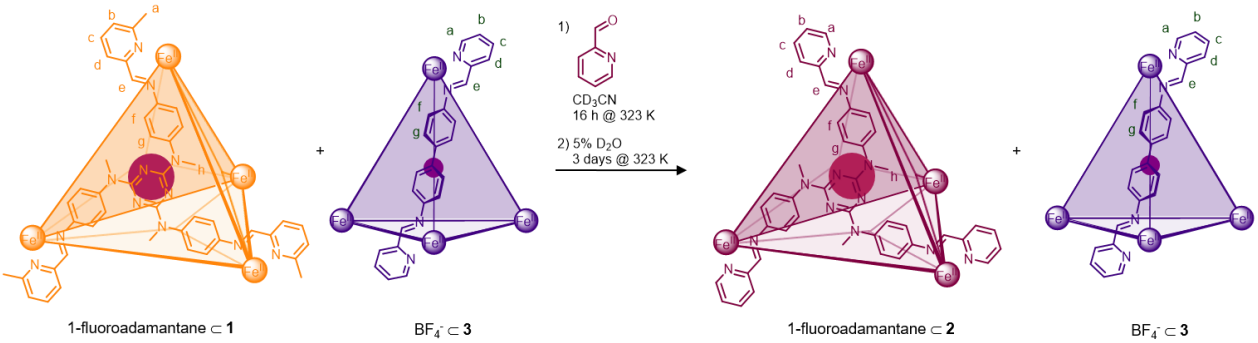

Scheme S5. Transformation from [1-fluoroadamantane $\subset$ **1**]$^{8+}$ to [1-fluoroadamantane $\subset$ **2**]$^{8+}$ in the presence of [$BF_4^- \subset$ **3**]$^{8+}$ induced by aldehyde exchange of 2-formyl-6-methylpyridine for 2-formylpyridine.

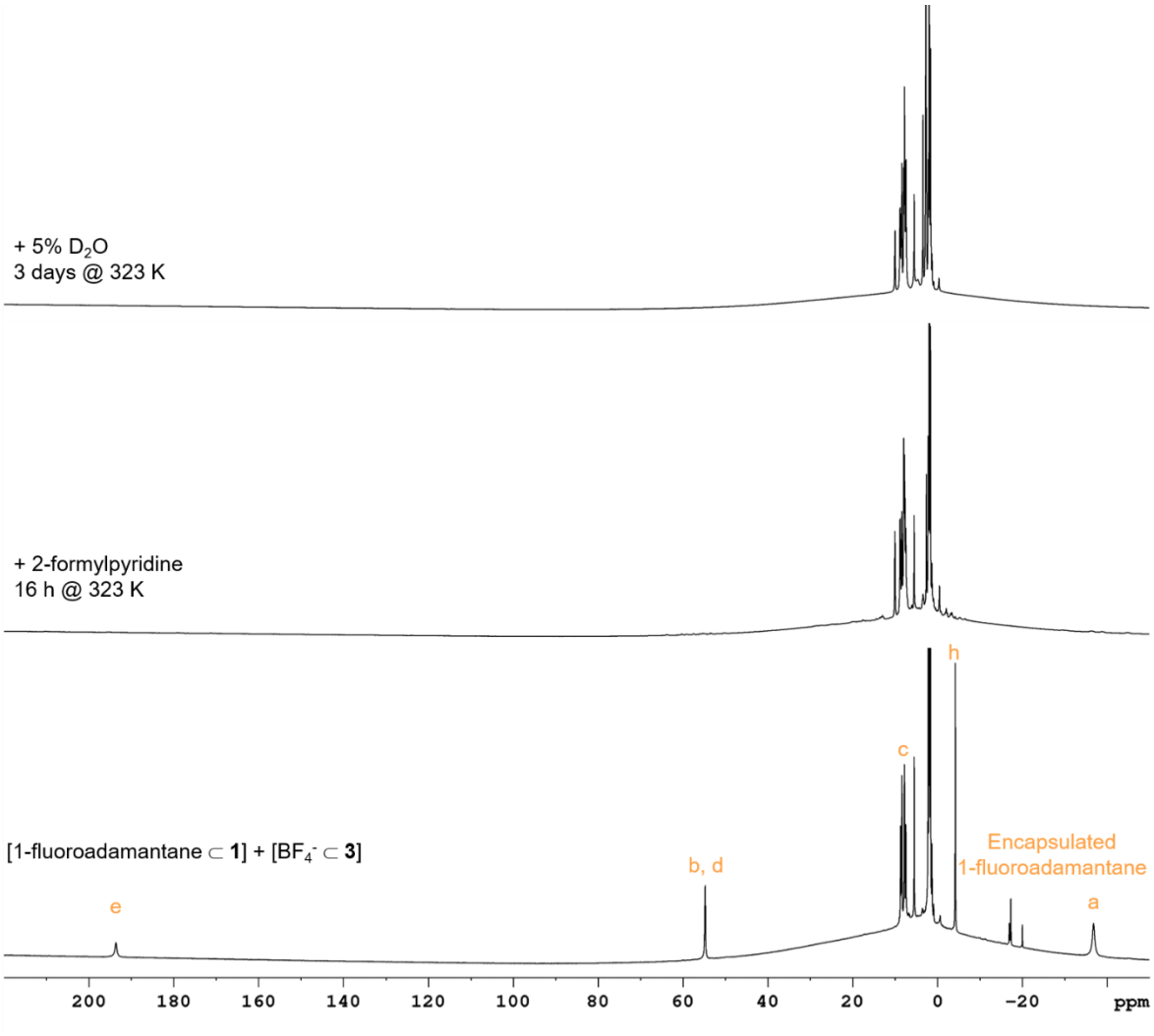

Figure S95. Paramagnetic ^{1}H NMR spectra of the transformation from [1-fluoroadamantane ⊂ **1**]$^{8+}$ (orange labels) to [1-fluoroadamantane ⊂ **2**]$^{8+}$ in the presence of [BF_4 ⊂ **3**]$^{8+}$ upon sequential addition of 24 eq. of 2-formylpyridine and 5% D_2O and heating at 323 K in CD_3CN. See Scheme S5 for proton assignments.

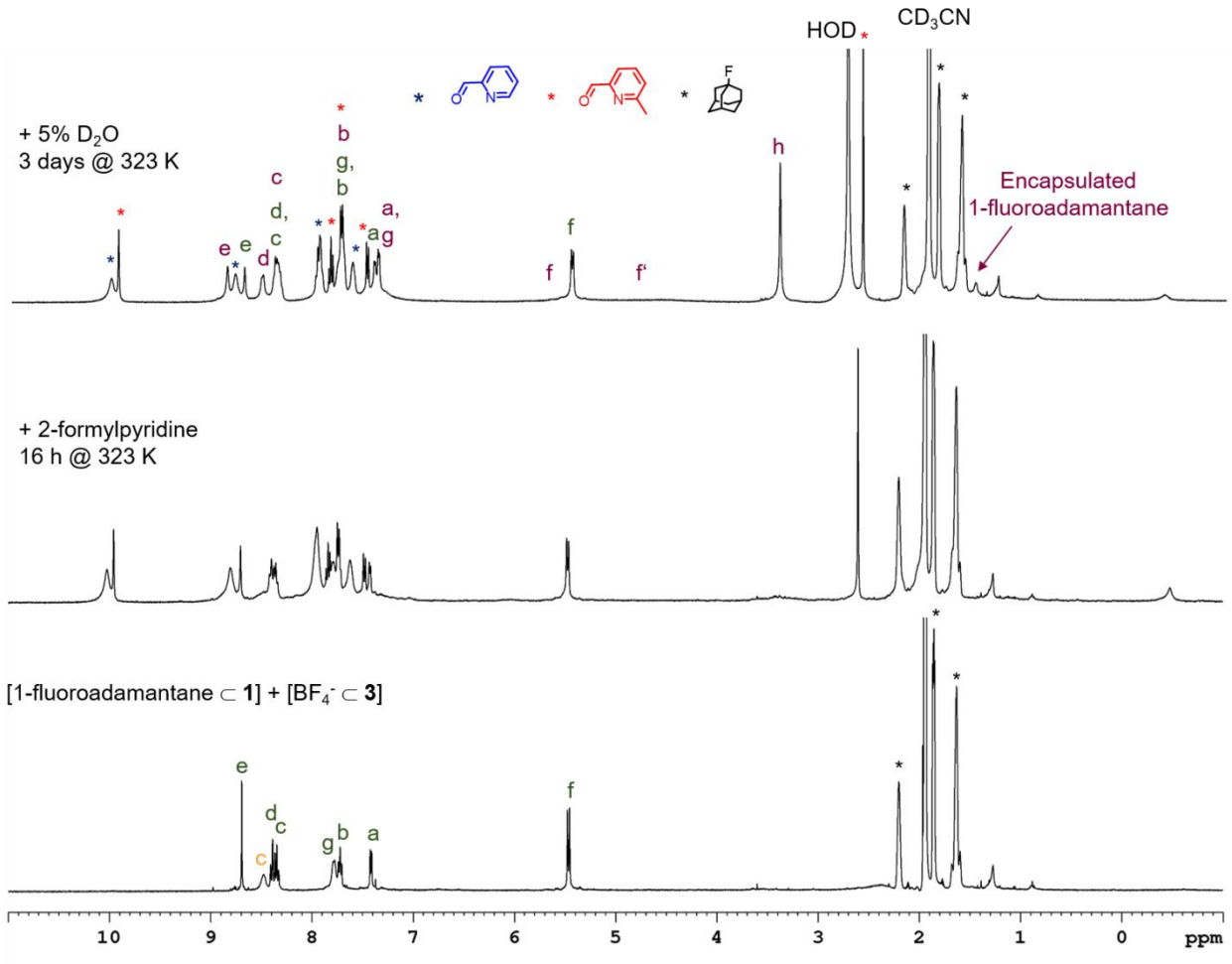

Figure S96. ^{1}H NMR spectra for the transformation from [1-fluoroadamantane ⊂ **1**]$^{8+}$ (orange labels) to [1-fluoroadamantane ⊂ **2**]$^{8+}$ (purple labels) in the presence of [BF_4^- ⊂ **3**]$^{8+}$ (green labels) upon sequential addition of 24 eq. of 2-formylpyridine and 5% D_2O and heating at 323 K in CD_3CN. See Scheme S5 for proton assignments.

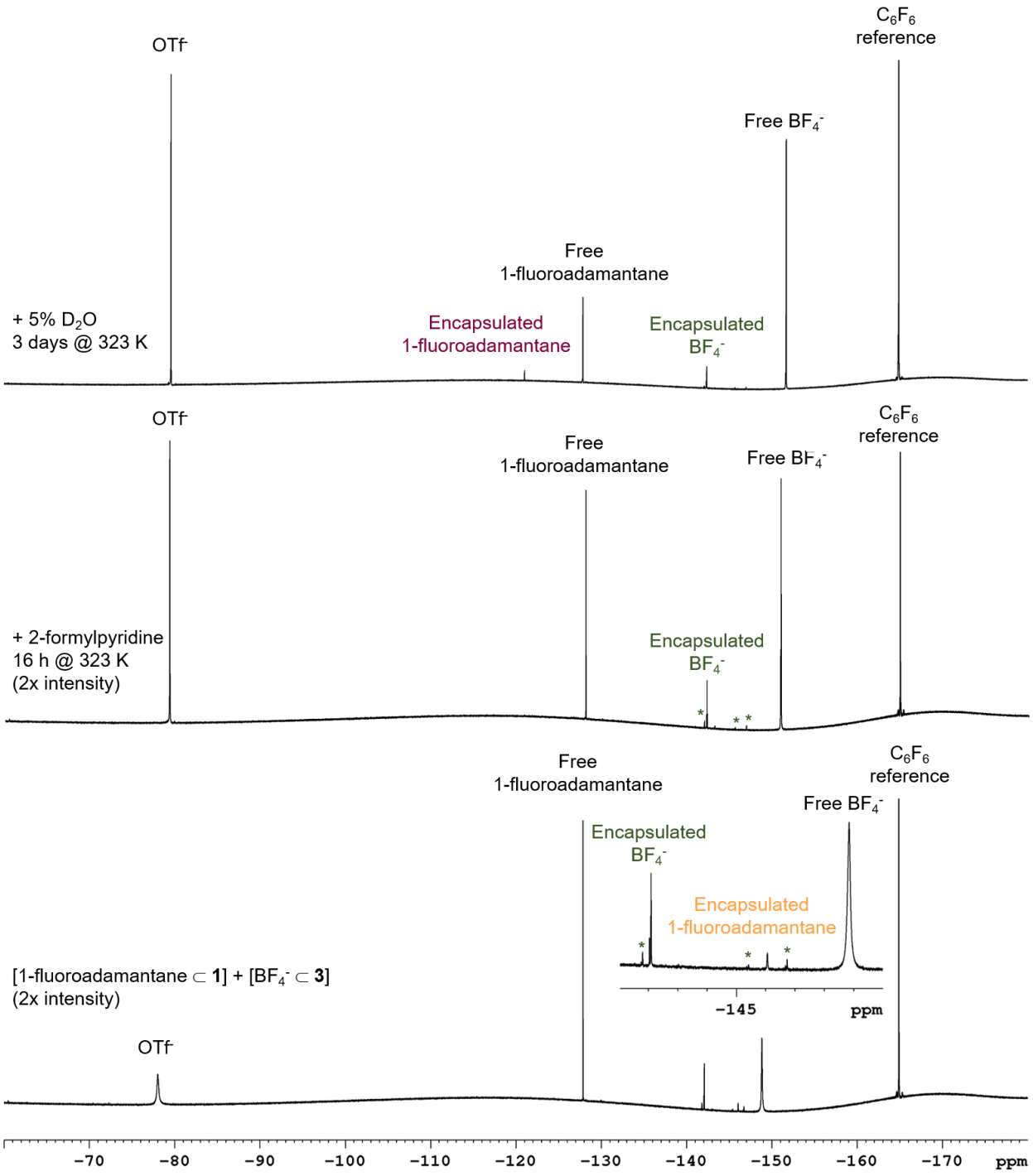

Figure S97. ^{19}F NMR spectra of the transformation from [1-fluoroadamantane ⊂ **1**]$^{8+}$ (orange labels) to [1-fluoroadamantane ⊂ **2**]$^{8+}$ (purple labels) in the presence of [BF_4^- ⊂ **3**]$^{8+}$ (green labels, * is attributed to encapsulation of BF_4^- within trace amounts of other diastereomers) upon heating at 323 K following addition of 24 eq. of 2-formylpyridine then addition of 5% D_2O in CD_3CN.

8.3.2 Disassembly

To the mixture of [1-fluoroadamantane ⊂ **2**]$^{8+}$ and [BF_4^- ⊂ **3**]$^{8+}$ (generated *in situ* from the subcomponent exchange in Section 8.3.1) was added 12 eq. *p*-anisidine (0.74 mg, 0.006 mmol) and the mixture was heated at 323 K for 1 day.

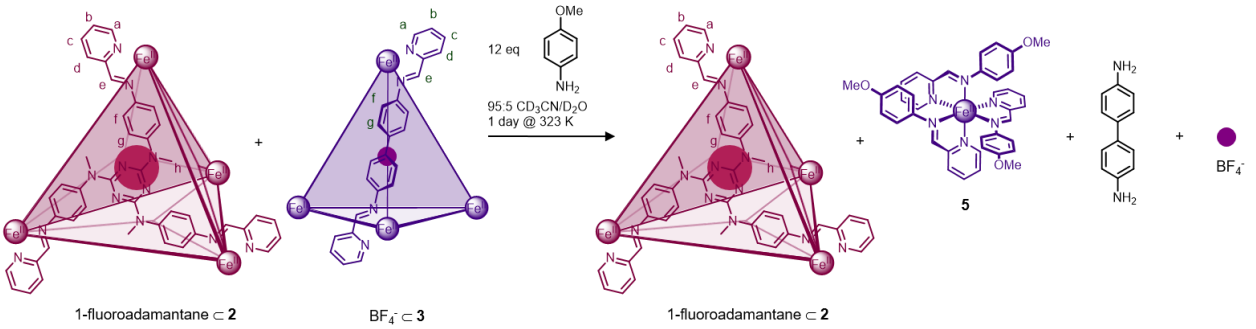

Scheme S6. Disassembly of [BF_4^- ⊂ **3**]$^{8+}$ in the presence of [1-fluoroadamantane ⊂ **2**]$^{8+}$ triggered by the chemical stimulus, *p*-anisidine.

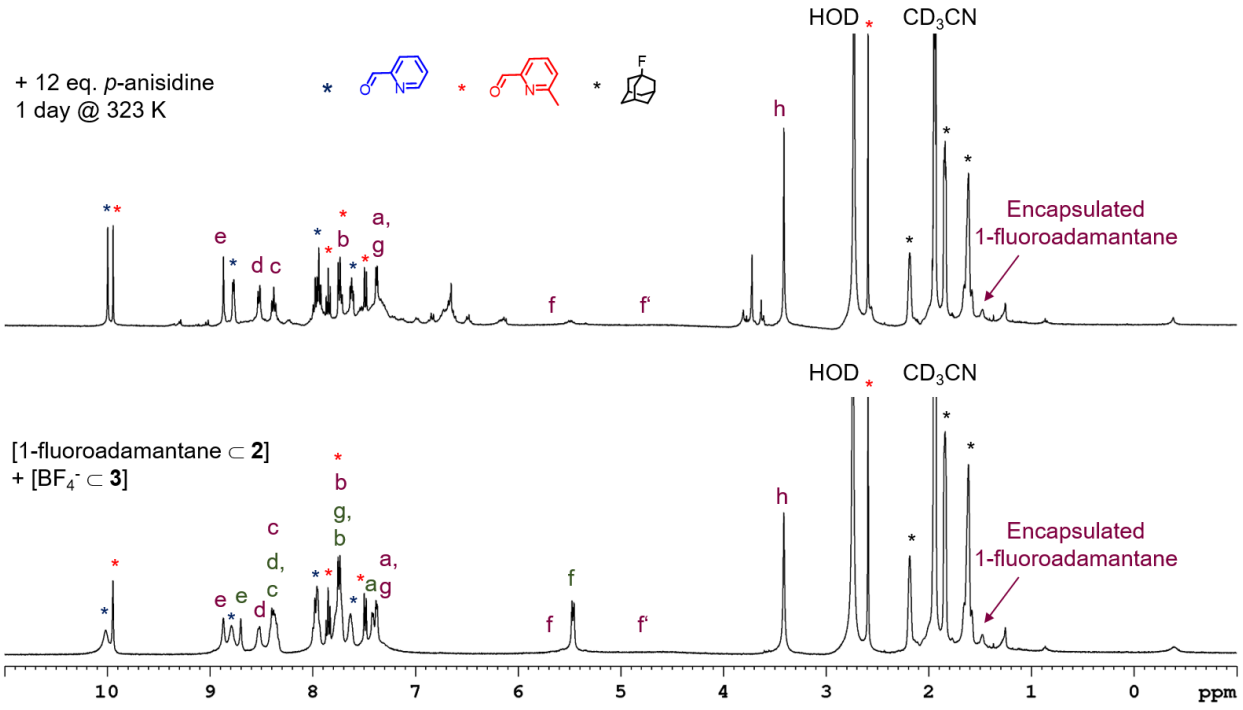

Figure S98. ^{1}H NMR spectra for the disassembly of [BF_4^- ⊂ **3**]$^{8+}$ (green labels) in the presence of [1-fluoroadamantane ⊂ **2**]$^{8+}$ (purple labels) in 95:5 CD_3CN/D_2O following the addition of 12 eq. *p*-anisidine and heating at 323 K. See Scheme S6 for proton assignments.

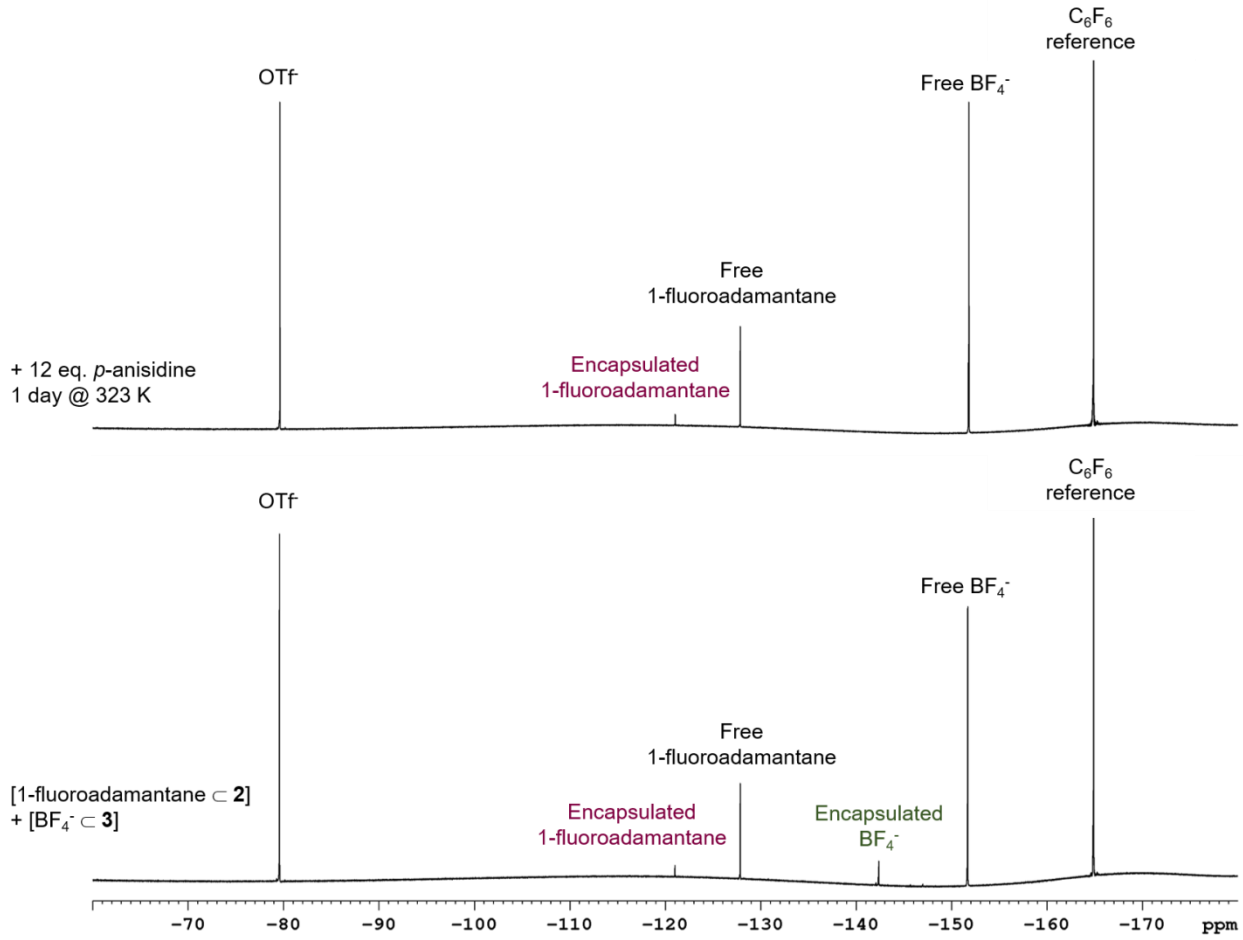

Figure S99. ^{19}F NMR spectra for the disassembly of $[BF_4^- \subset \mathbf{3}]^{8+}$ (green labels) in the presence of [1-fluoroadamantane $\subset$ **2**]$^{8+}$ (purple labels) in 95:5 CD_3CN/D_2O following the addition of 12 eq. *p*-anisidine and heating at 323 K.

8.4 Titrations of Cages 2 and 3

To a solution of [1-fluoroadamantane ⊂ **2**]$^{8+}$ (prepared as in Section 8.2 using 2.11 mg cage **2** and an equilibration time of at least 3 days) and/or [BF_4 ⊂ **3**]$^{8+}$ (1.55 mg, 0.0005 mmol) was added aliquots of 6 eq. *p*-anisidine (10 µL, 300 mM). After each addition, the mixture was equilibrated at 323 K for 1 day and NMR spectra were recorded.

8.4.1 Mixture of [1-Fluoroadamantane ⊂ **2**]$^{8+}$ and [BF_4 ⊂ **3**]$^{8+}$

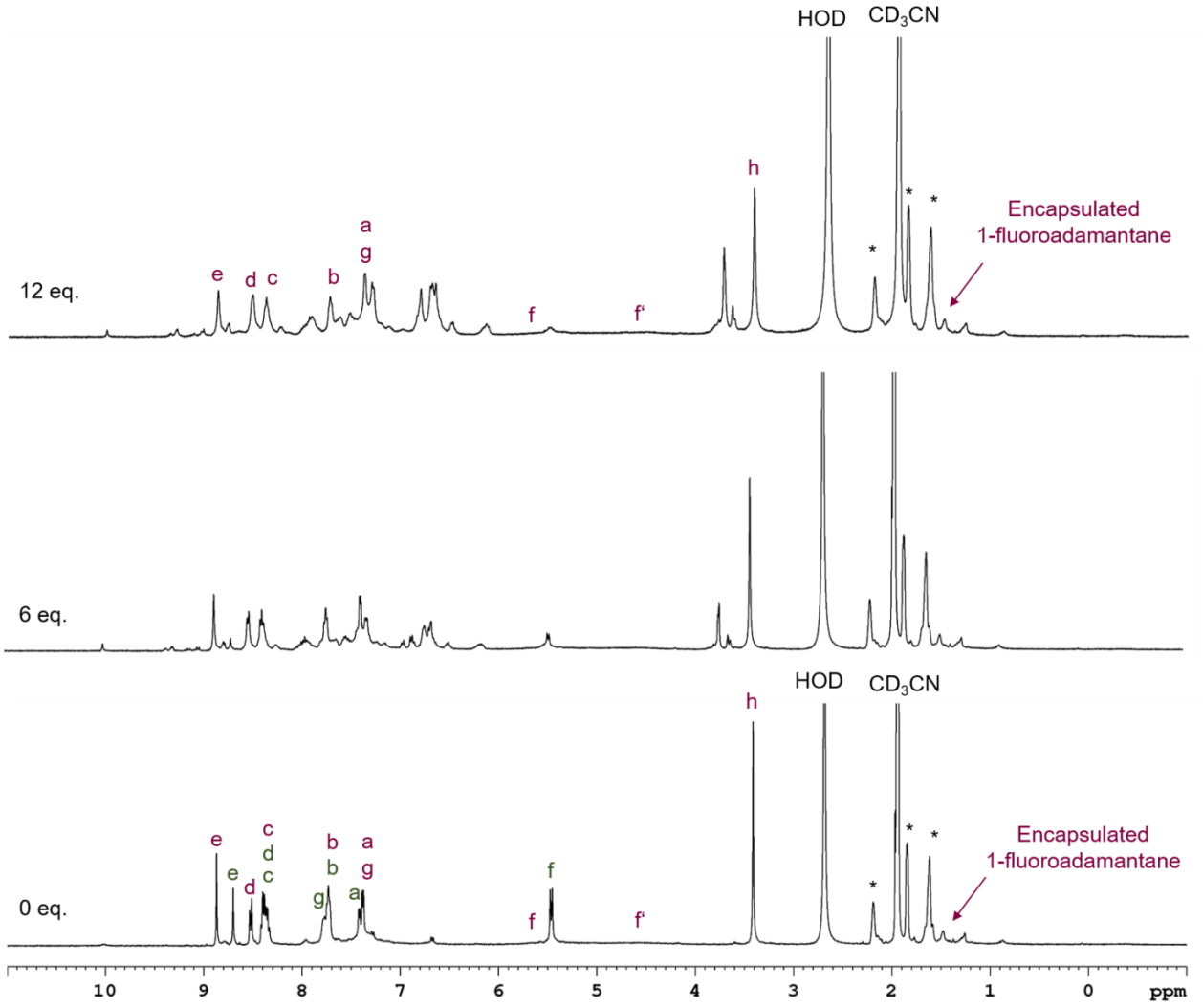

Figure S100. ^{1}H NMR spectra for the titration of [1-fluoroadamantane ⊂ **2**]$^{8+}$ (purple labels) and [BF_4 ⊂ **3**]$^{8+}$ (green labels) with 0-12 eq. *p*-anisidine in 95:5 CD_3CN/D_2O. See Scheme S6 for cage proton assignments and signals marked with * correspond to free 1-fluoroadamantane.

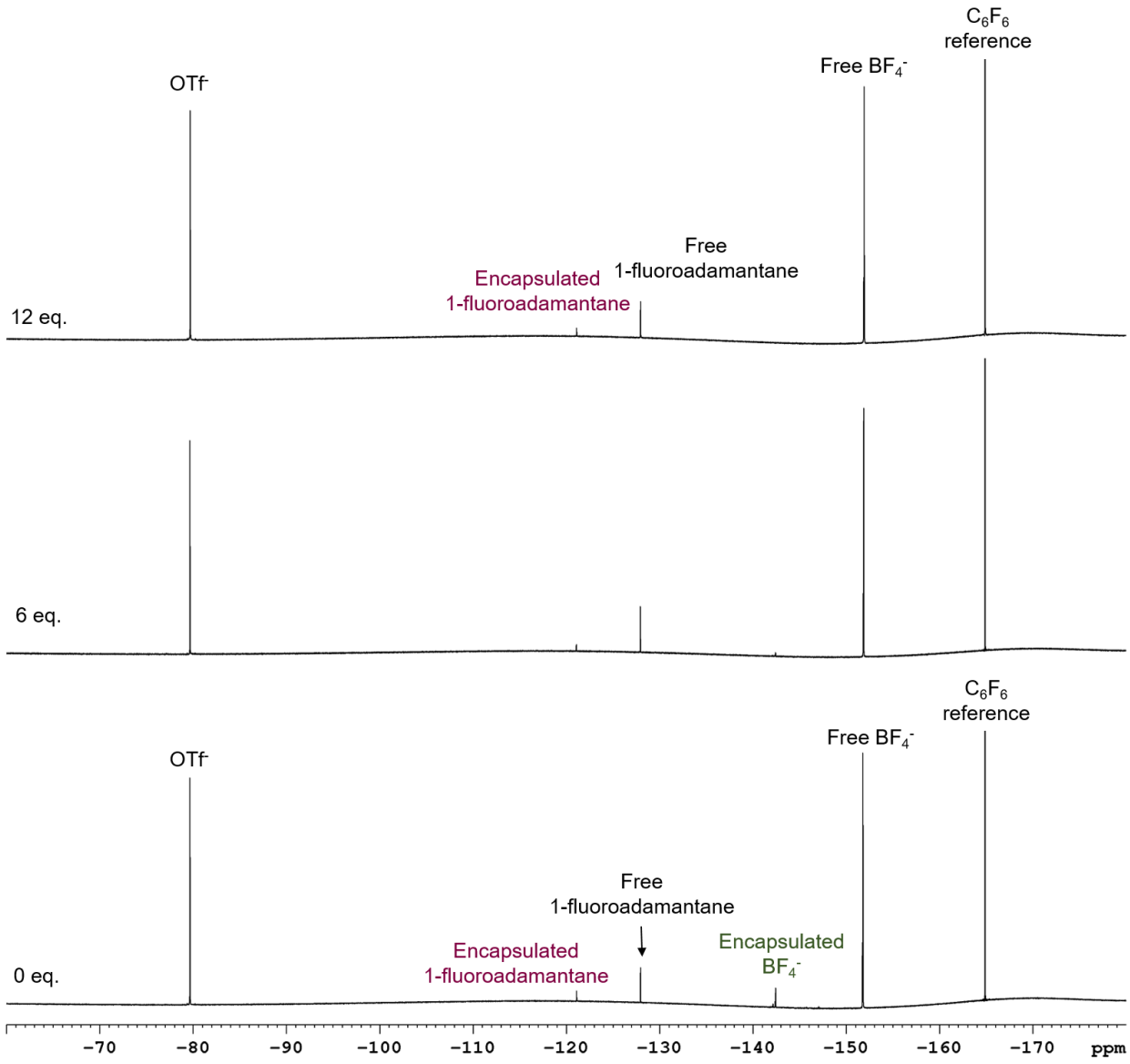

Figure S101. ^{19}F NMR spectra for the titration of [1-fluoroadamantane ⊂ **2**]$^{8+}$ (purple labels) and [BF_4 ⊂ **3**]$^{8+}$ (green labels) with 0-12 eq. *p*-anisidine in 95:5 CD_3CN/D_2O.

8.4.2 [1-Fluoroadamantane ⊂ **2**]$^{8+}$

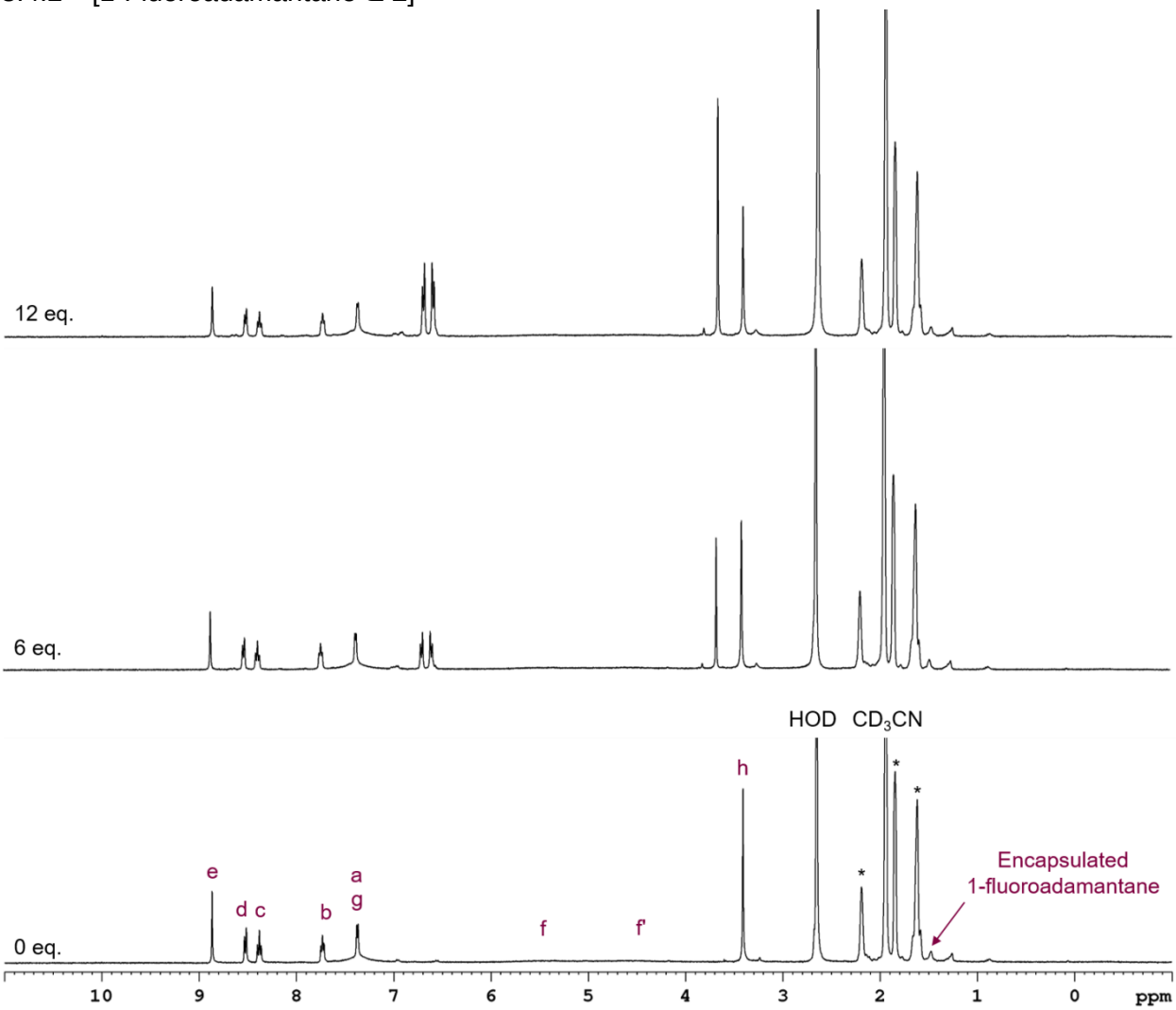

Figure S102. ^{1}H NMR spectra for the titration of [1-fluoroadamantane ⊂ **2**]$^{8+}$ (purple labels) with 0-12 eq. *p*-anisidine in 95:5 CD_3CN/D_2O. See Scheme S6 for cage proton assignments and signals marked with * correspond to free 1-fluoroadamantane.

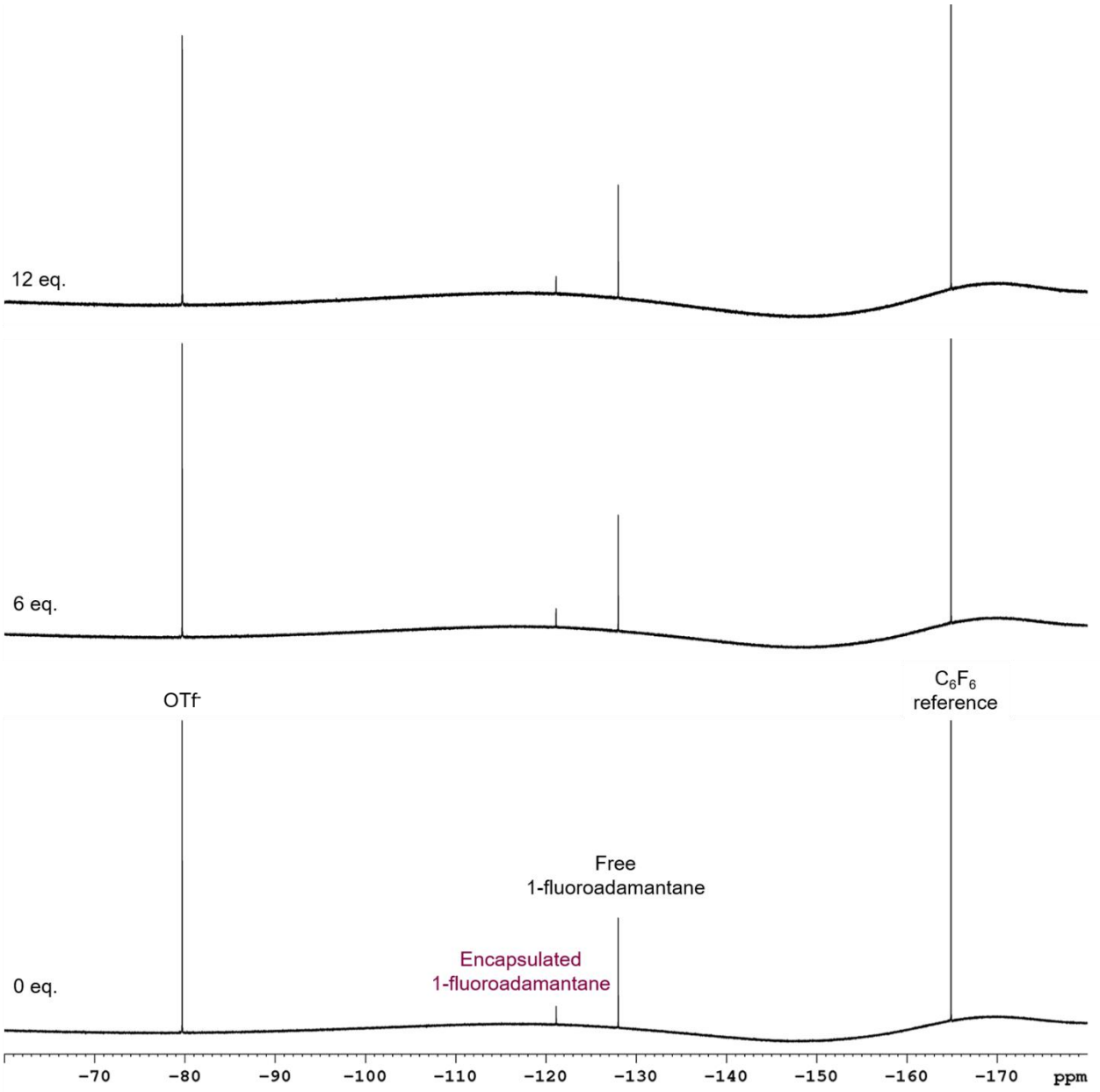

Figure S103. ^{19}F NMR spectra for the titration of [1-fluoroadamantane ⊂ **2**]$^{8+}$ (purple labels) with 0-12 eq. *p*-anisidine in 95:5 CD_3CN/D_2O.

8.4.3 $[BF_4 \subset \mathbf{3}]^{8+}$

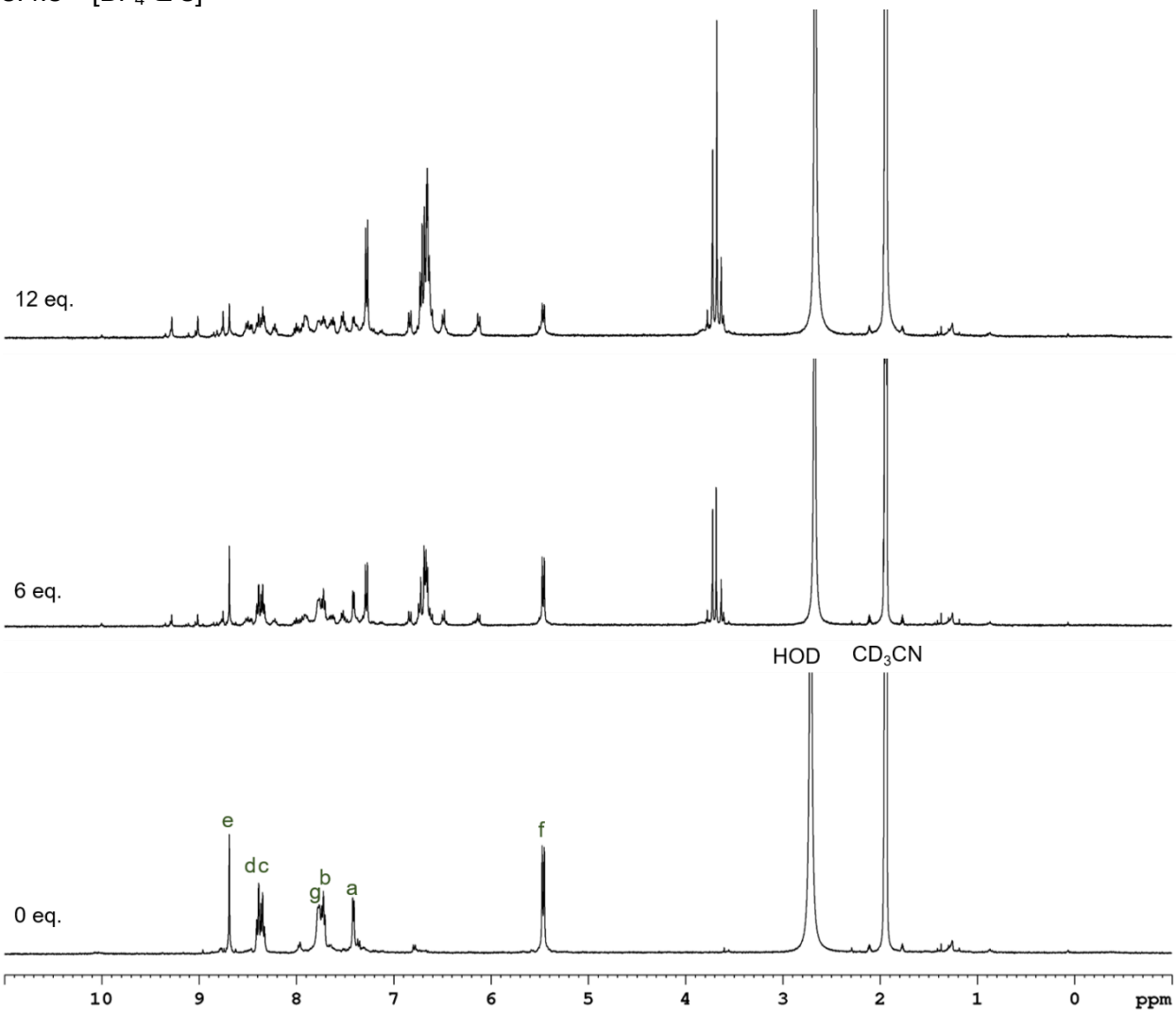

Figure S104. ^{1}H NMR spectra for the titration of $[BF_4 \subset \mathbf{3}]^{8+}$ (green labels) with 0-12 eq. *p*-anisidine in 95:5 CD_3CN/D_2O. See Scheme S6 for cage proton assignments.

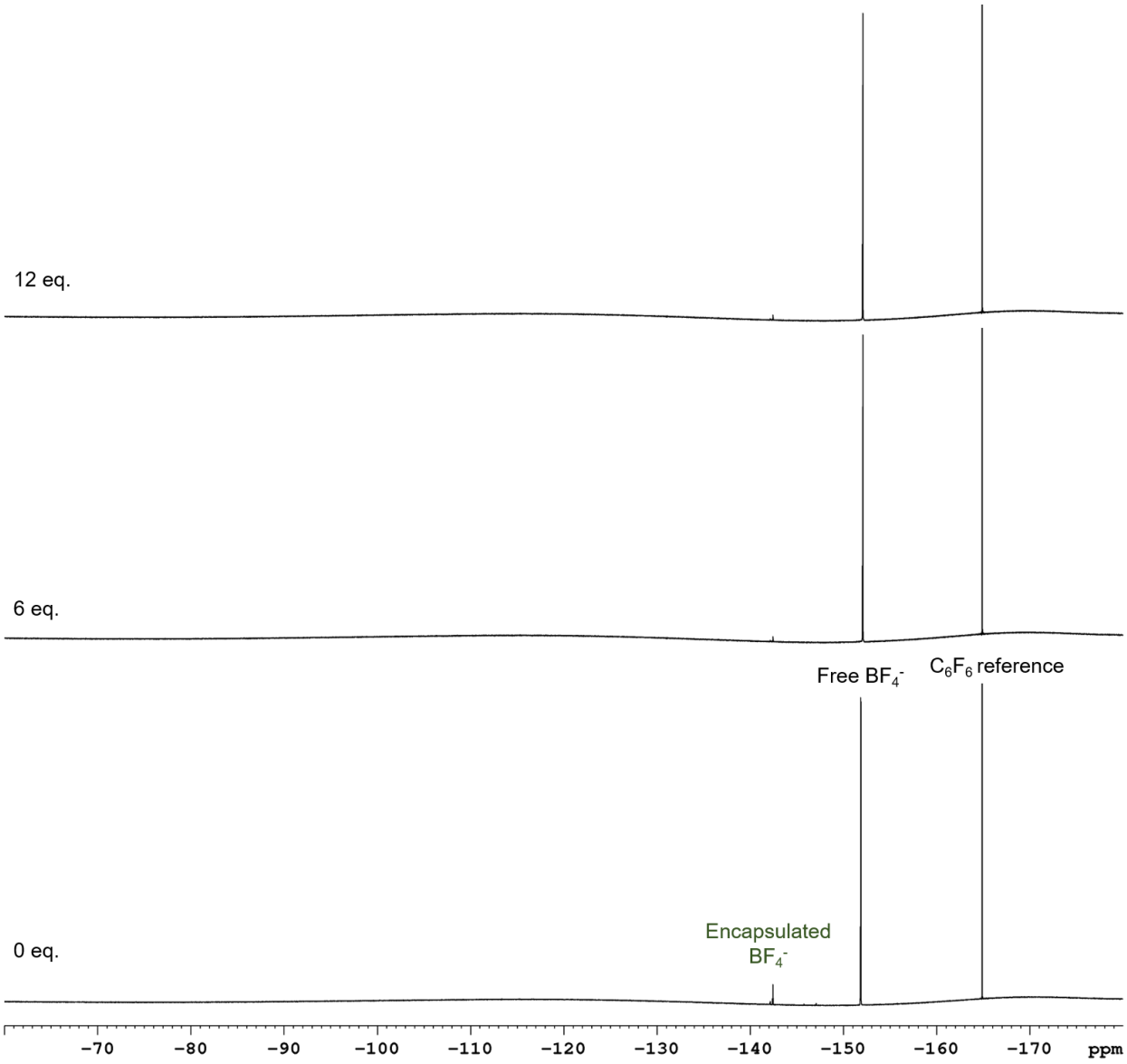

Figure S105. ^{19}F NMR spectra for the titration of $[BF_4 \subset \mathbf{3}]^{8+}$ (green labels) with 0-12 eq. *p*-anisidine in 95:5 CD_3CN/D_2O.

9 Additional Characterisation of Cage 1

9.1 IR Spectrum of 1

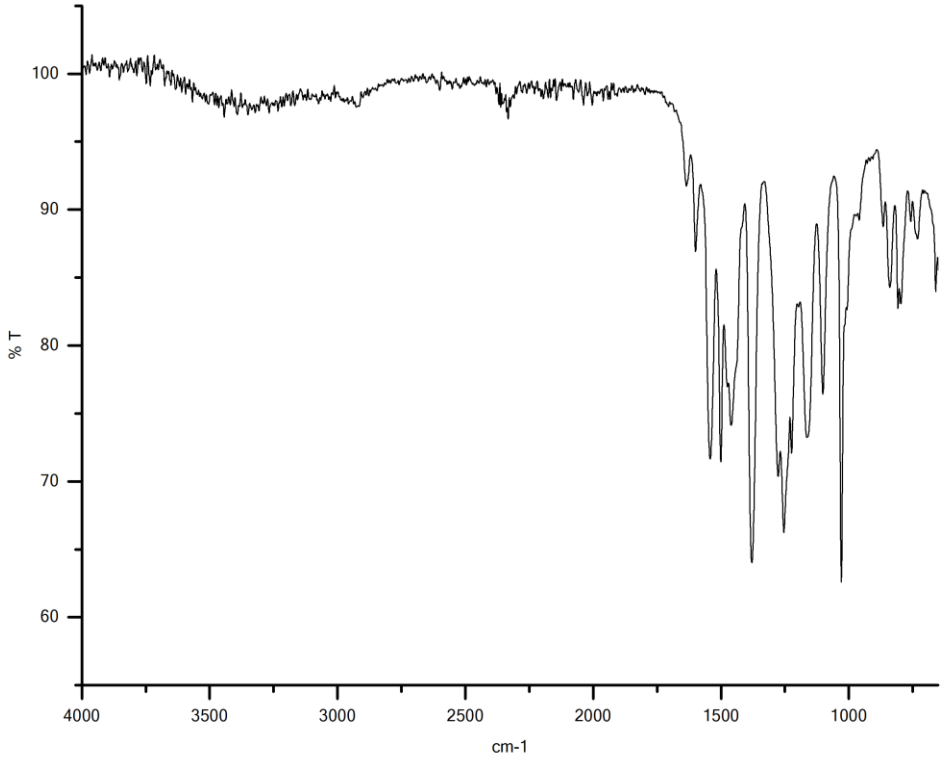

Figure S106. IR spectrum of high-spin cage **1**.

9.2 Magnetic Susceptibility

According to the Evans' method,[1] the mass susceptibility χ_g of the dissolved substance is given by equation 2 where Δf is the frequency shift in Hz of the reference compound, f is the fixed probe frequency of the spectrometer, χ_o is the mass susceptibility of CD_3CN (-0.534×10^{-6} cm^3 g^{-1}), m is the mass in g of the complex in 1 cm^3 of solution. The 3/2π factor in the original Evans equation has been replaced with -3/4π for a sample axis parallel to the magnetic field.

$$\chi_g = \frac{-3\Delta f}{4\pi f m} + \chi_o \qquad \text{Eq. 2}$$

The molar susceptibility χ_M was calculated according to equation 3 by multiplying the mass susceptibility by the molecular weight (M).

$$\chi_M = \chi_g M \qquad \text{Eq. 3}$$

The molar susceptibility χ_M contains the diamagnetic contribution (χ_M^{dia}) and according to Piguet,[10] this contribution cannot be neglected for large supramolecular complexes and therefore, the corrected molar susceptibility $\chi_{M'}$ was calculated according to equation 4 using tabulated values of Pascal's constants[11] to correct for the diamagnetic contributions from the ligands, Fe(II) core electrons and counteranions. χ_M^{dia} for cage **1** is -0.01319 cm^3 mol^{-1}.

$$\chi_{M'} = \chi_M - \chi_M dia \qquad \text{Eq. 4}$$

The molar susceptibilities support the ^{1}H NMR variable temperature experiments that cage **1** is high spin between 268 K and 318 K (Table S3).

Table S3. Molar susceptibilities (χ_M) and corrected molar susceptibilities ($\chi_{M'}$) for cage **1**.

T/K	Δf/Hz	χ_M /cm^3 mol^{-1}	$\chi_{M'}$ /cm^3 mol^{-1}
268	152.13	0.0581	0.0713
298	129.17	0.0490	0.0621
318	115.77	0.0436	0.0568

10 References

1. Evans, D. F., *J. Chem. Soc.* **1959**, 2003-2005.
2. Bolliger, J. L.; Ronson, T. K.; Ogawa, M.; Nitschke, J. R., *J. Am. Chem. Soc.* **2014,** *136*, 14545-14553.
3. Solomon, I., *Phys. Rev.* **1955,** *99*, 559-565.
4. Amouri, H.; Mimassi, L.; Rager, M. N.; Mann, B. E.; Guyard-Duhayon, C.; Raehm, L., *Angew. Chem. Int. Ed.* **2005,** *44*, 4543-4546.
5. Tidmarsh, I. S.; Taylor, B. F.; Hardie, M. J.; Russo, L.; Clegg, W.; Ward, M. D., *New J. Chem.* **2009,** *33*, 366-375.
6. Isley, W. C.; Zarra, S.; Carlson, R. K.; Bilbeisi, R. A.; Ronson, T. K.; Nitschke, J. R.; Gagliardi, L.; Cramer, C. J., *Phys. Chem. Chem. Phys.* **2014,** *16*, 10620-10628.
7. Cai, S.; Seu, C.; Kovacs, Z.; Sherry, A. D.; Chen, Y., *J. Am. Chem. Soc.* **2006,** *128*, 13474-13478.
8. Turega, S.; Whitehead, M.; Hall, B. R.; Meijer, A. J. H. M.; Hunter, C. A.; Ward, M. D., *Inorg. Chem.* **2013,** *52*, 1122-1132.
9. Clegg, J. K.; Cremers, J.; Hogben, A. J.; Breiner, B.; Smulders, M. M. J.; Thoburn, J. D.; Nitschke, J. R., *Chem. Sci.* **2013,** *4*, 68-76.
10. Piguet, C., *J. Chem. Educ.* **1997,** *74*, 815.
11. Drago, R. S., *Physical Methods for Chemists*. 2nd ed.; Surfside Scientific Publishers: Gainsville, FL, 1992.